AUSSOIS 2019

Interaction entre localisation et endommagement lors de la rupture ductile : mesures tridimensionnelles *in situ*

Thilo F. MORGENEYER

Centre des Matériaux (CdM) UMR CNRS 7633 / B.P. 87 91003 Evry cedex France

The chicken and egg question

Strain localisation

?

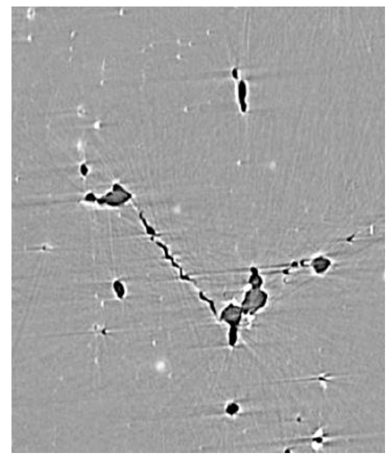

Damage softening

What is the origin of slant fracture?

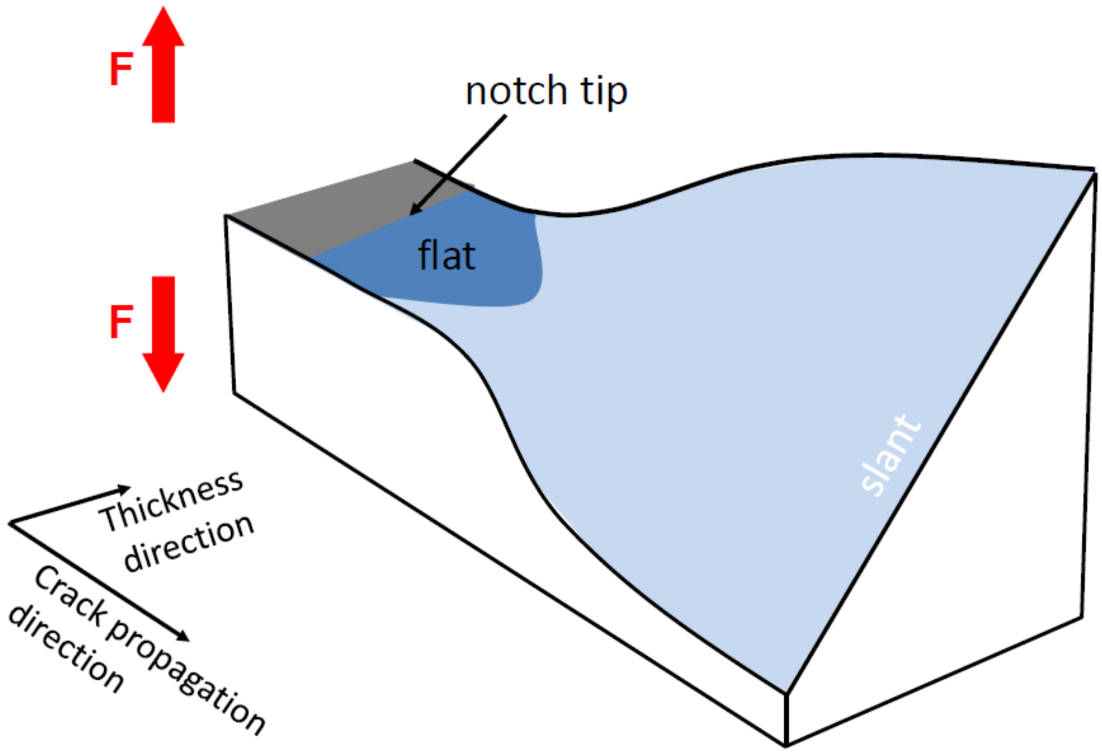

Approach:
Measure damage and strain *in situ* and simultaneously
via two novel techniques

Outline

- Materials
- Synchrotron laminography:
  - imaging and damage analysis
- Digital volume correlation: volume strain measurement
- Strain and damage interactions ahead of a notch
  - Different materials
  - Origins?

- *In situ* damage evolution under shear loading
- Multiscale observations with enhanced resolution

2139 T3/T8 tensile stress stain curves

T3

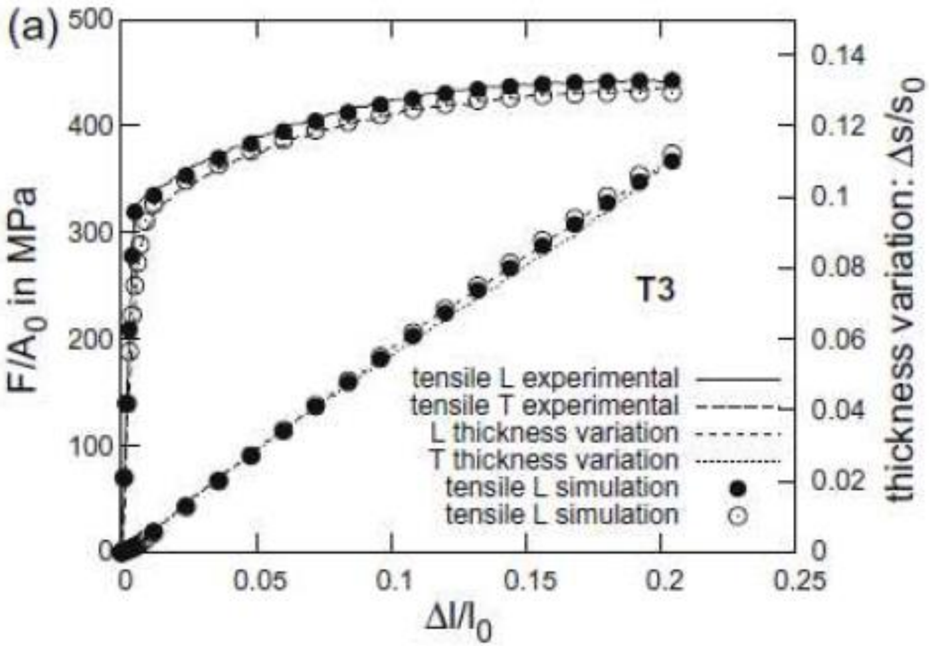

T8

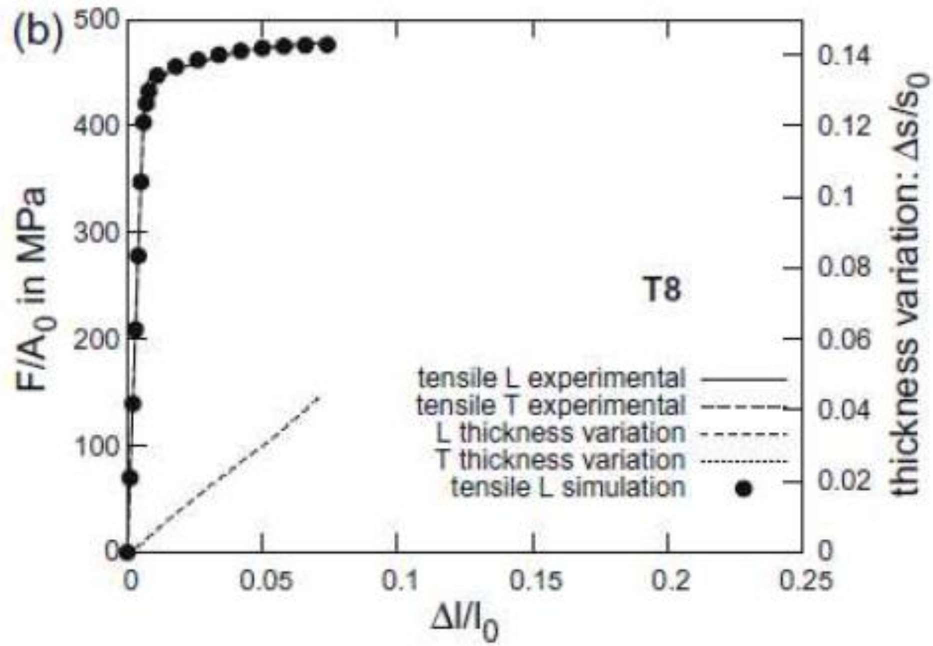

Morgeneyer et al. Acta Mat 2009

Application to AA2139-T3

Al-Cu alloy

- Grain size

initial porosity: 0.3%

intermetallic content: 0.45%

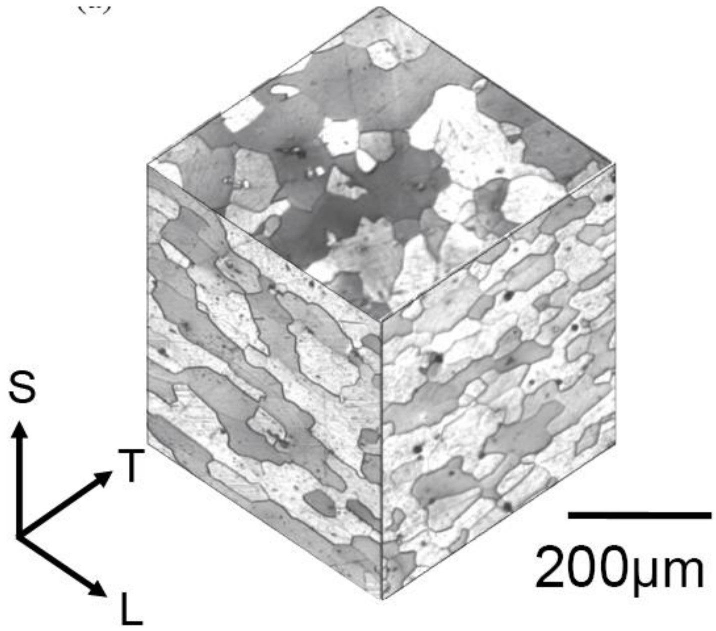

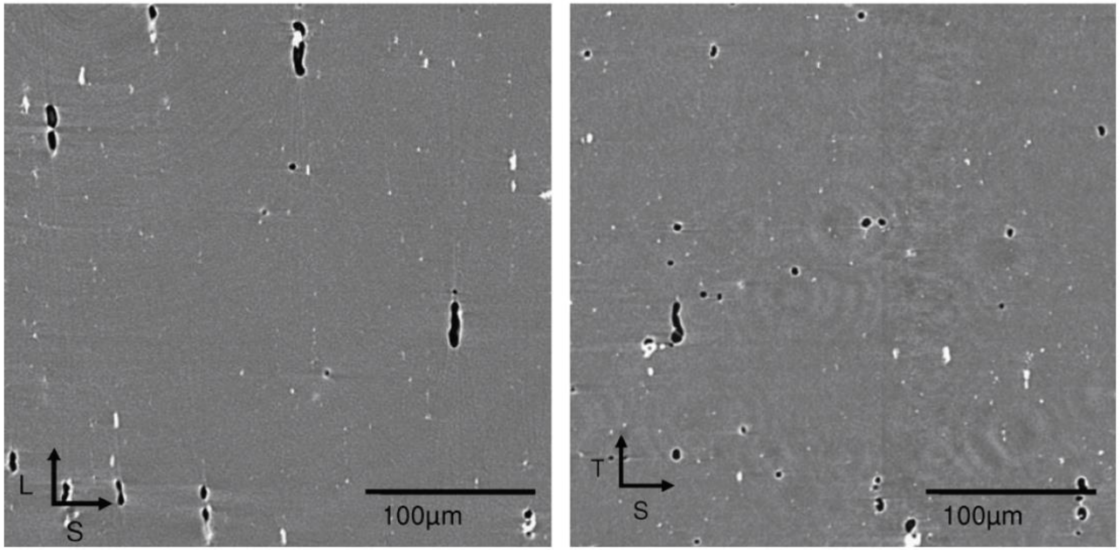

[Morgeneyer *et al., 2008, Acta Mat.* 56 (8), 1671-1679]

Ductile fracture: tomography observation

Principle

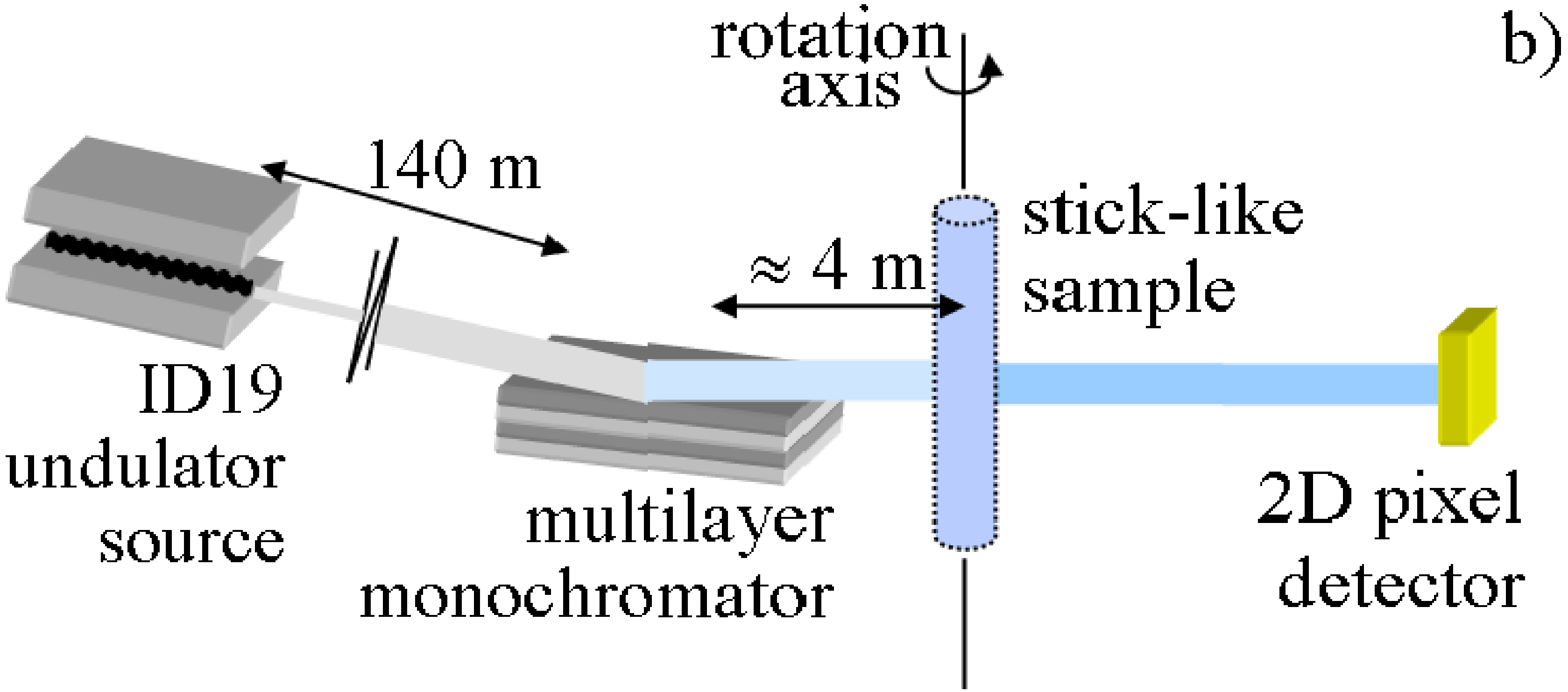

- Stick like samples
- Typical diameter 1 mm for µm resolution
- Observation of sheets for ductile tearing not possible!

Ductile fracture: laminography observation

Principle

L. Helfen *et al.*, *Appl. Phys. Lett.* 2005
L. Helfen *et al.*, *Appl. Phys. Lett.* 2009

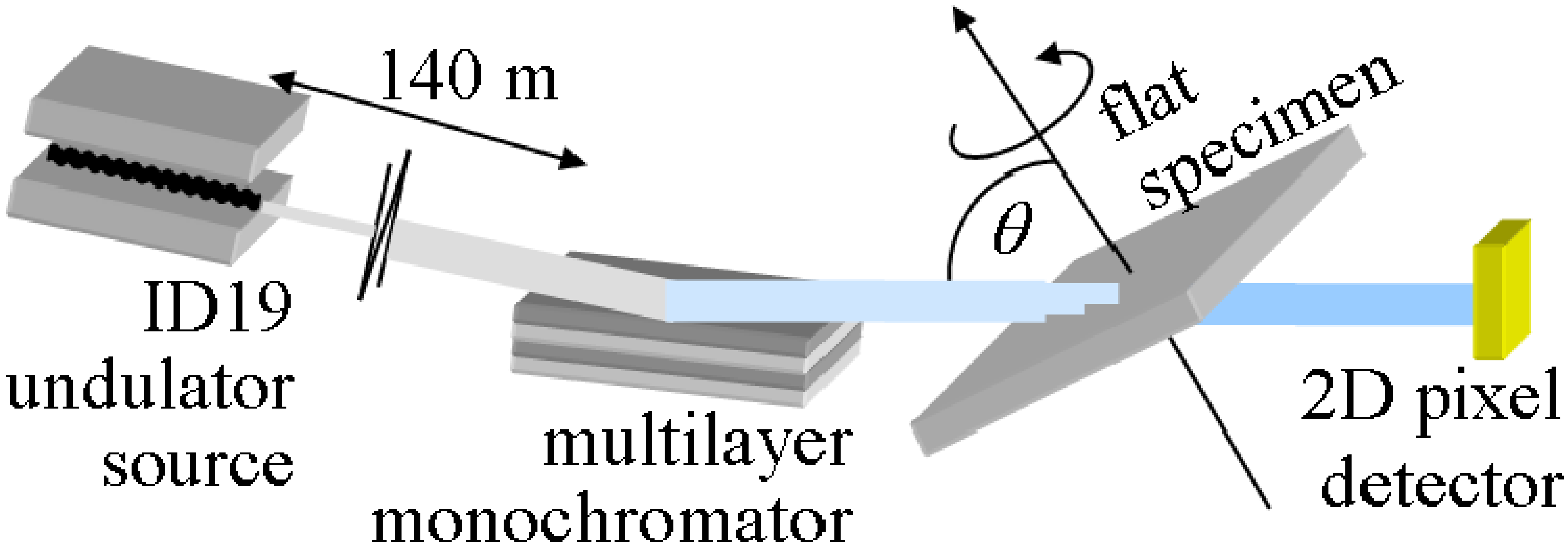

•

- Specimen can be much larger than lateral field of view of detector!
- Major benefit: Possibility to observe ***in situ*** large thin samples at realistic sizes/ length scales
- Additional artefacts due to missing information
- Available at ESRF (ID15; ID19), KARA (TOPOTOMO; IMAGE-beamline)

In situ laminography

○ end-station and loading device

- Dedicated *in situ* machines as there are specifications on:
  - geometry
  - weight

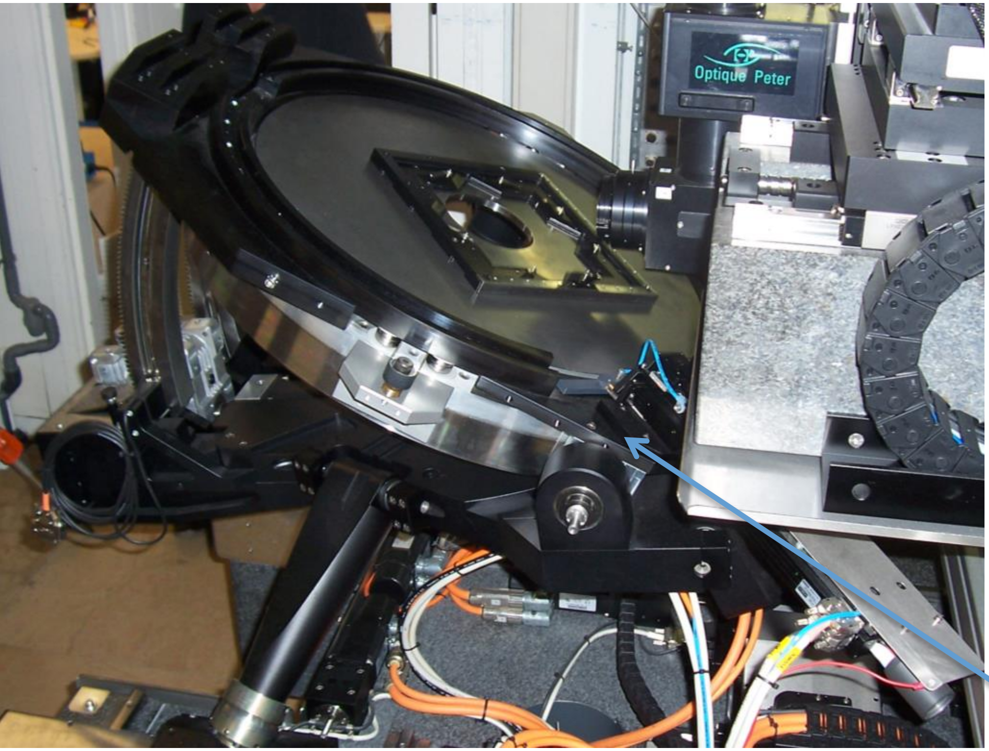

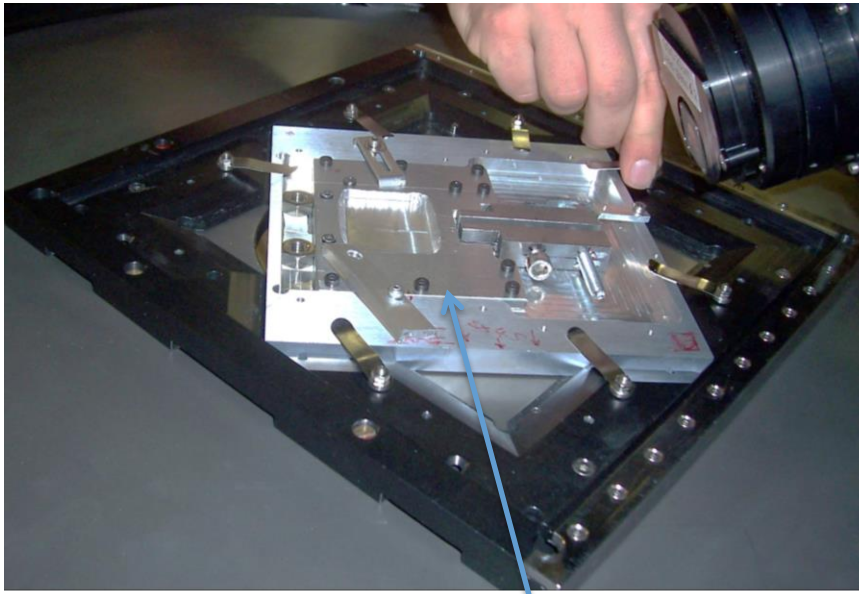

2 screw loading device
Anti-buckling frame
specimen

KIT- Laminography device at ESRF ID19

Aluminium sheet investigated by laminography

- 2139 Al alloy in T3 condition,
- Specimen thickness 1mm
- ~20 load steps via 2 load screws
  - T-L configuration

anti-buckling device
not shown here

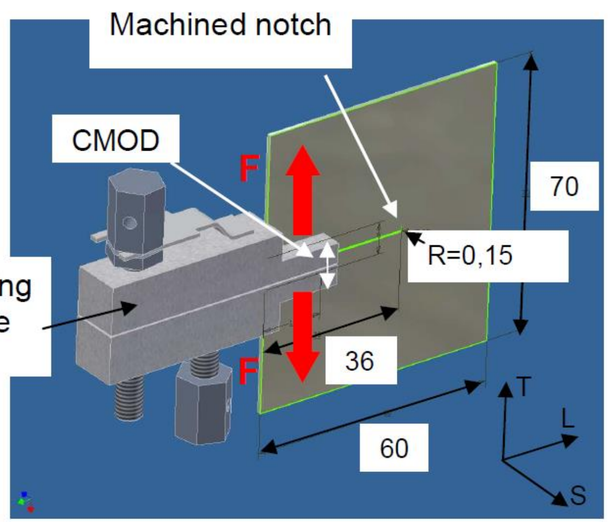

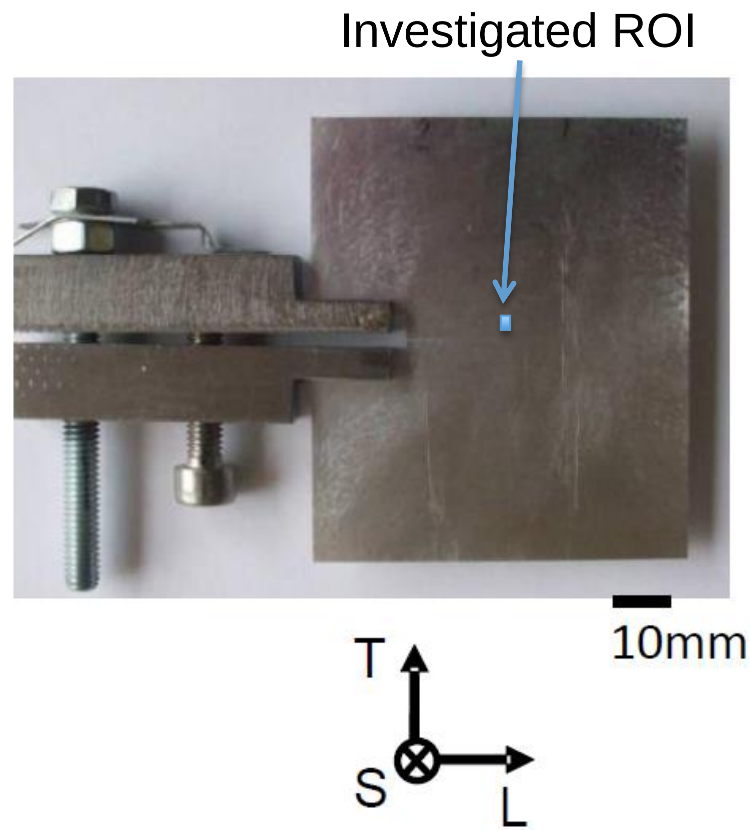

- Scan conditions, at ESRF ID19
  - Tilt angle 25 degree
  - Voxel size 0.7 µm
  - Scan time ~12 mins

*Morgeneyer et al. Scripta Mat. 2011

In-situ SRCLaminography

- 2139 T3: 2D section at mid-thickness

Crack progression
(and rolling) direction

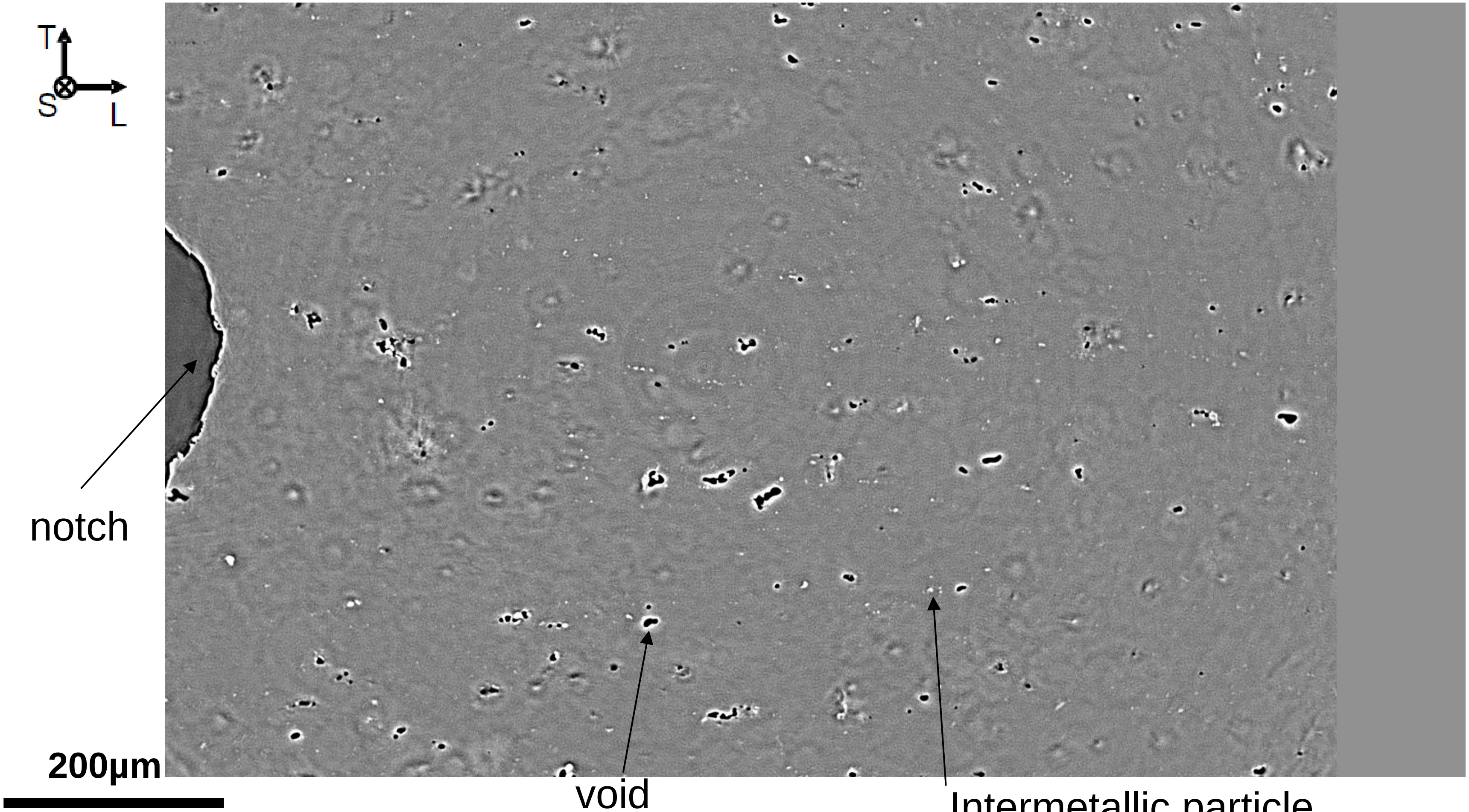

*Morgeneyer et al. Scripta Mat. 2011

In-situ SRCLaminography

- 2139 T3: 2D section at mid-thickness

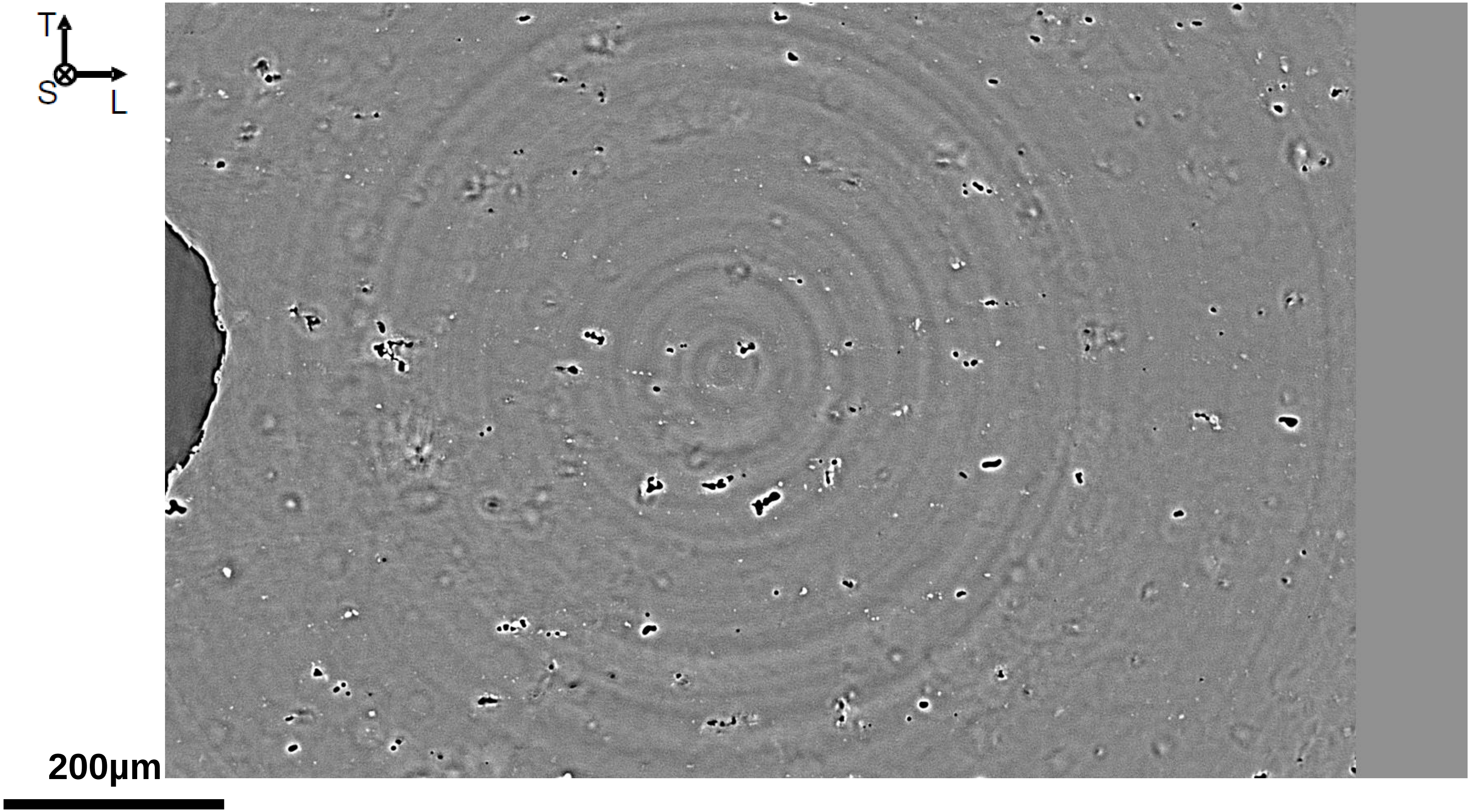

In-situ SRCLaminography

- 2139 T3: 2D section at mid-thickness

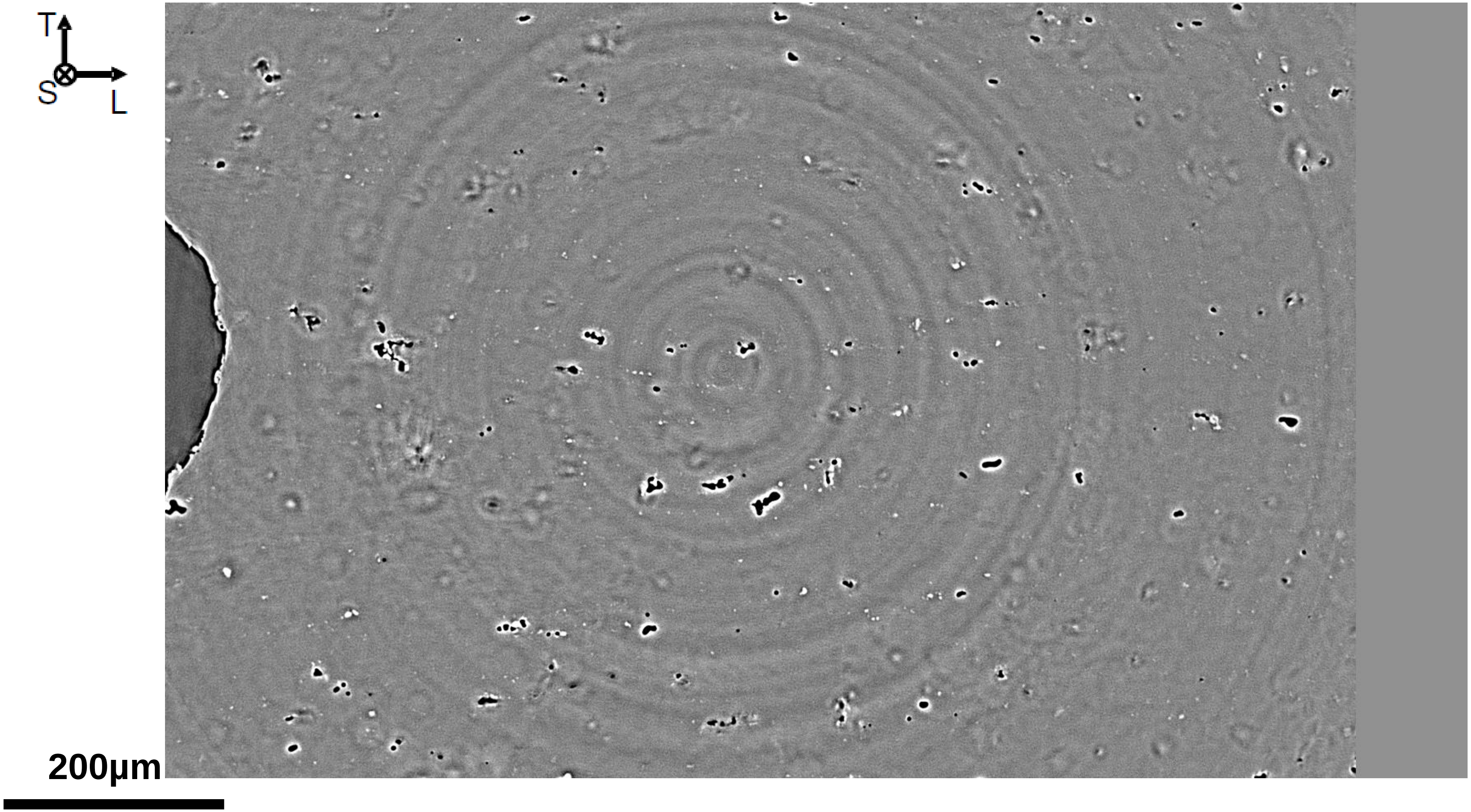

In-situ SRCLaminography

- 2139 T3: 2D section at mid-thickness

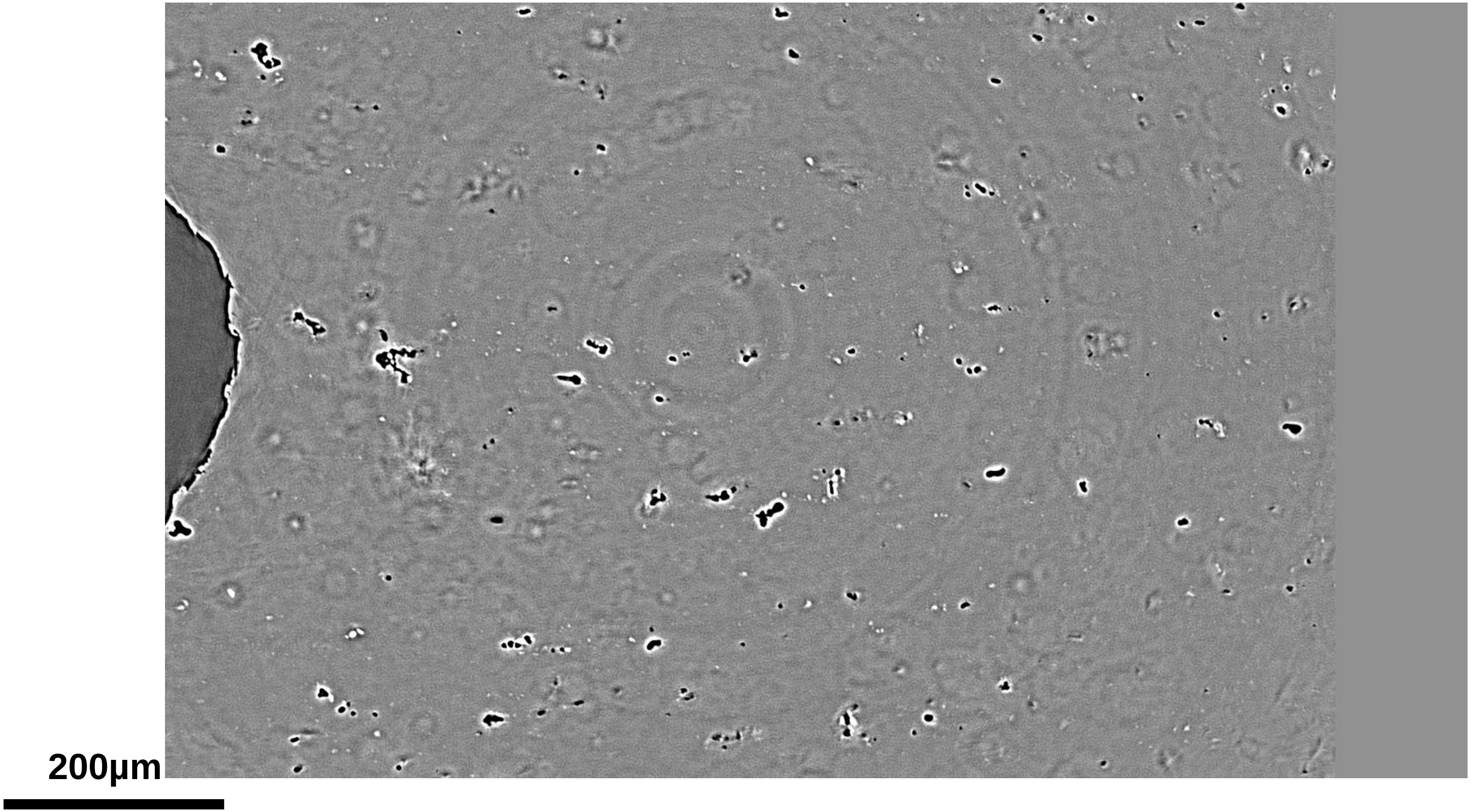

In-situ SRCLaminography

- 2139 T3: 2D section at mid-thickness

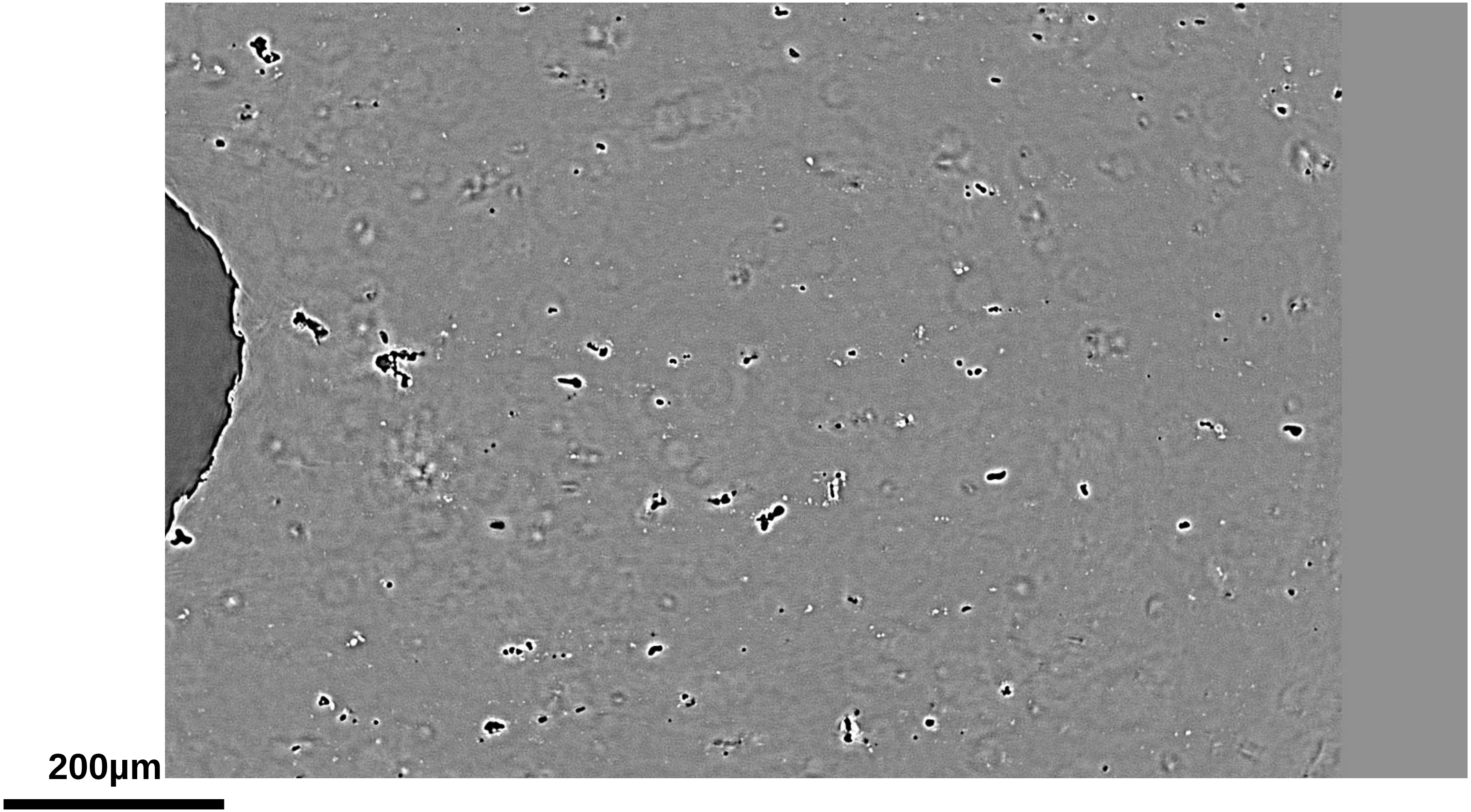

In-situ SRCLaminography

- 2139 T3: 2D section at mid-thickness

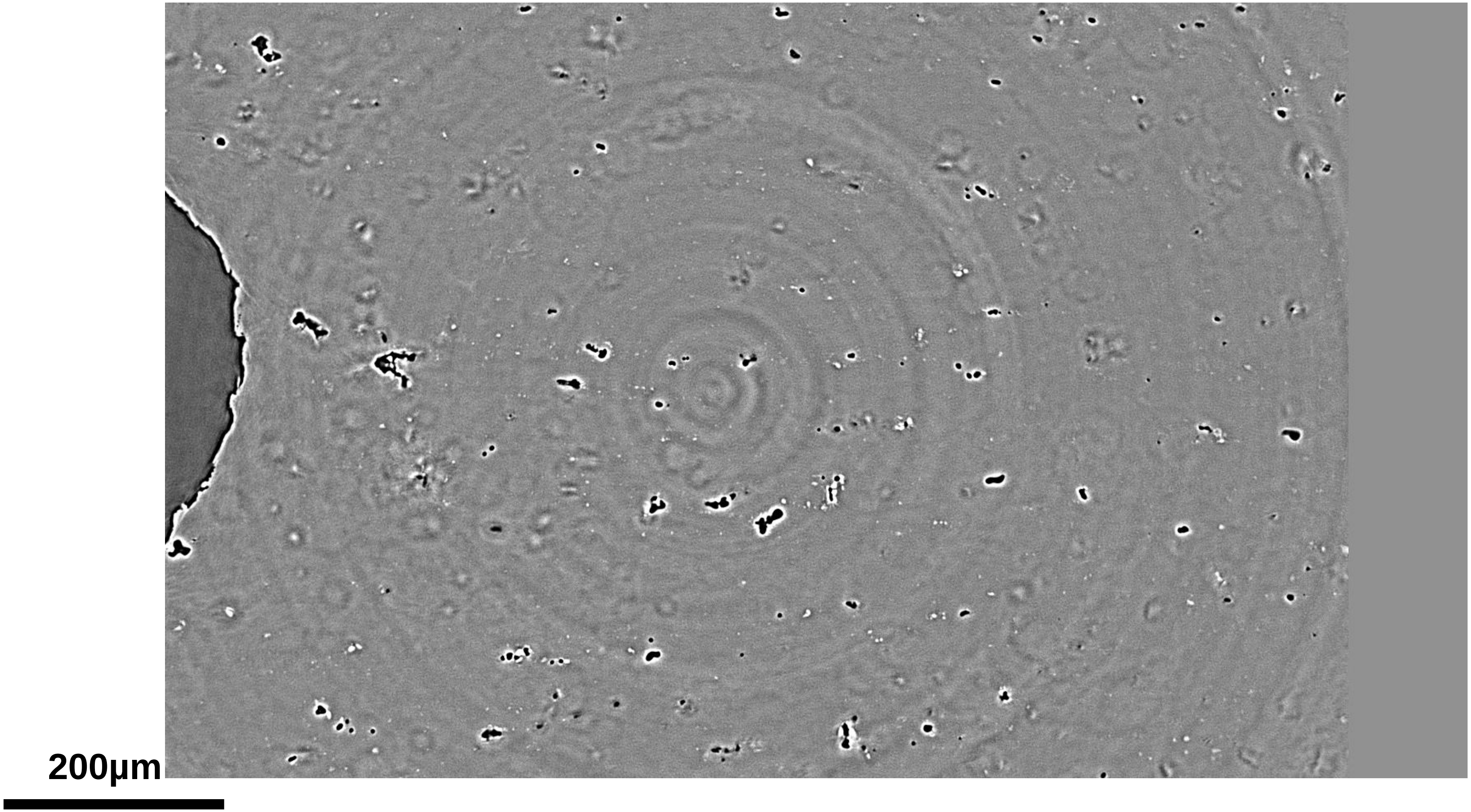

In-situ SRCLaminography

- 2139 T3: 2D section at mid-thickness

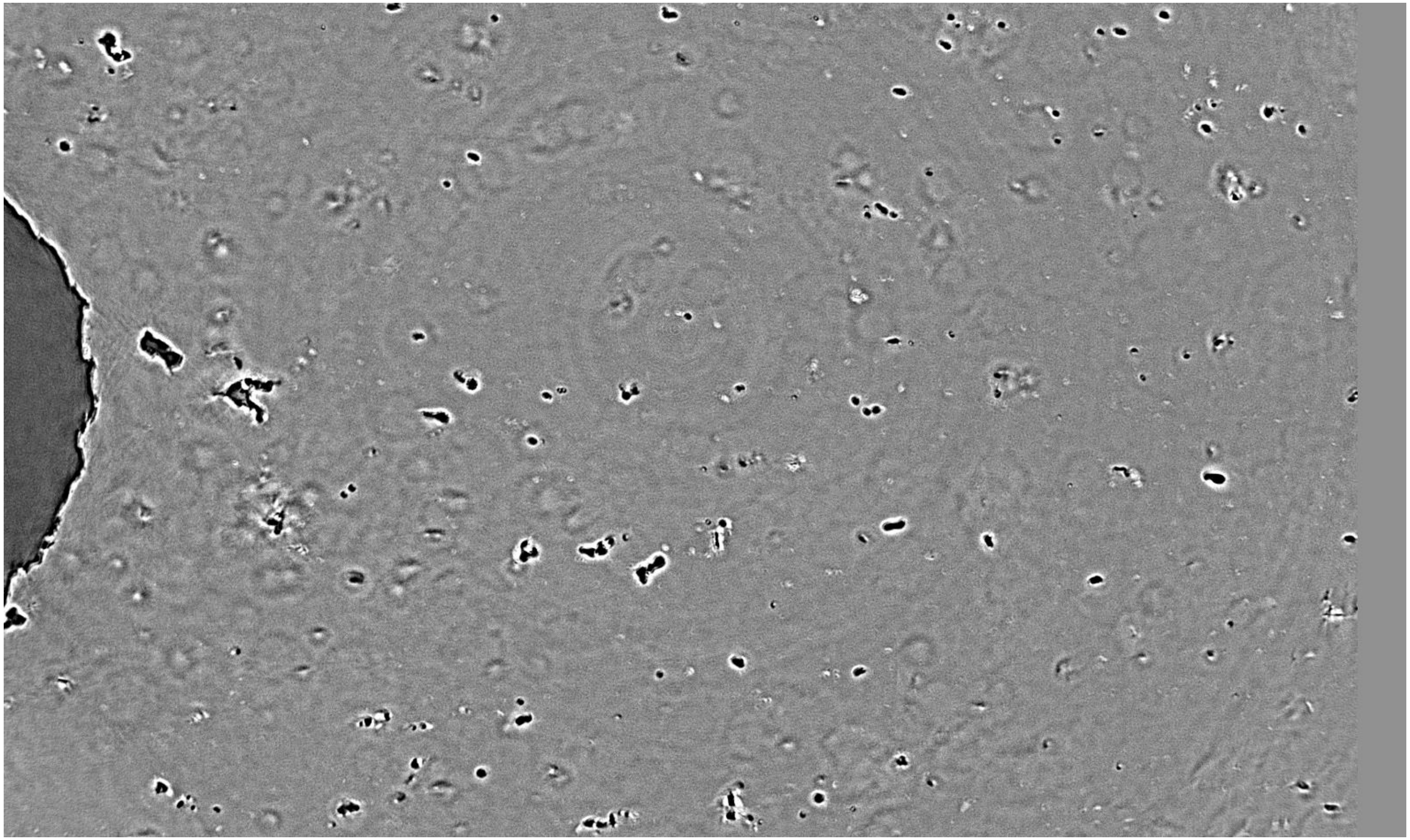

200µm

In-situ SRCLaminography

- 2139 T3: 2D section at mid-thickness

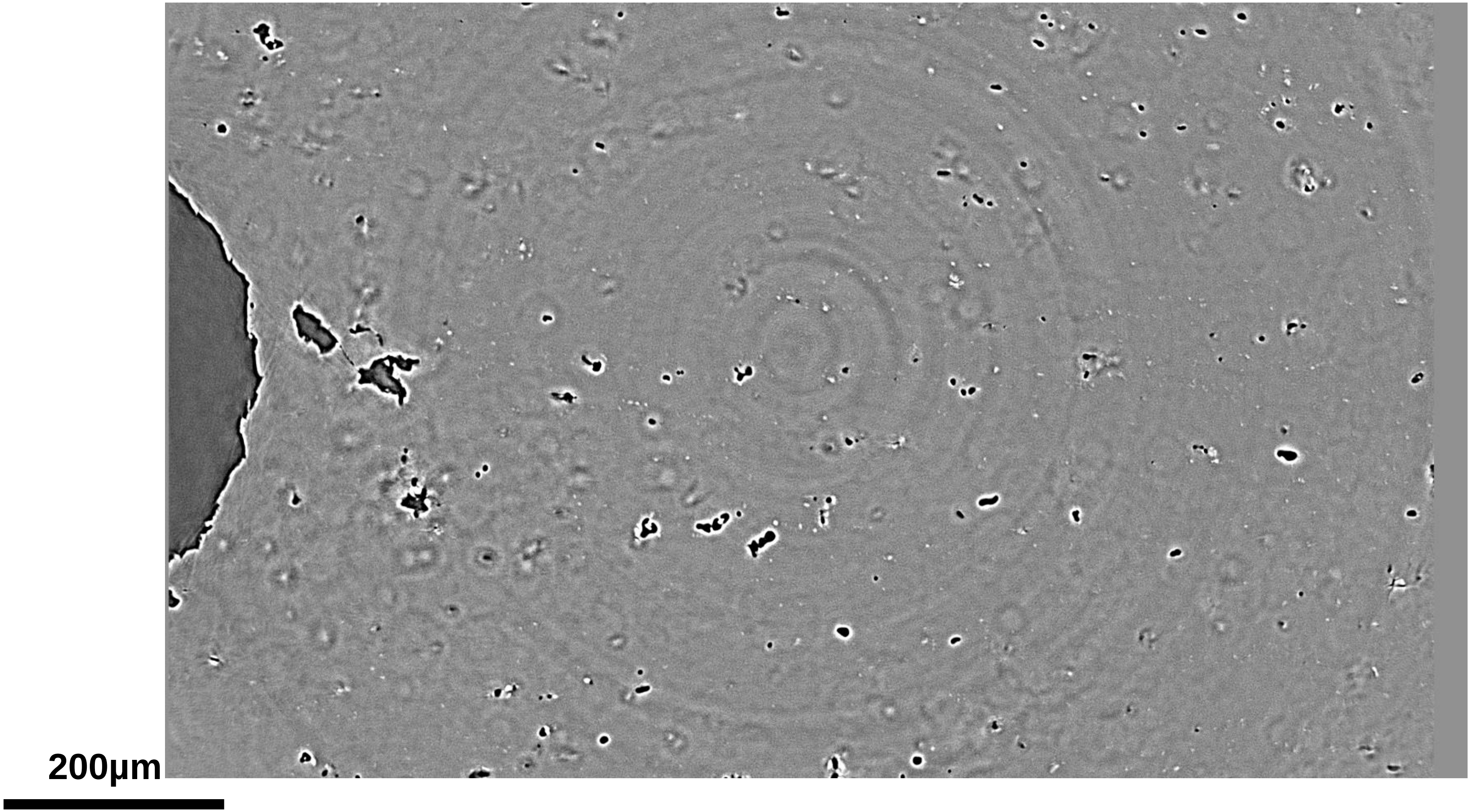

In-situ SRCLaminography

- 2139 T3: 2D section at mid-thickness

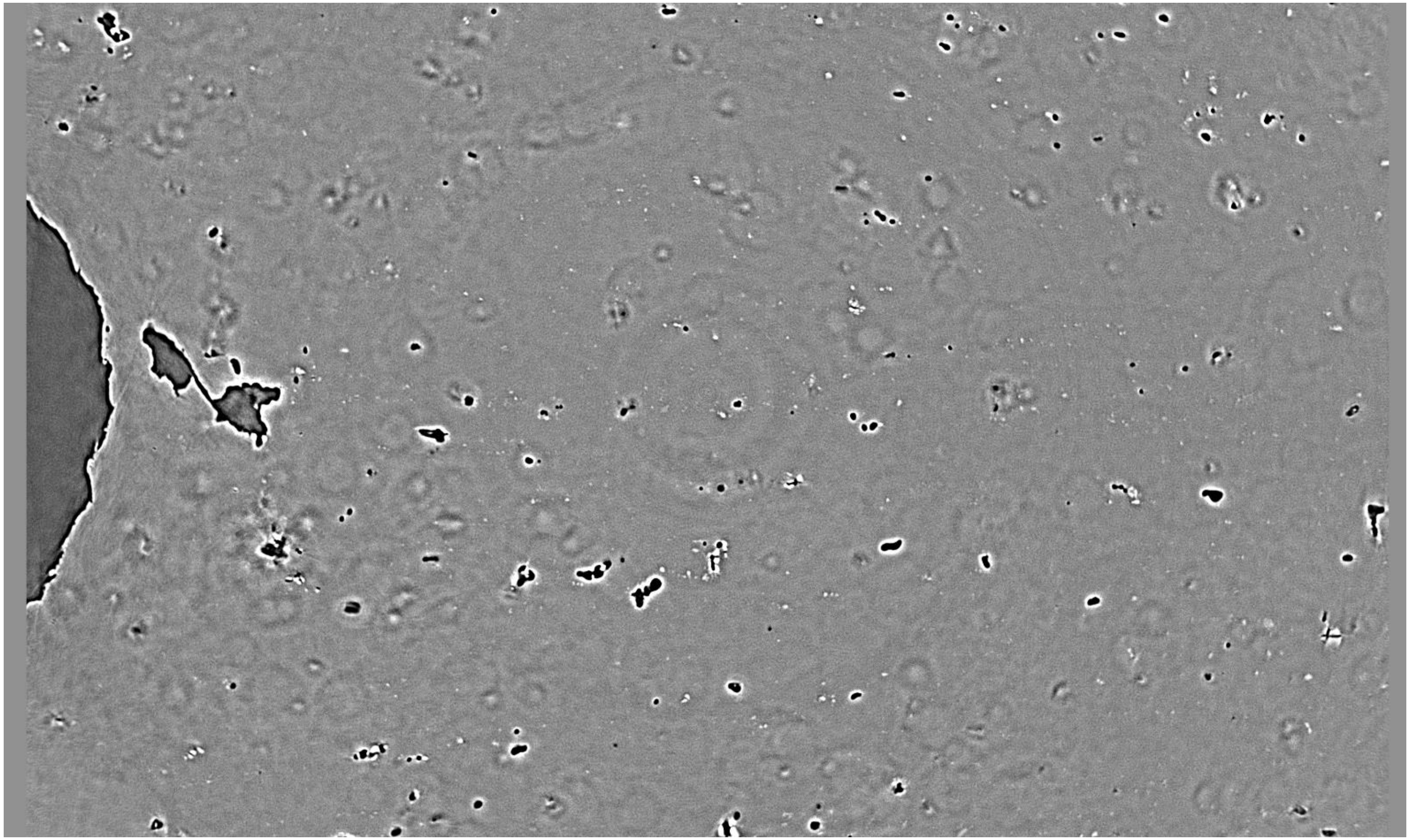

200µm

In-situ SRCLaminography

- 2139 T3: 2D section at mid-thickness

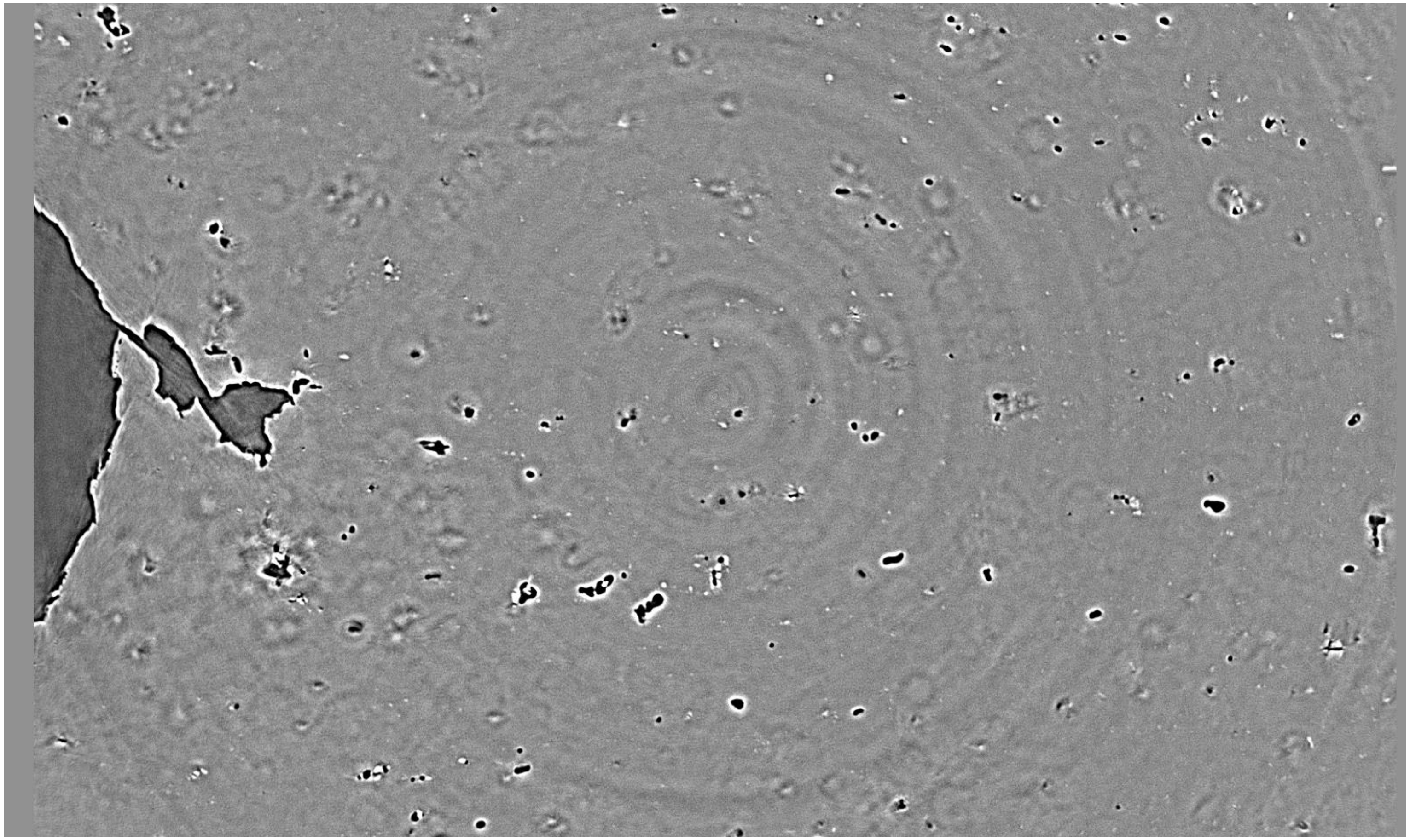

200µm

In-situ SRCLaminography

- 2139 T3: 2D section at mid-thickness

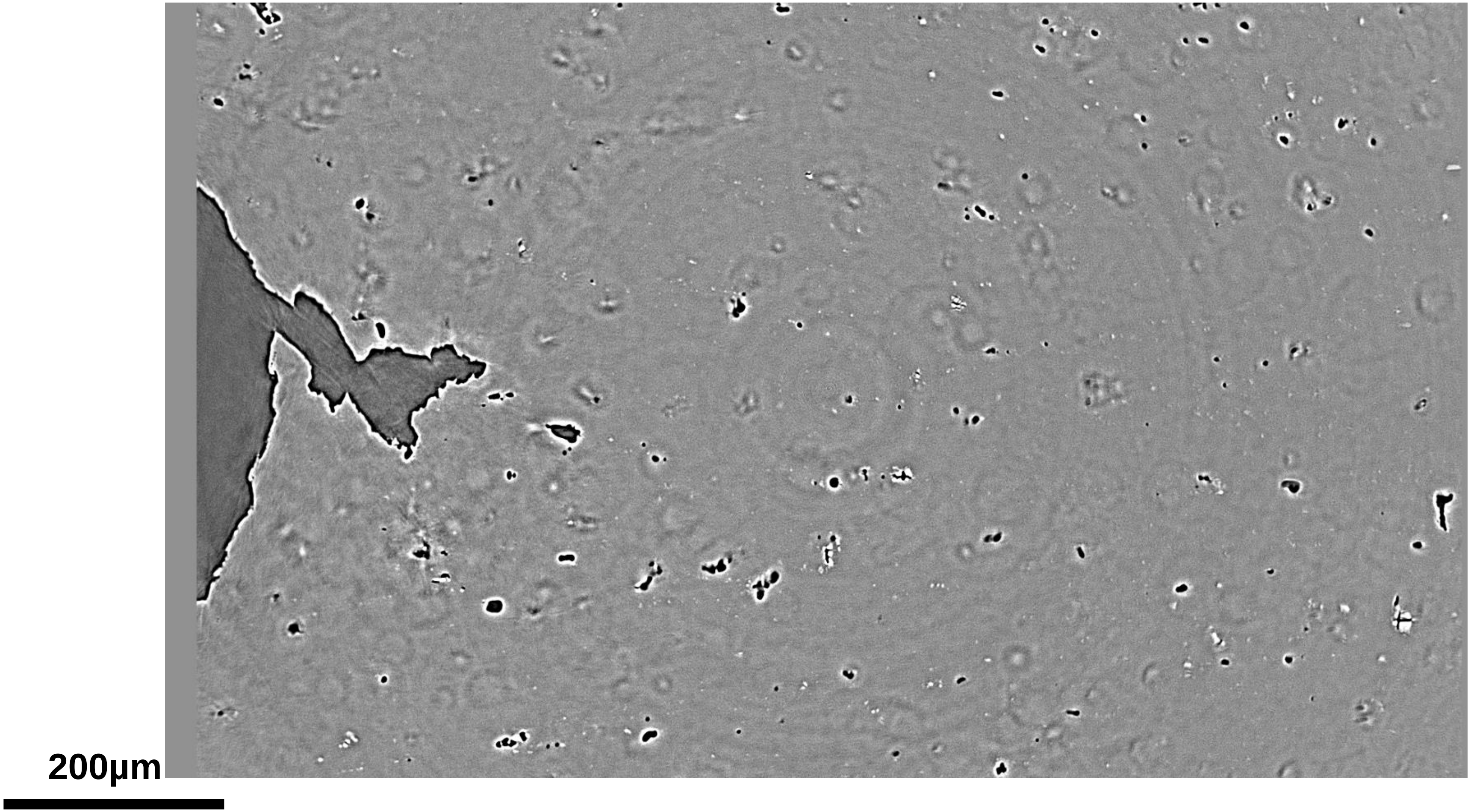

In-situ SRCLaminography

- 2139 T3: 2D section at mid-thickness

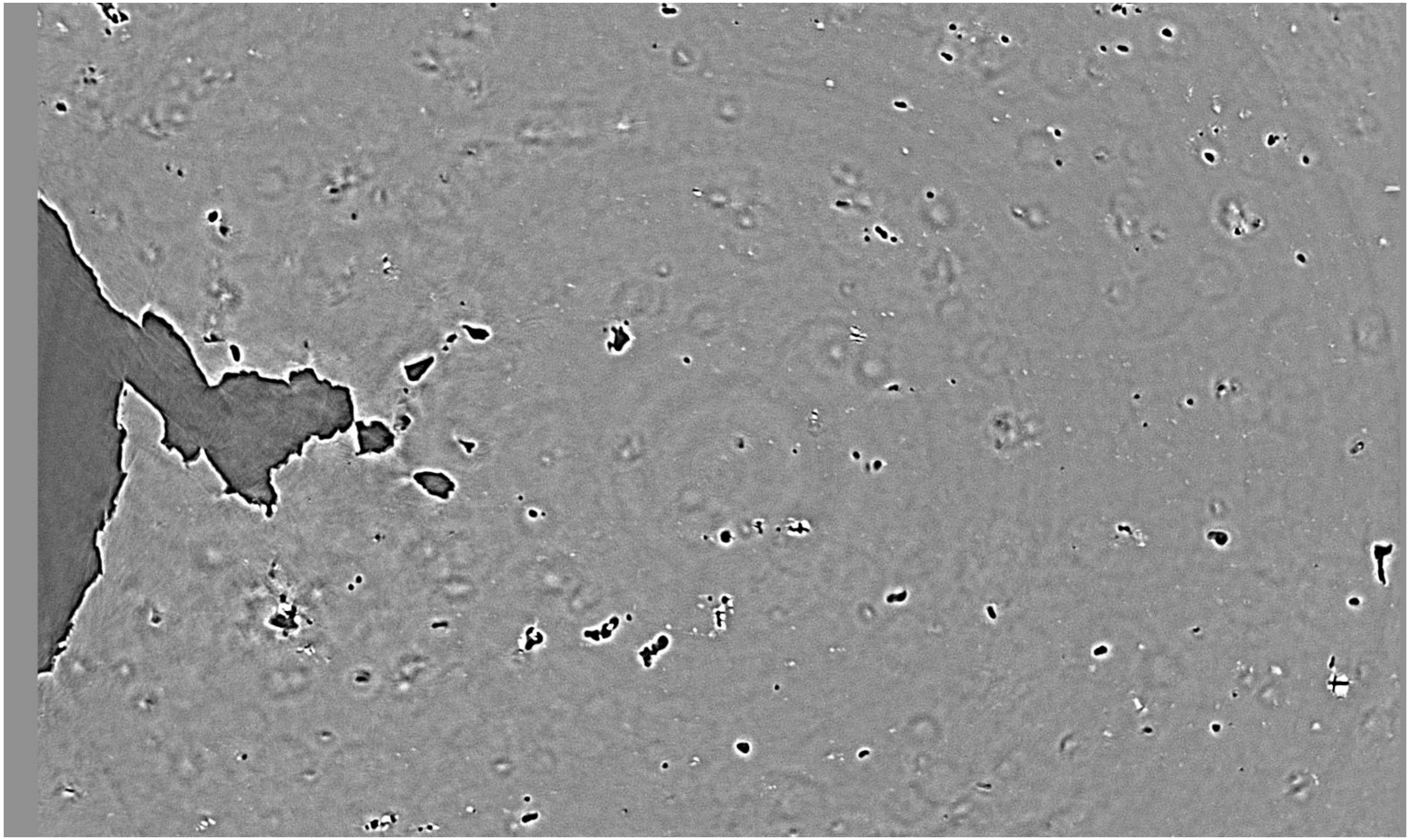

200µm

In-situ SRCLaminography

- 2139 T3: 2D section at mid-thickness

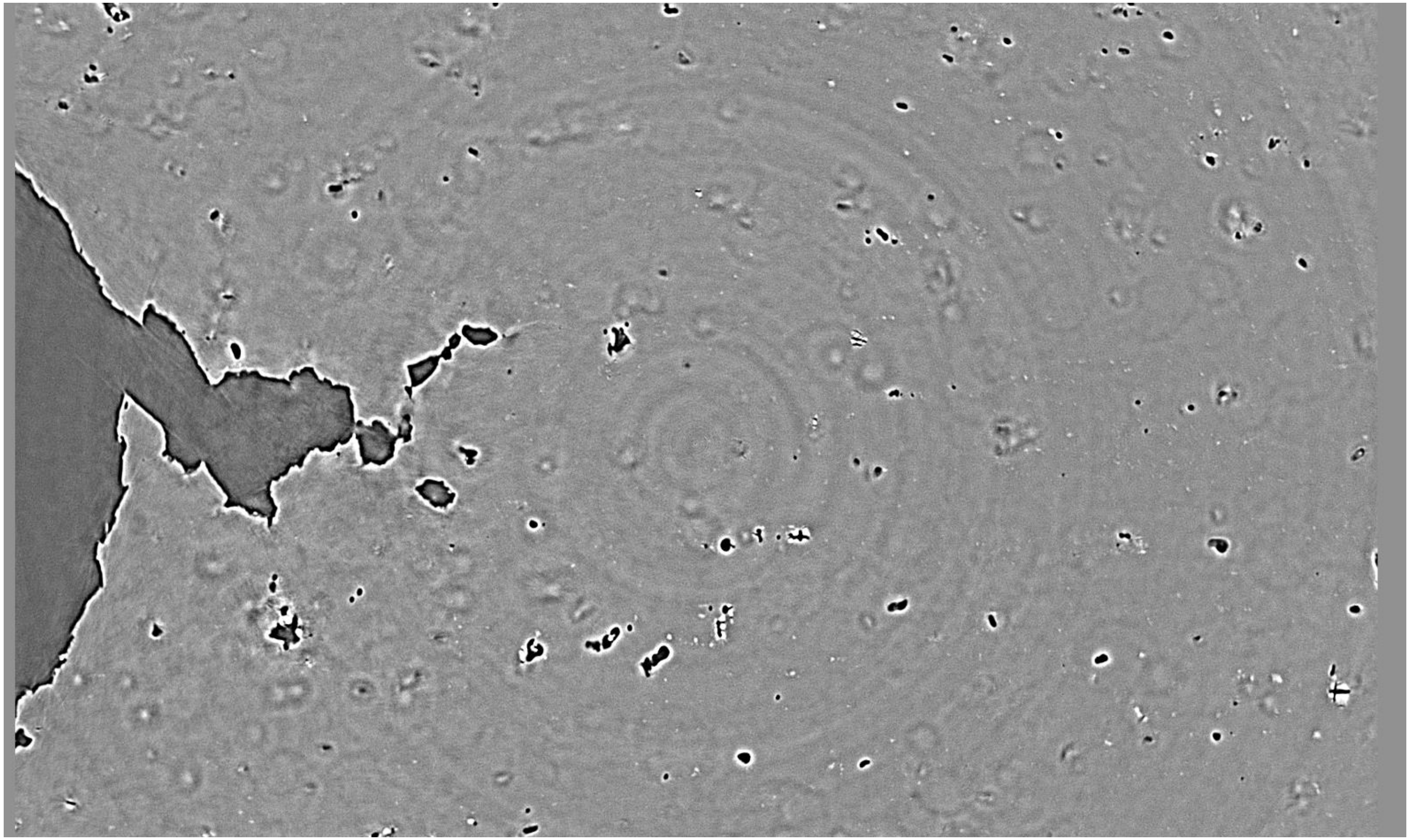

200µm

In-situ SRCLaminography

- 2139 T3: 2D section at mid-thickness

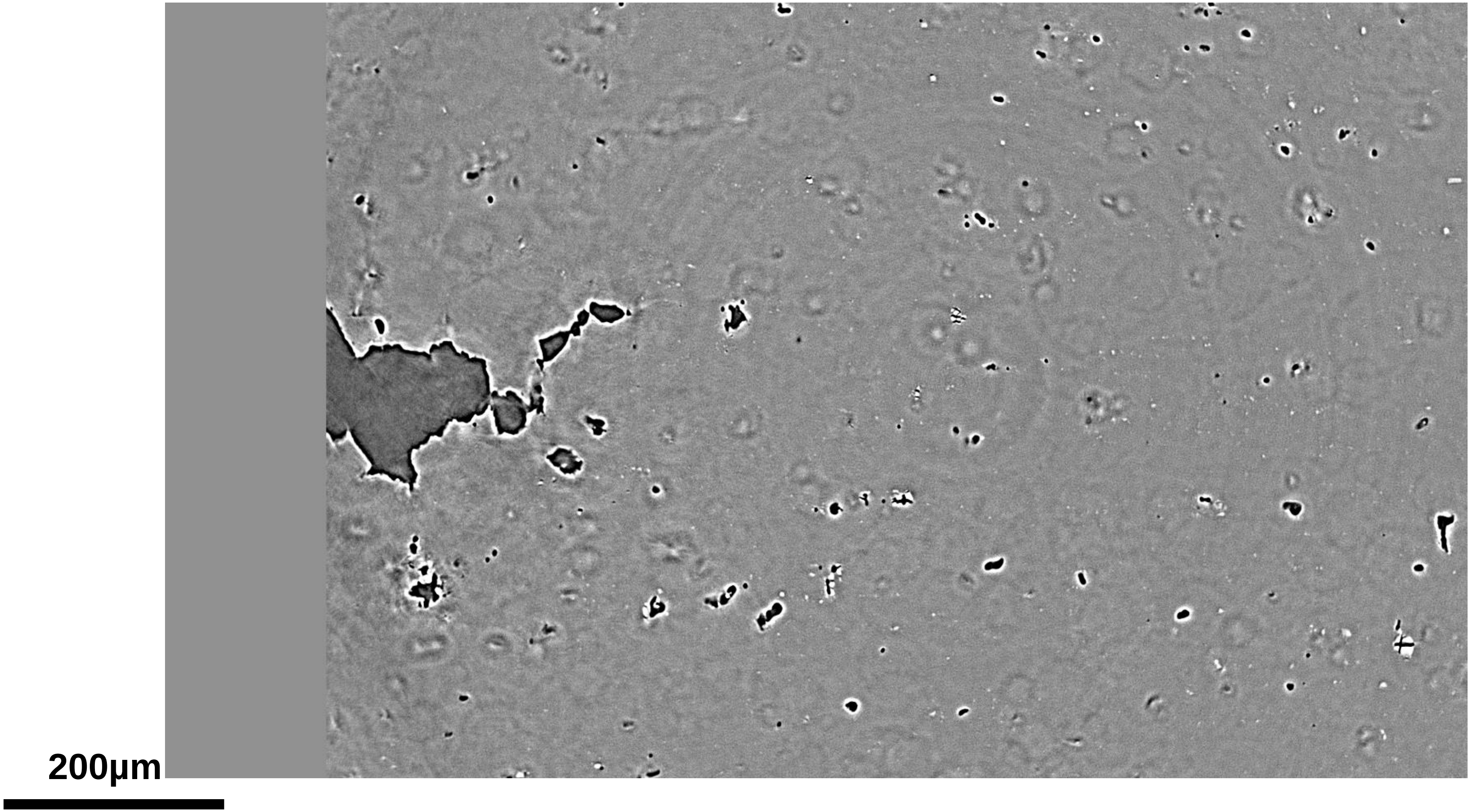

In-situ SRCLaminography

- 2139 T3: 2D section at mid-thickness

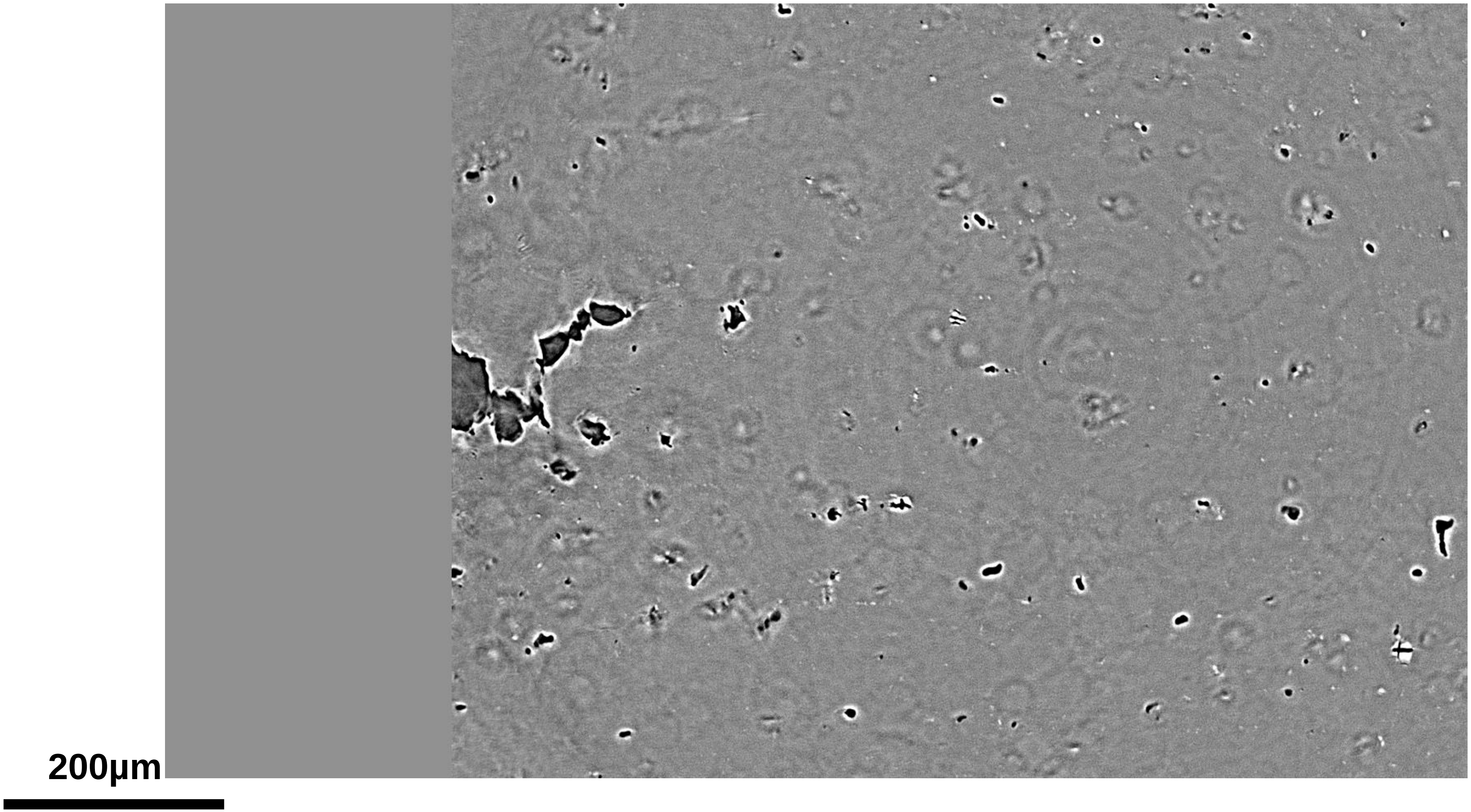

In-situ SRCLaminography

- 2139 T3: 2D section at mid-thickness

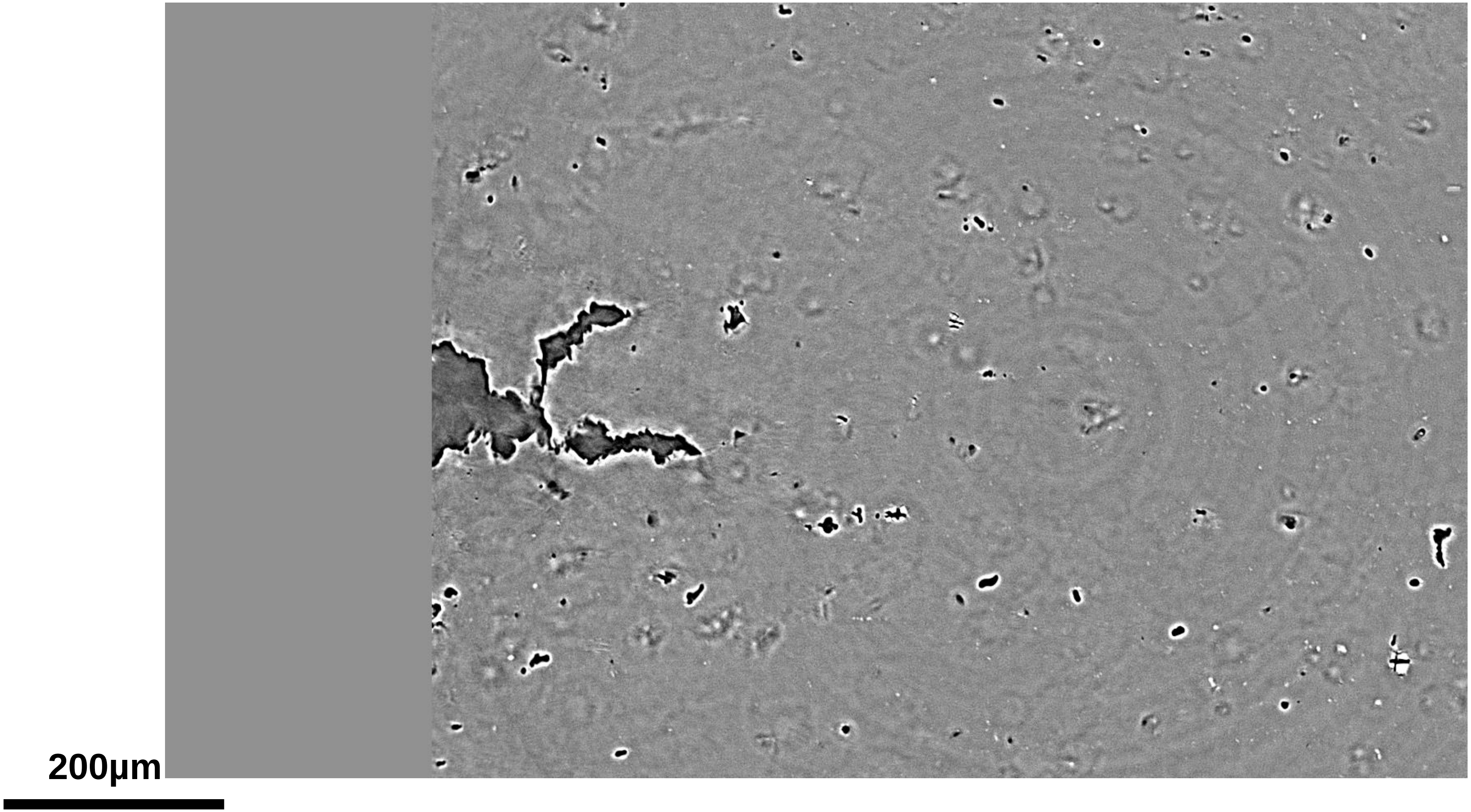

In-situ SRCLaminography

- 2139 T3: 2D section at mid-thickness

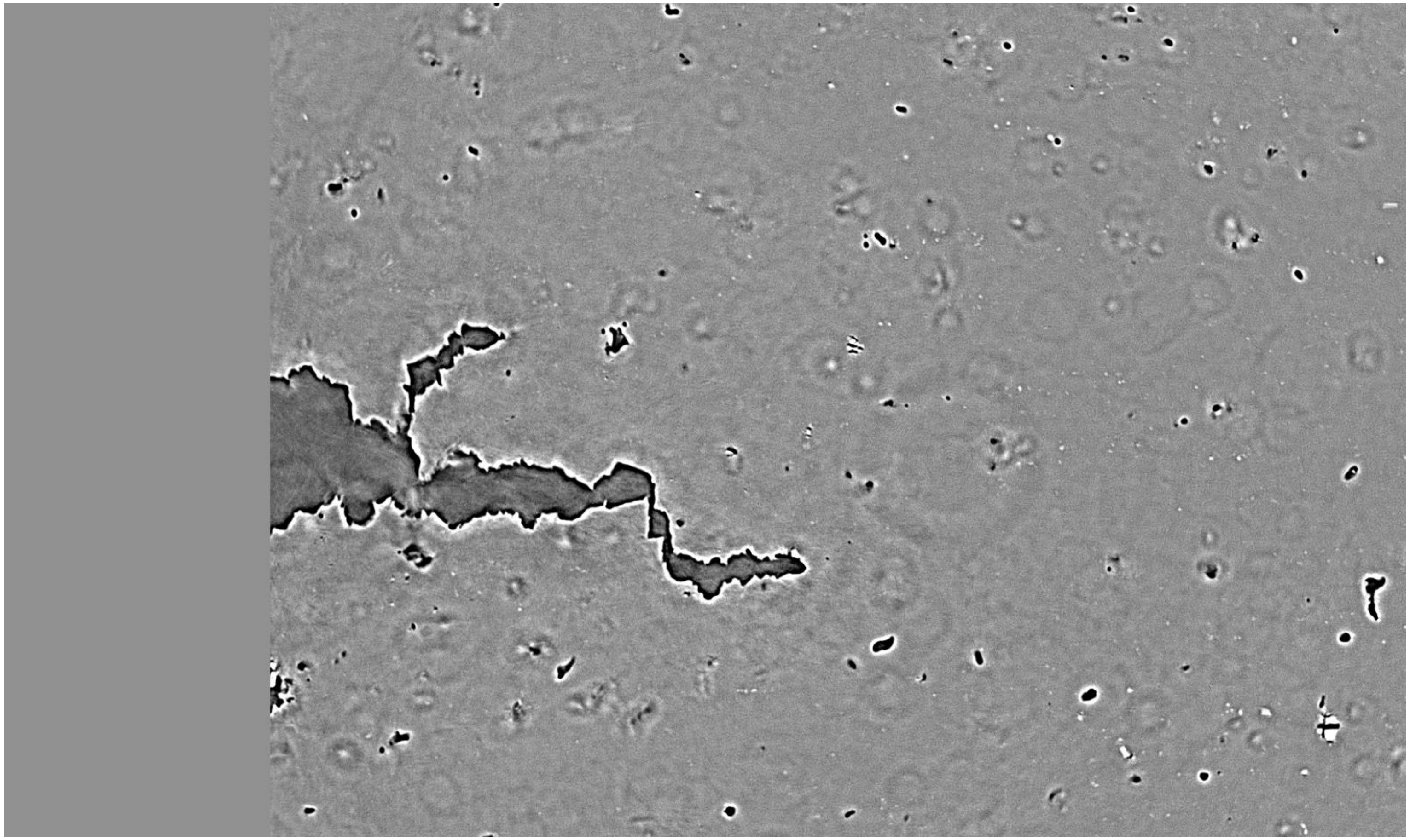

200µm

In-situ SRCLaminography

- 2139 T3: 2D section at mid-thickness

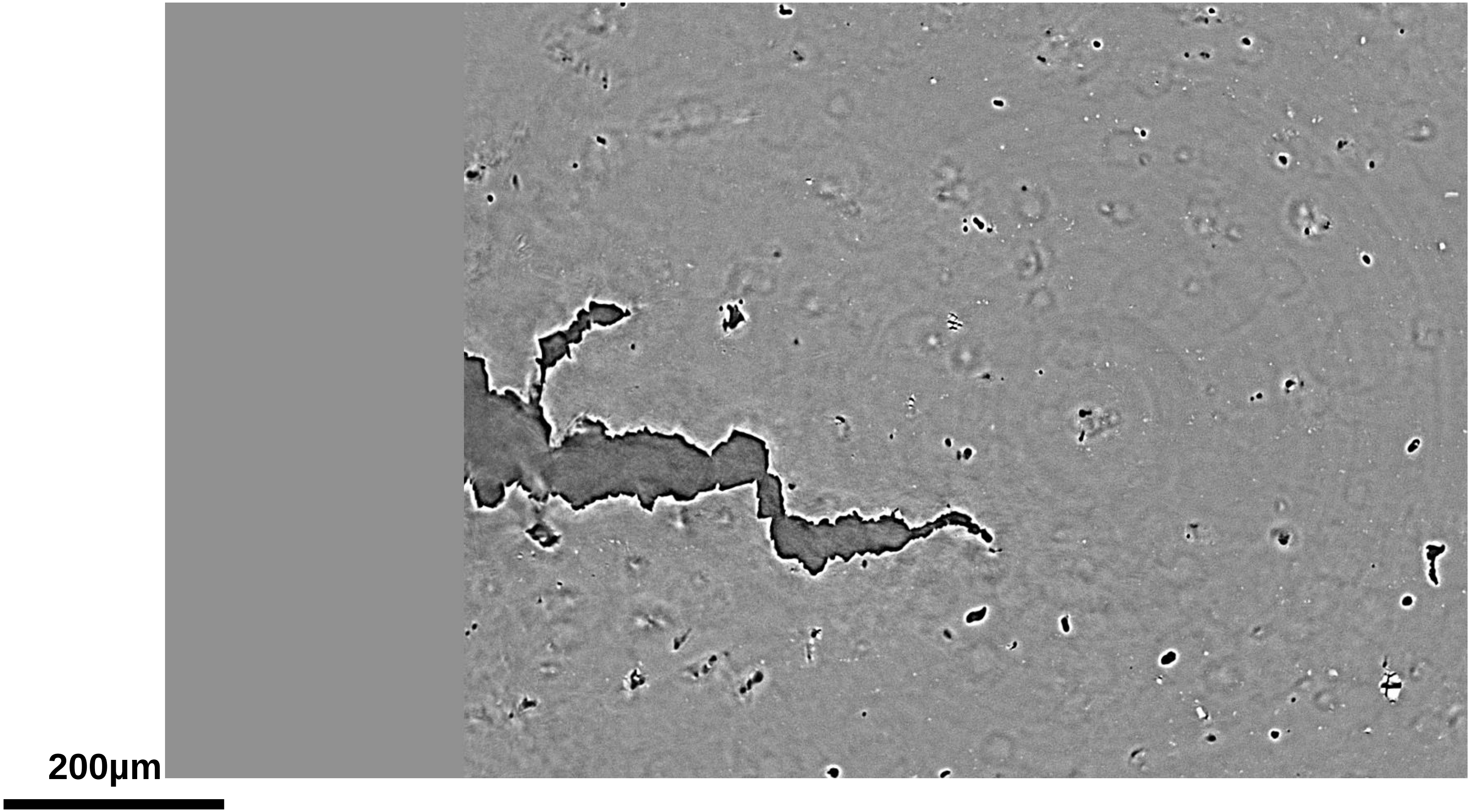

In-situ SRCLaminography

- 2139 T3: 2D section at mid-thickness

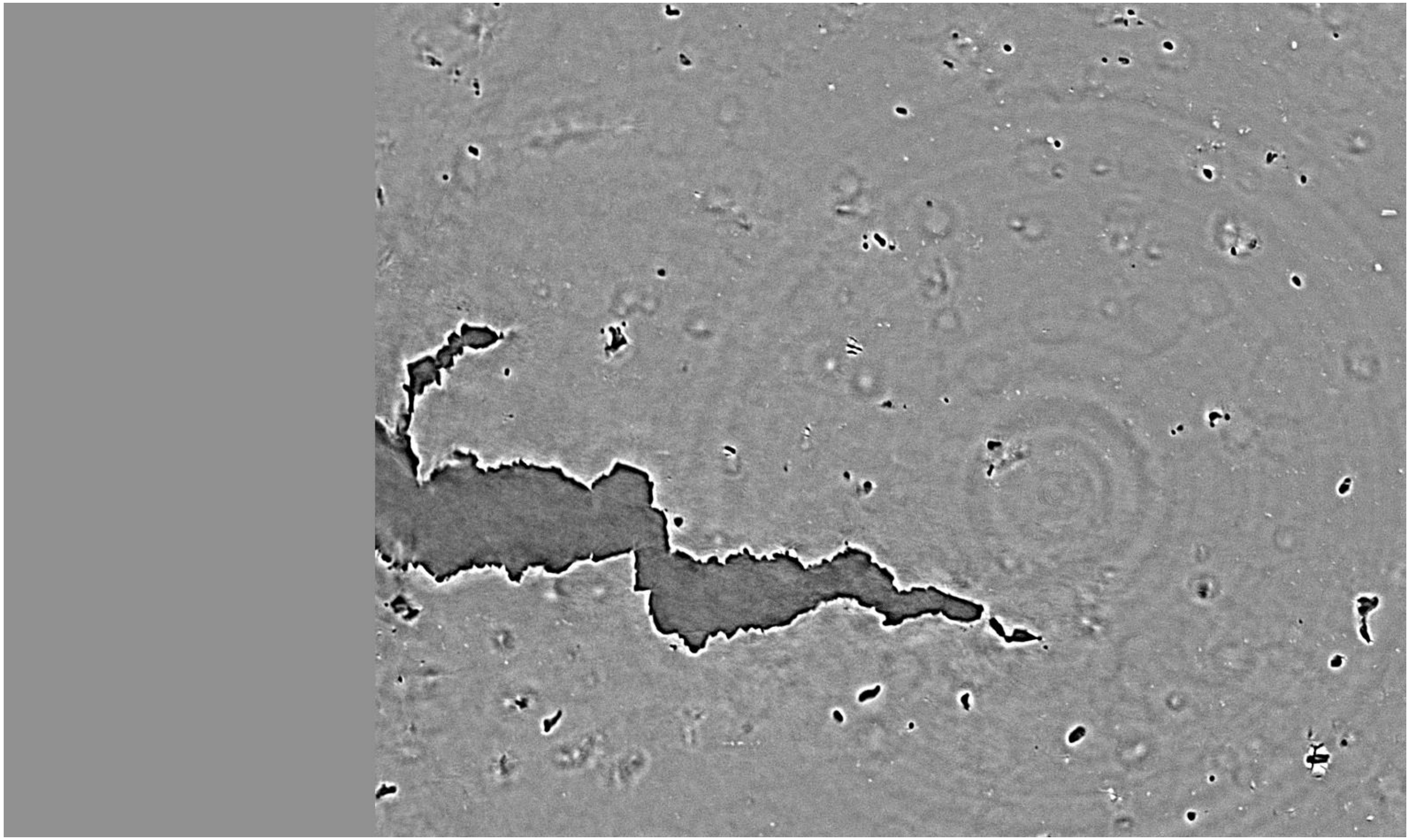

200µm

In-situ SRCLaminography

- 2139 T3: 2D section at mid-thickness

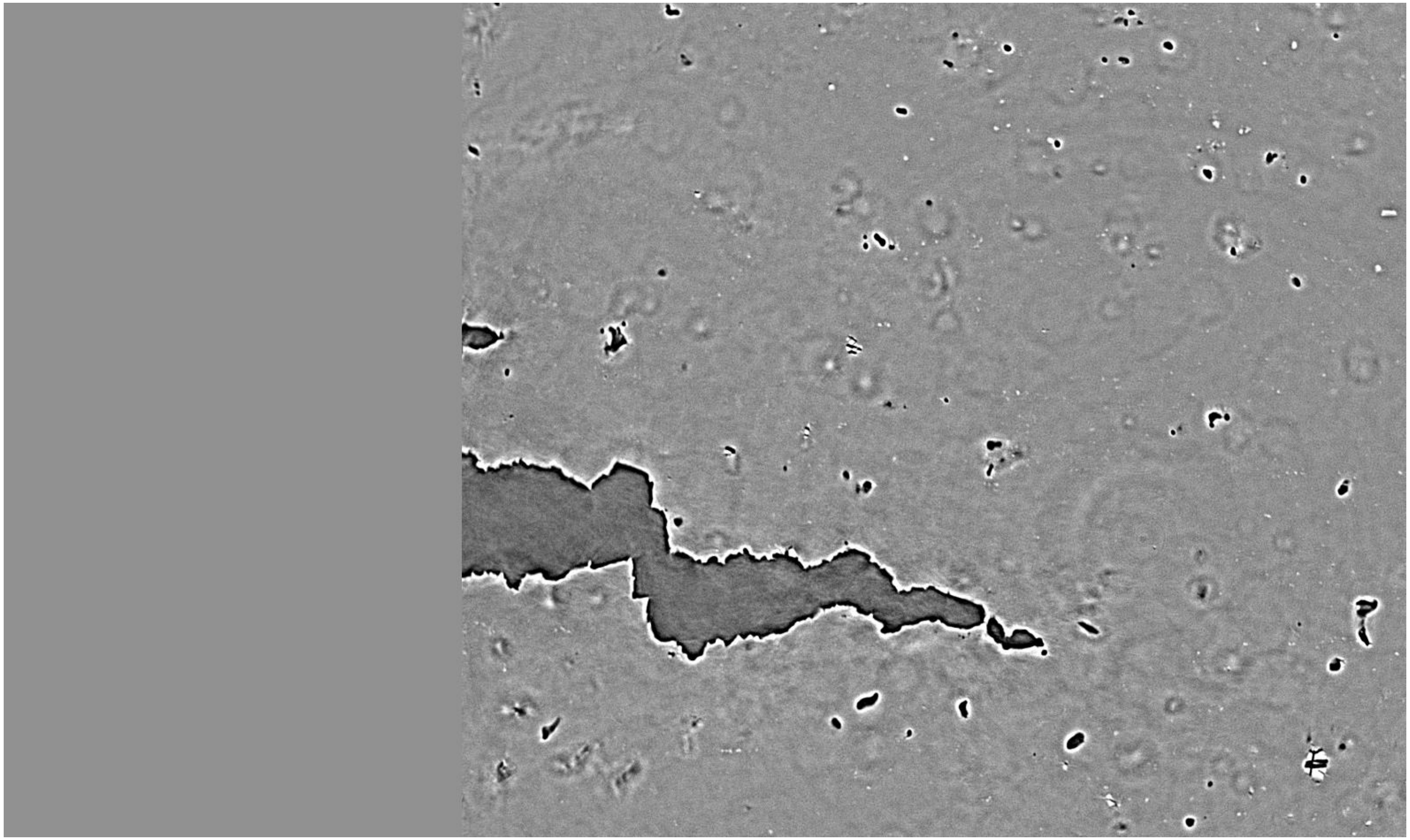

200µm

In-situ SRCLaminography

- 2139 T3: 2D section at mid-thickness

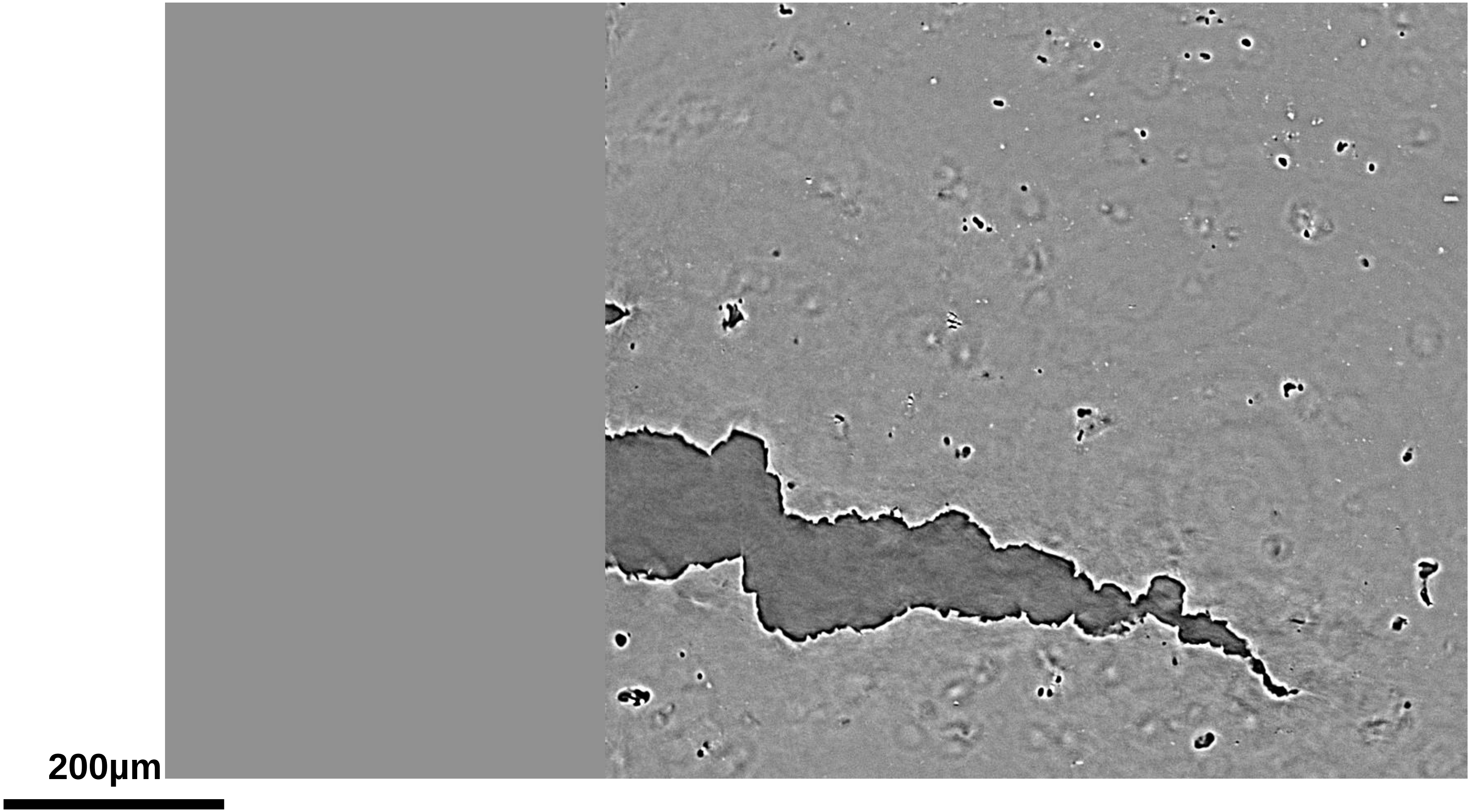

In-situ SRCLaminography

- 2139 T3: 2D section at mid-thickness

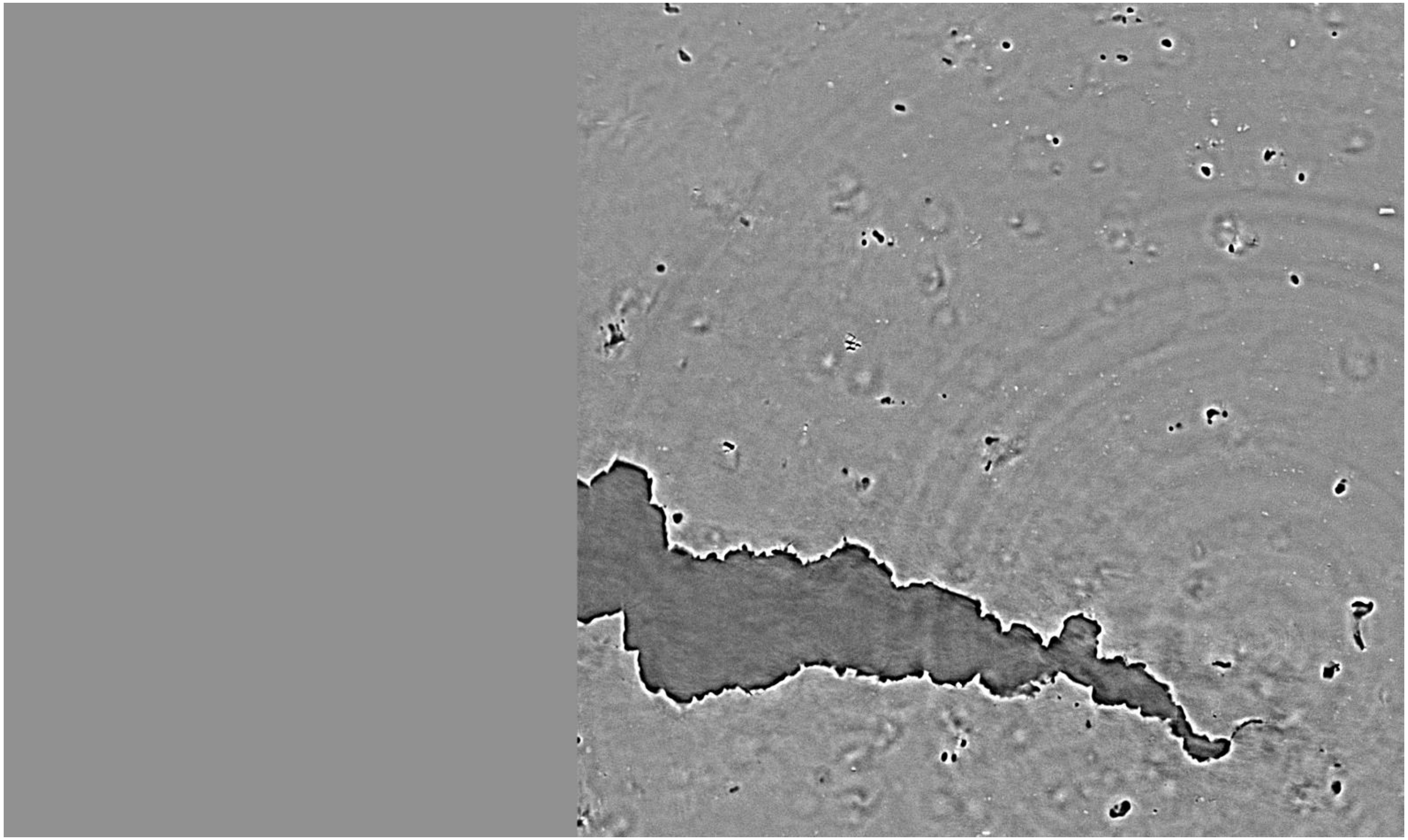

200µm

In-situ SRCLaminography

- 2D section at mid-thickness

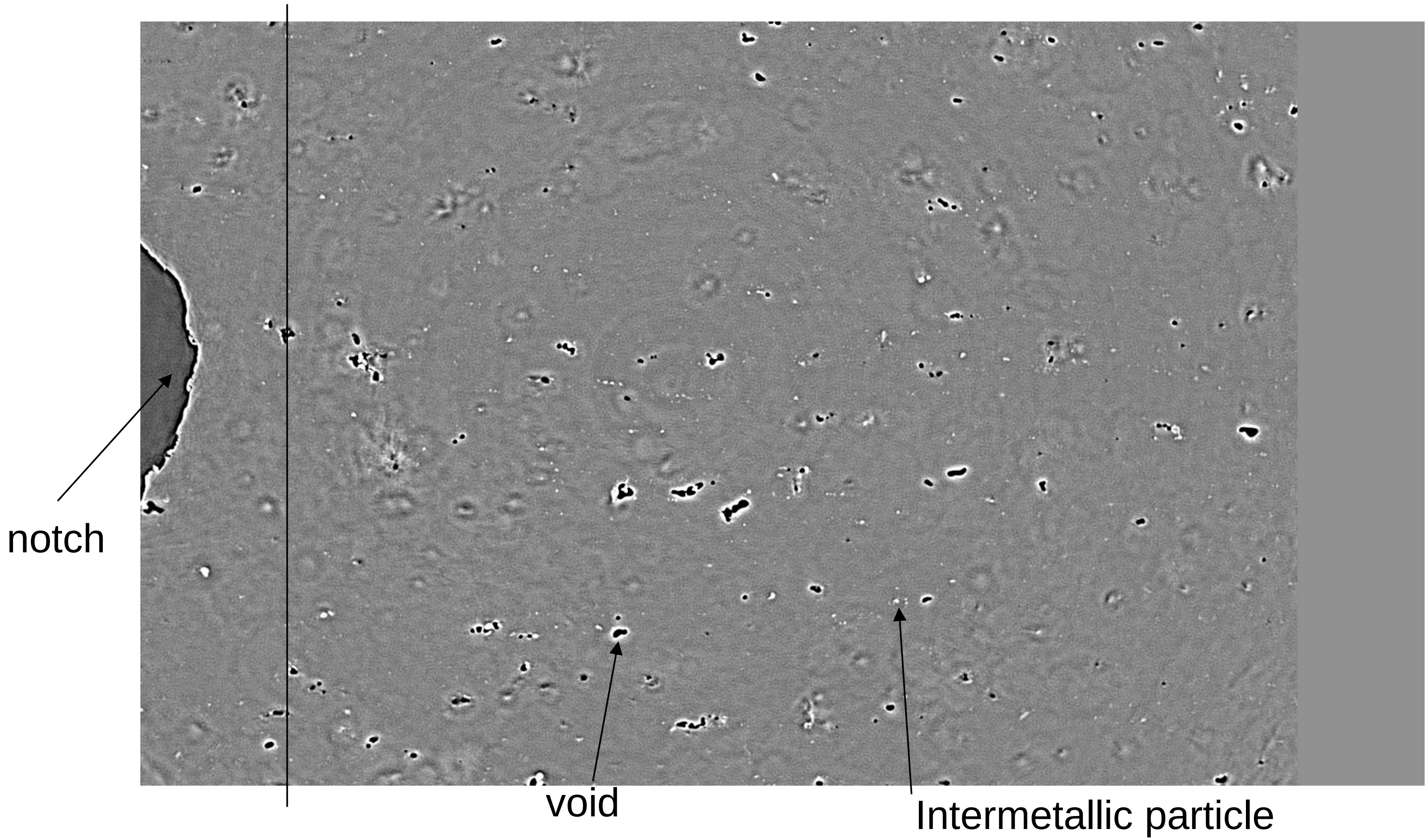

In-situ SRCLaminography

- 2D view in propagation direction ~50µm ahead of notch
  - Laminography aretacts become visible

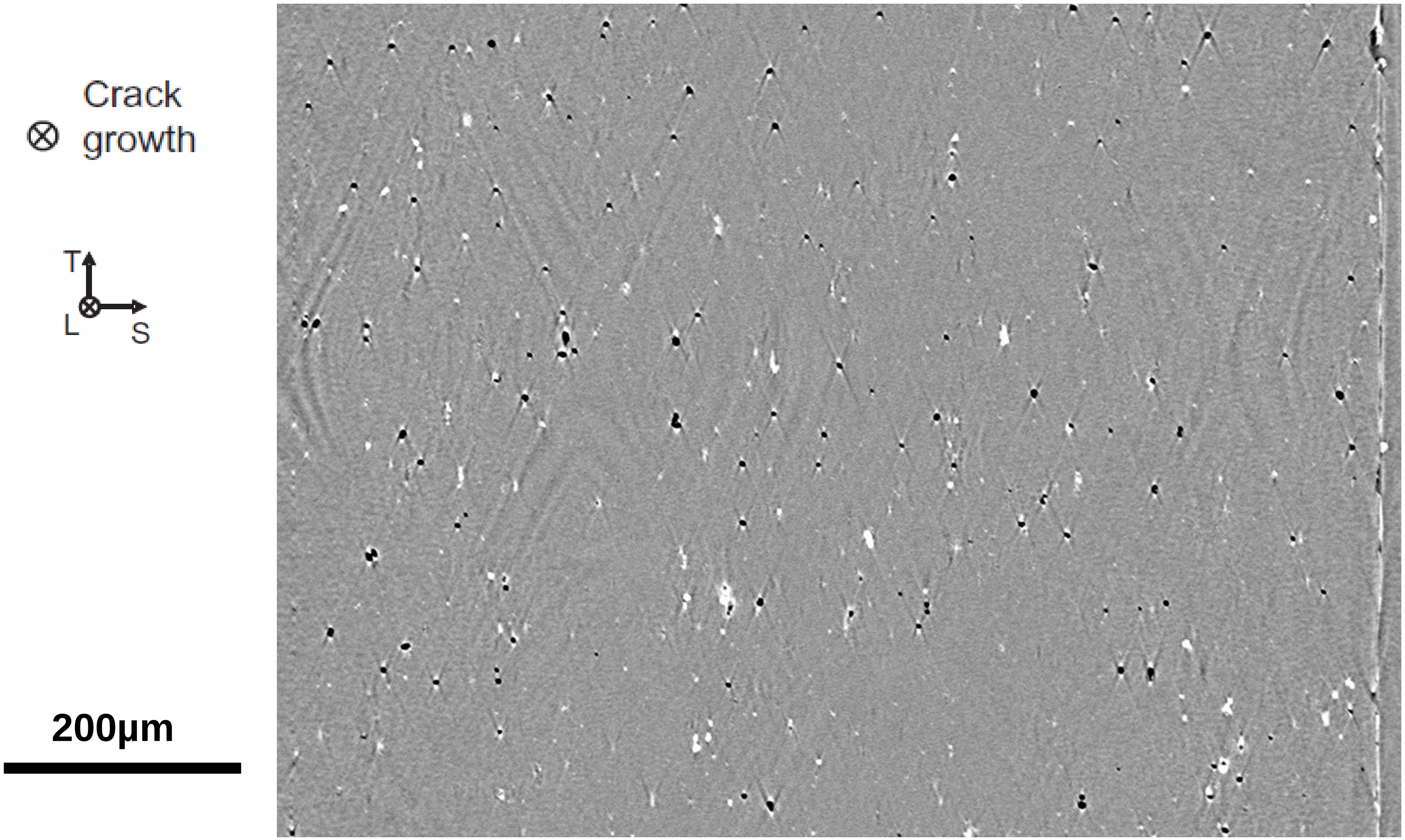

In-situ SRCLaminography

- 2D view in propagation direction ~50µm ahead of notch

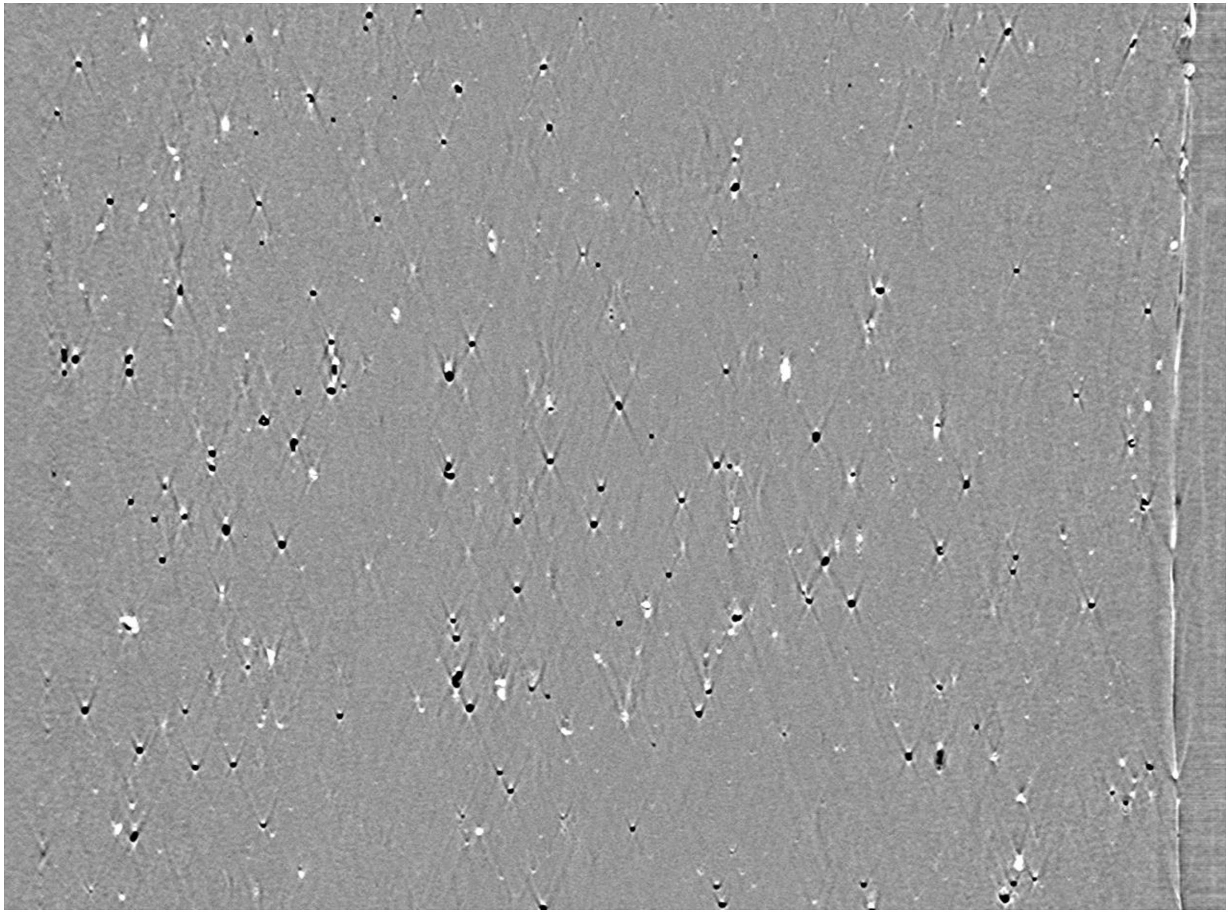

200µm

In-situ SRCLaminography

- 2D view in propagation direction ~50µm ahead of notch

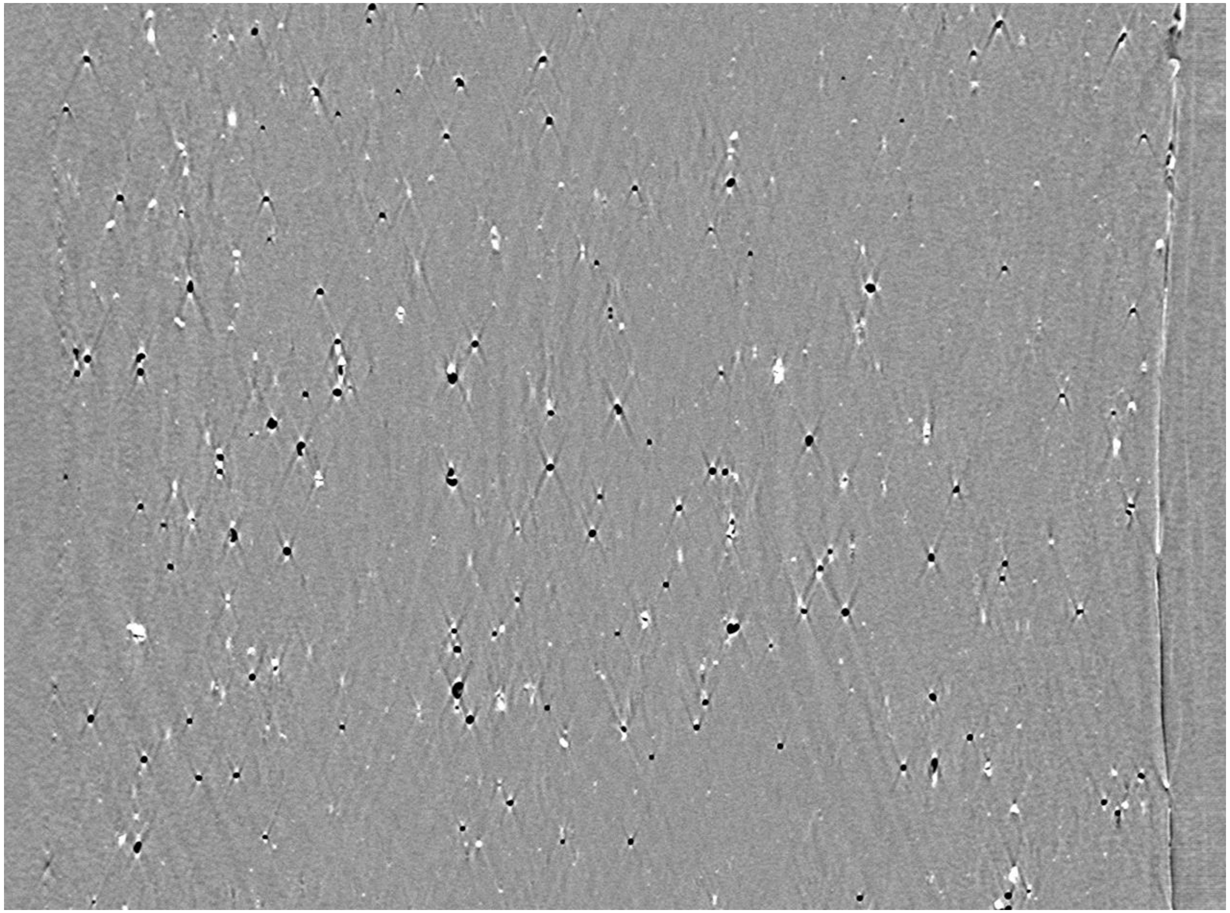

200µm

In-situ SRCLaminography

- 2D view in propagation direction ~50µm ahead of notch

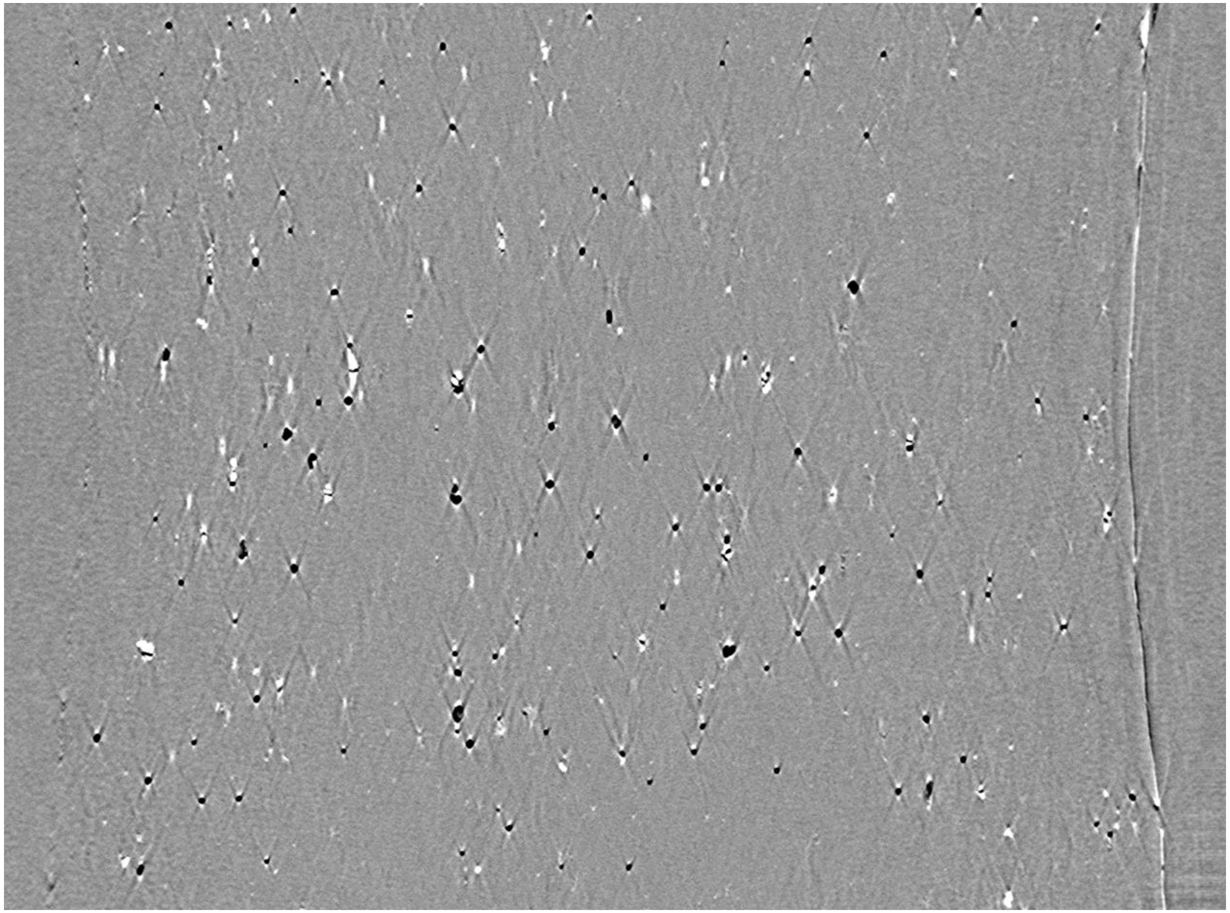

200µm

In-situ SRCLaminography

- 2D view in propagation direction ~50µm ahead of notch

200µm

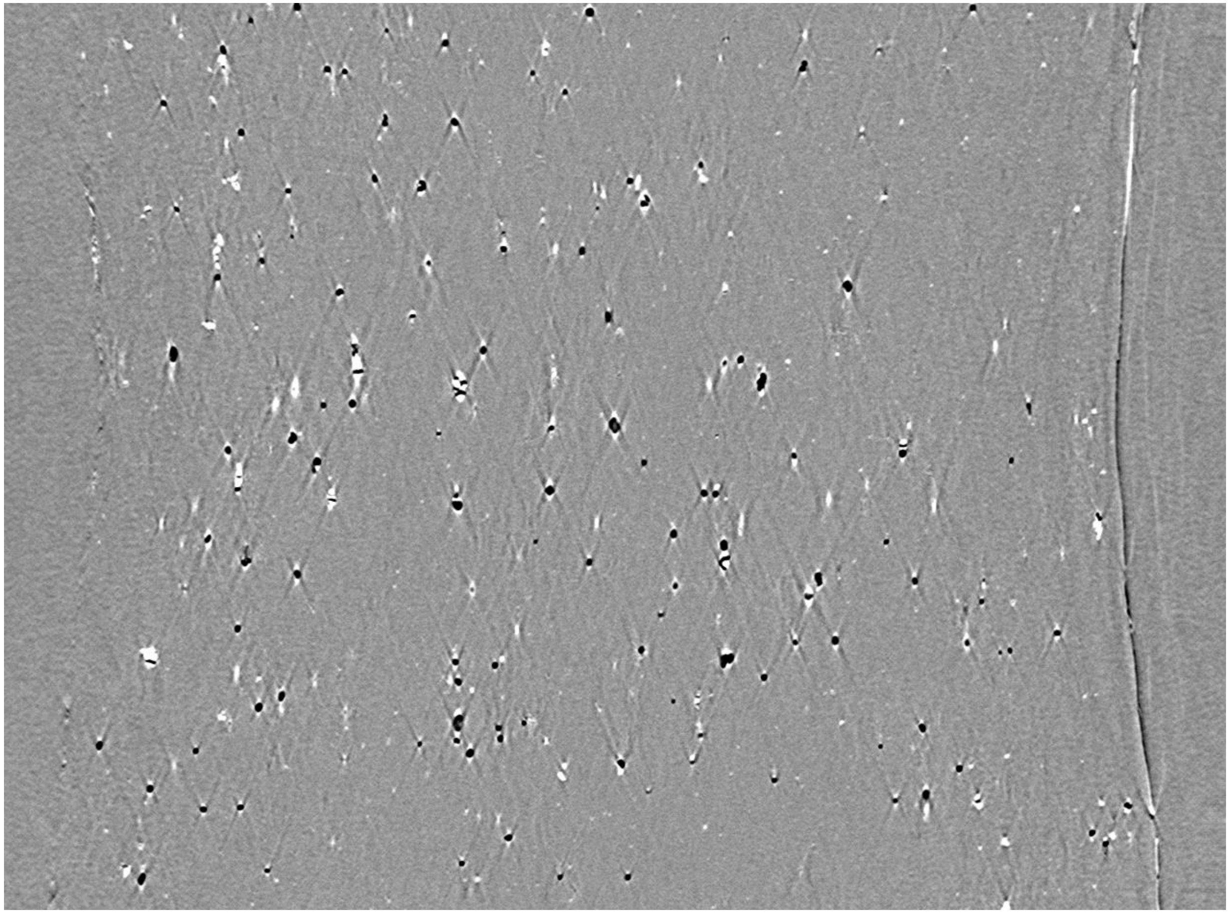

In-situ SRCLaminography

- 2D view in propagation direction ~50µm ahead of notch

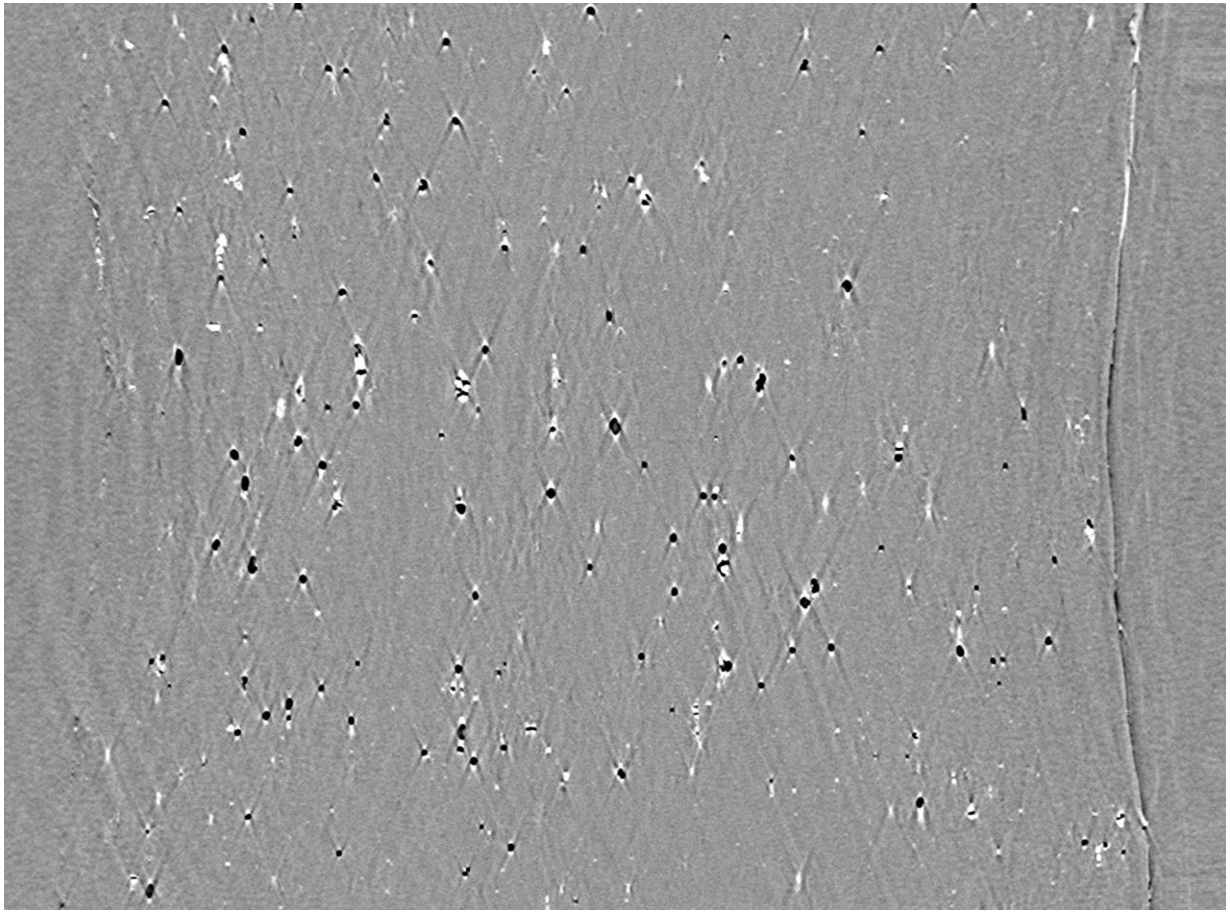

200µm

In-situ SRCLaminography

- 2D view in propagation direction ~50µm ahead of notch

200µm

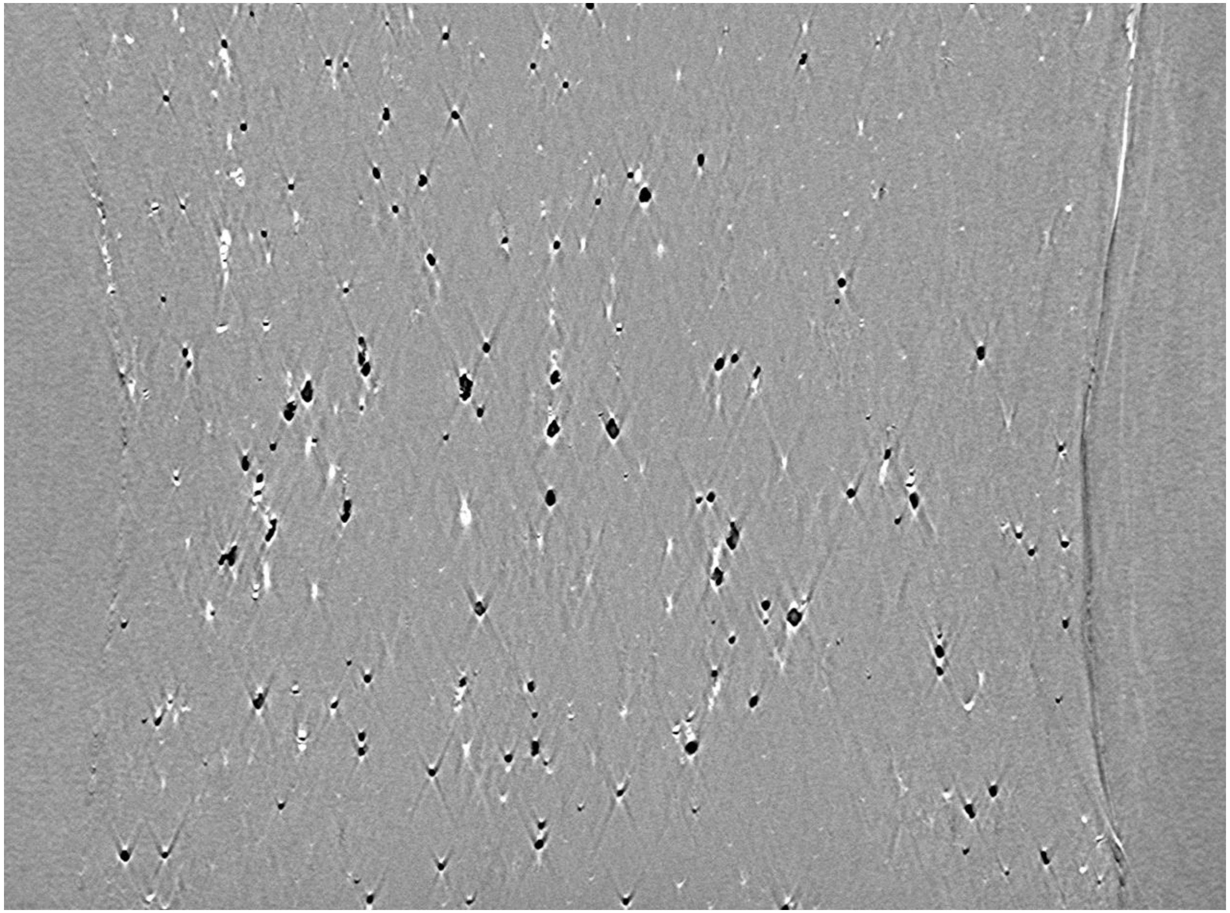

In-situ SRCLaminography

- 2D view in propagation direction ~50µm ahead of notch

200µm

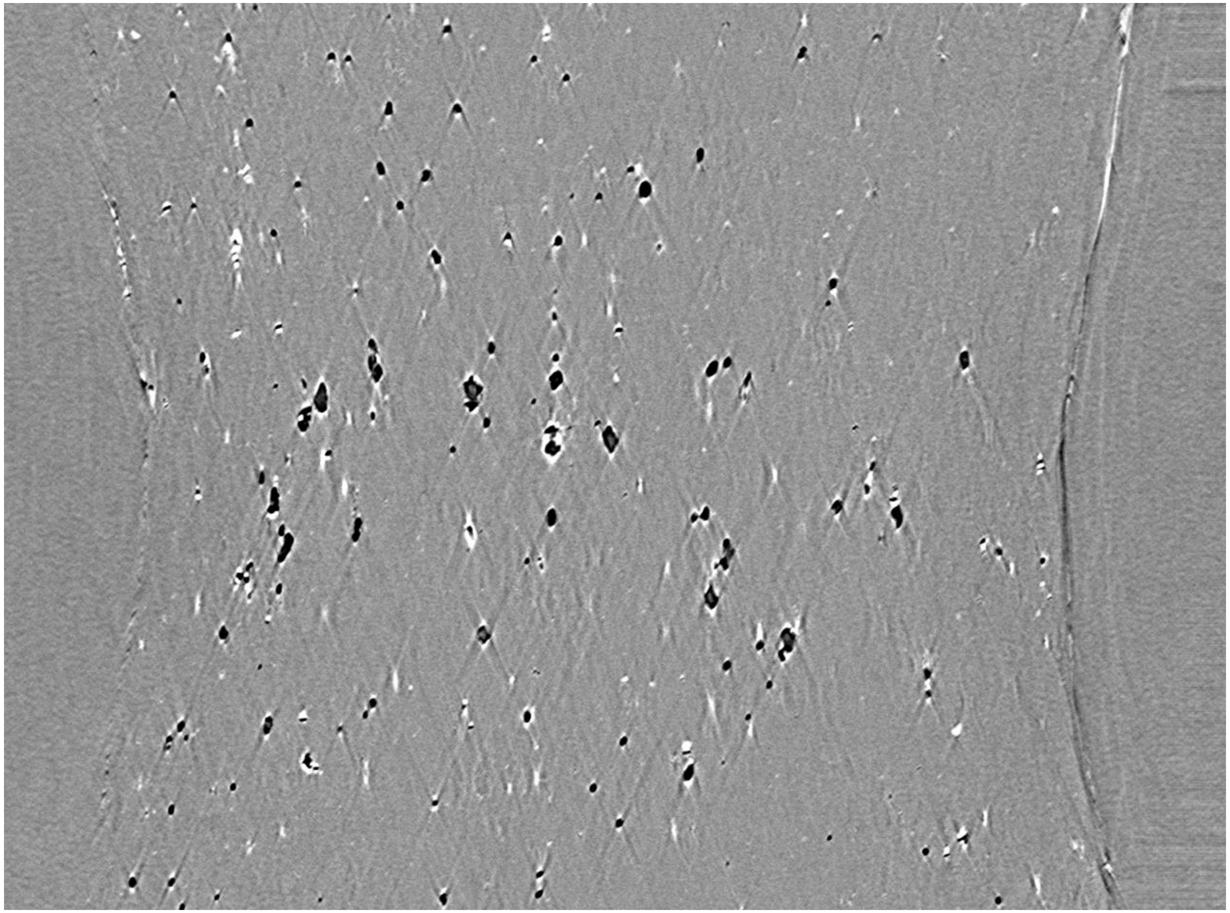

In-situ SRCLaminography

- 2D view in propagation direction ~50µm ahead of notch

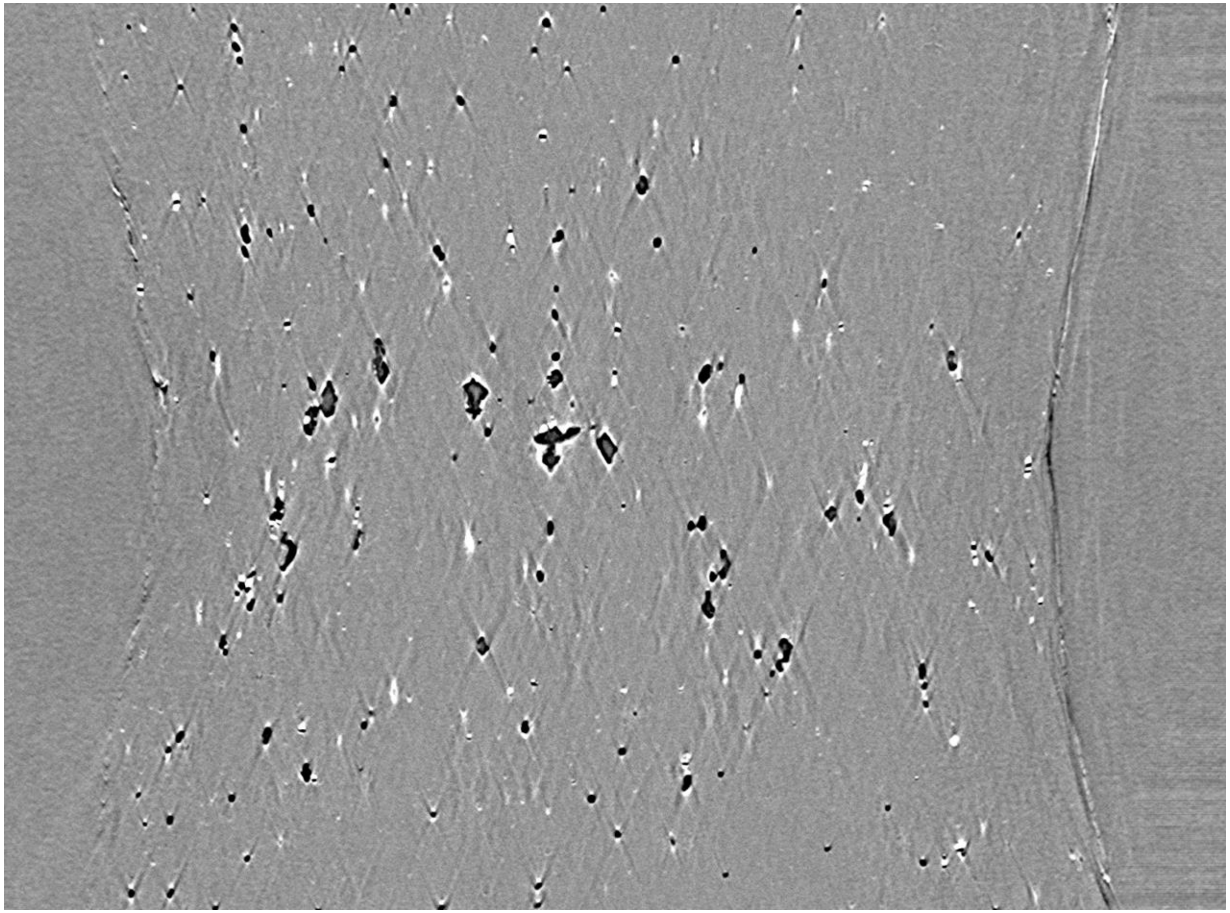

200µm

In-situ SRCLaminography

- 2D view in propagation direction ~50µm ahead of notch

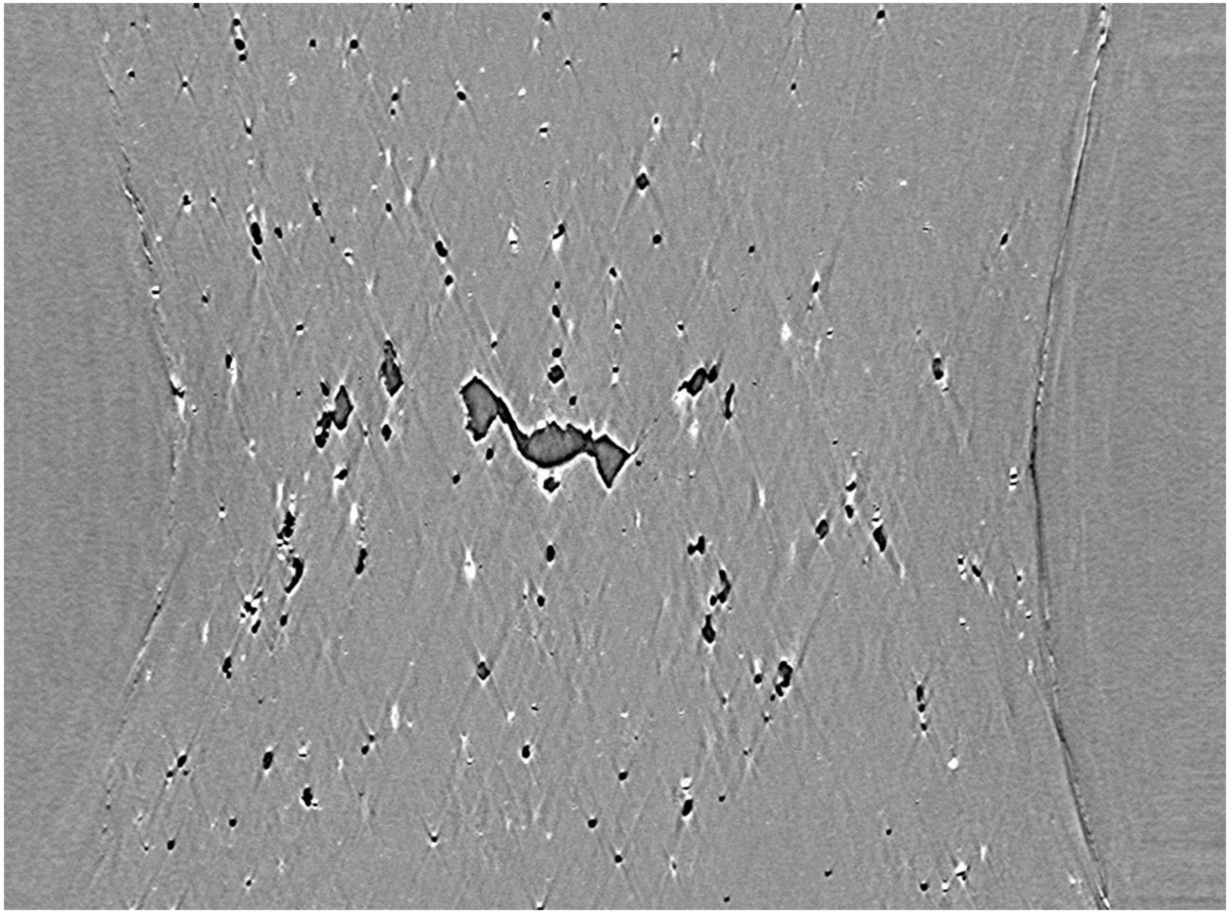

200µm

In-situ SRCLaminography

- 2D view in propagation direction ~50µm ahead of notch

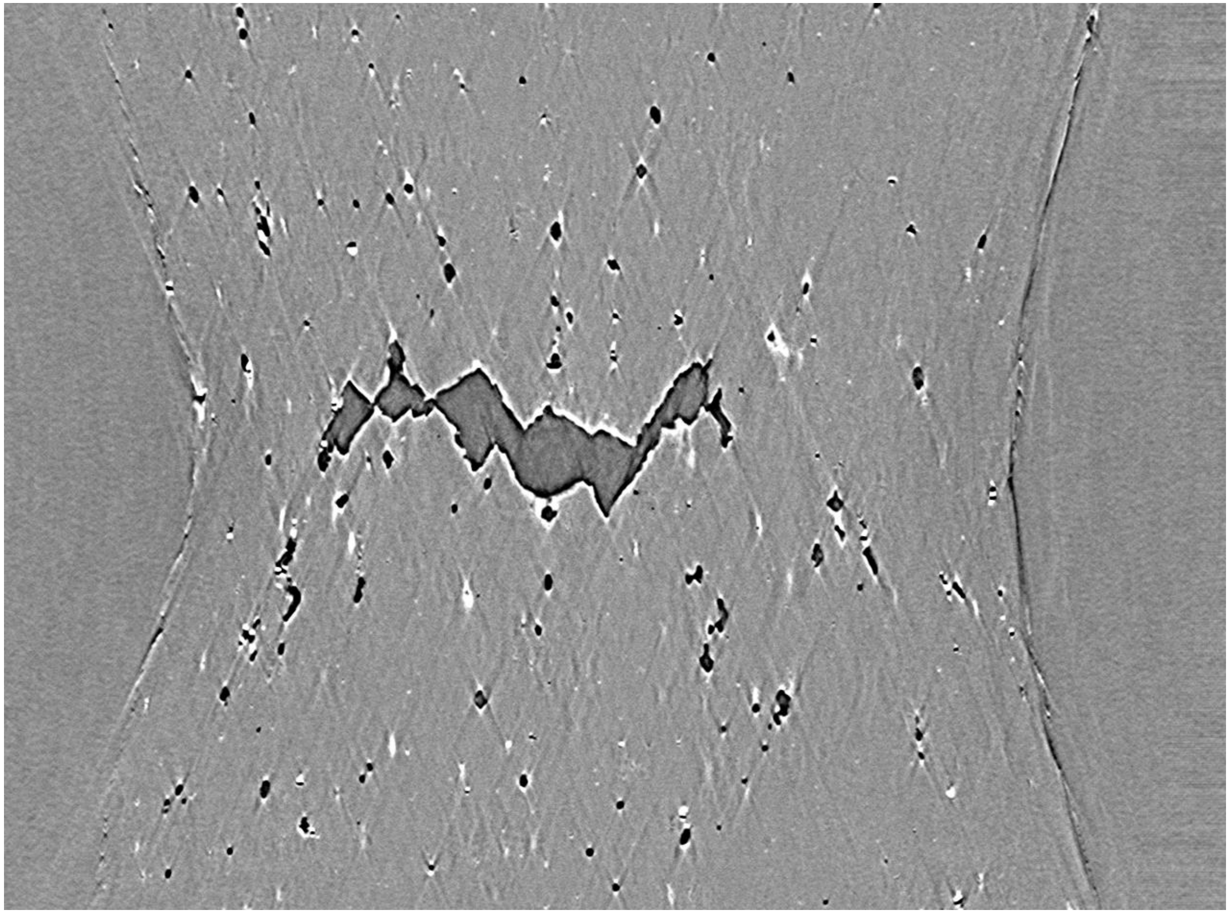

200µm

In-situ SRCLaminography

- 2D view in propagation direction ~50µm ahead of notch

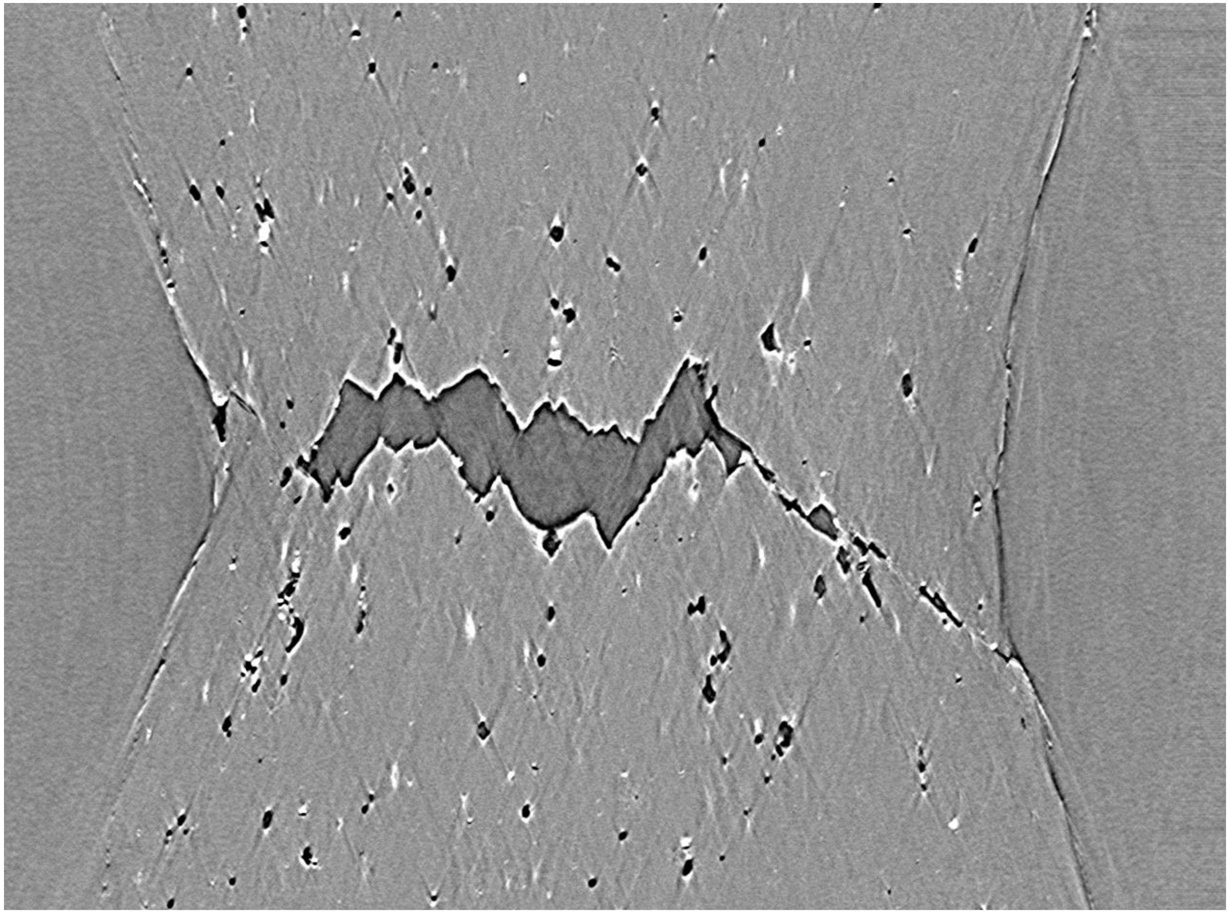

200µm

In-situ SRCLaminography

- 2D view in propagation direction ~50µm ahead of notch

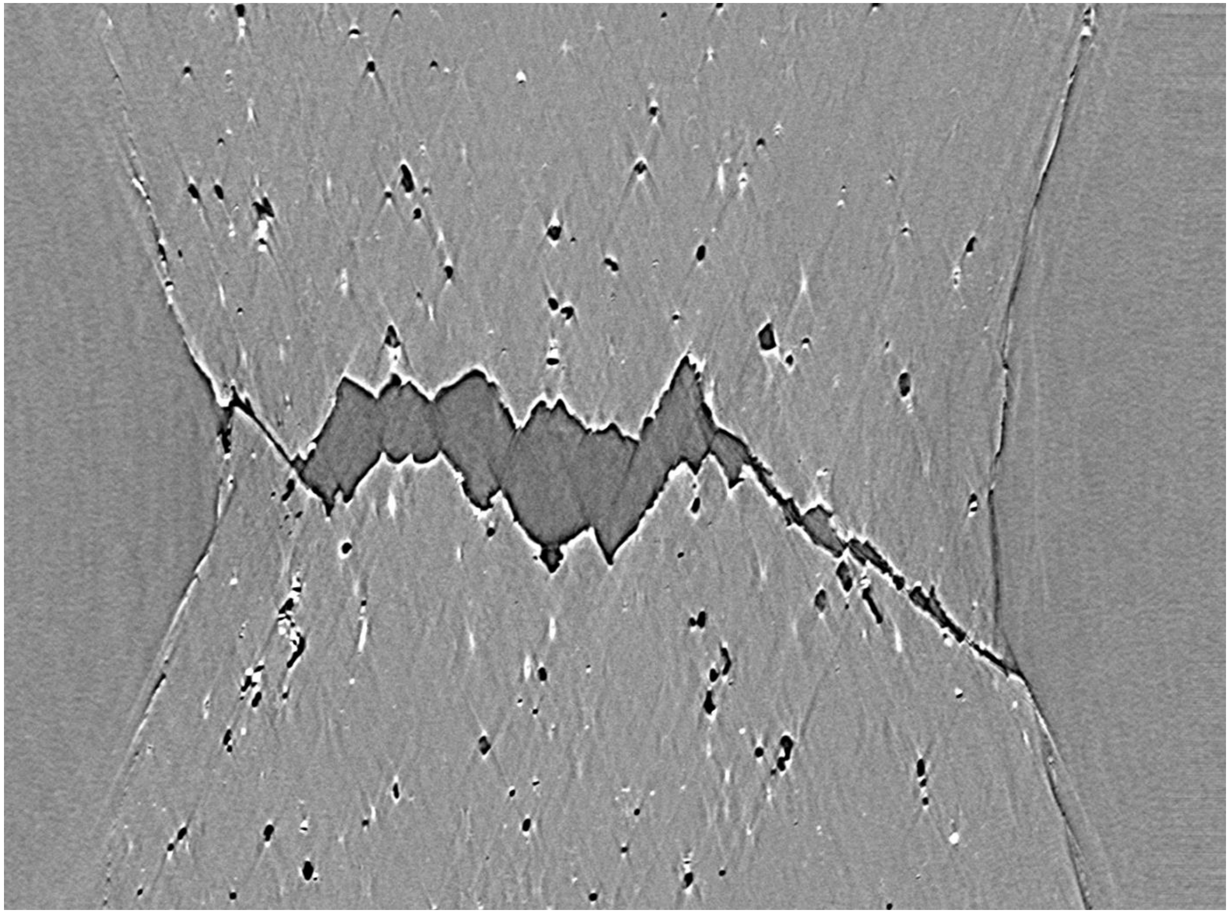

200µm

Zoom: Choice of voids

- 4 voids that will contribute to the final crack
- Investigate: shape change
  orientation change
  how they contribution to final crack

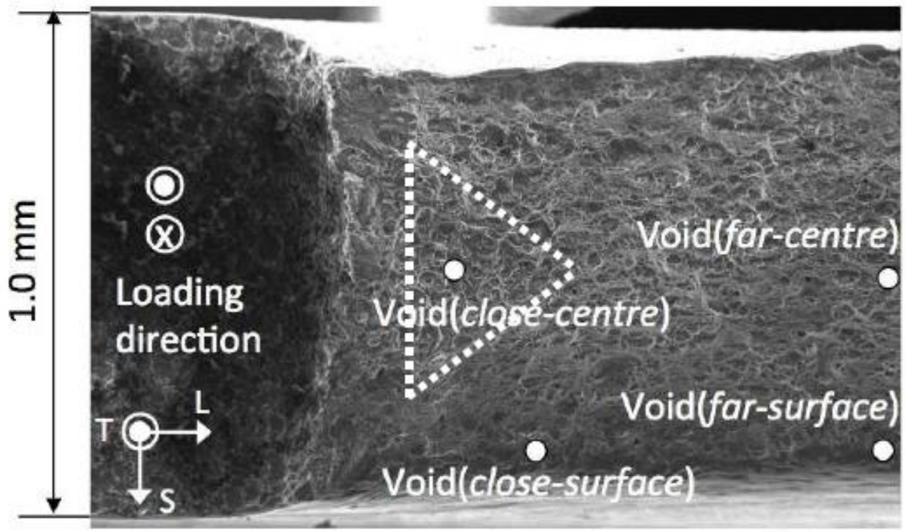

(a) L-S configuration

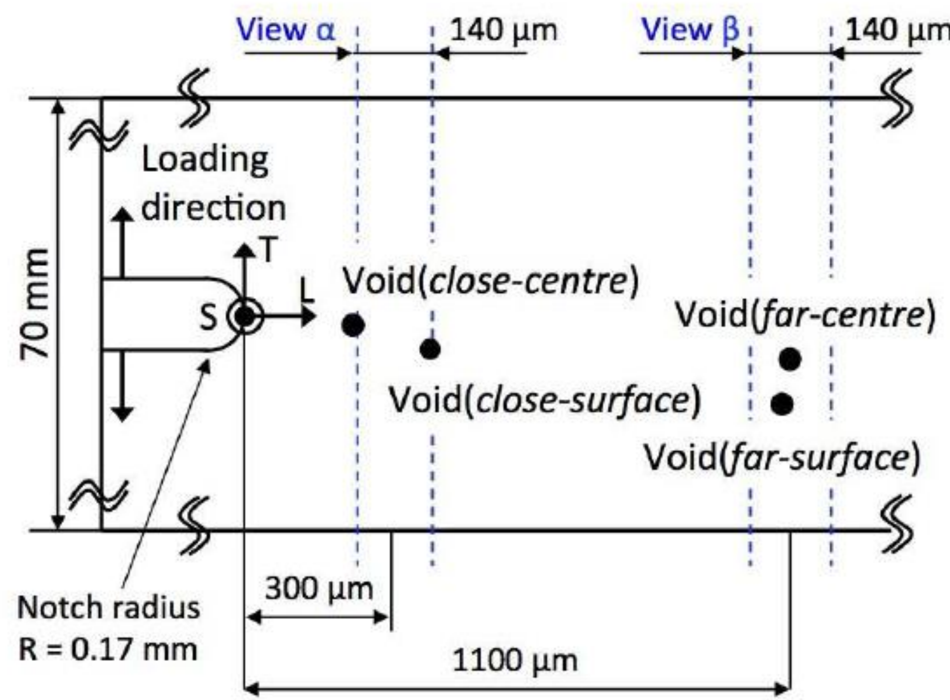

(b) L-T configuration

*[T. Ueda *et al.*, 2014, *Acta Mat*]

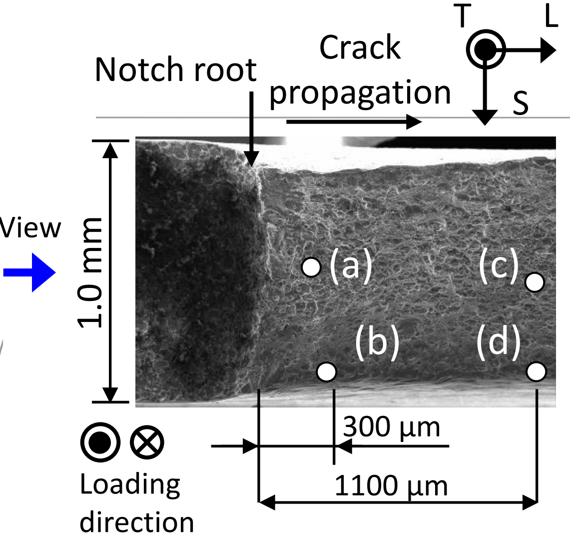

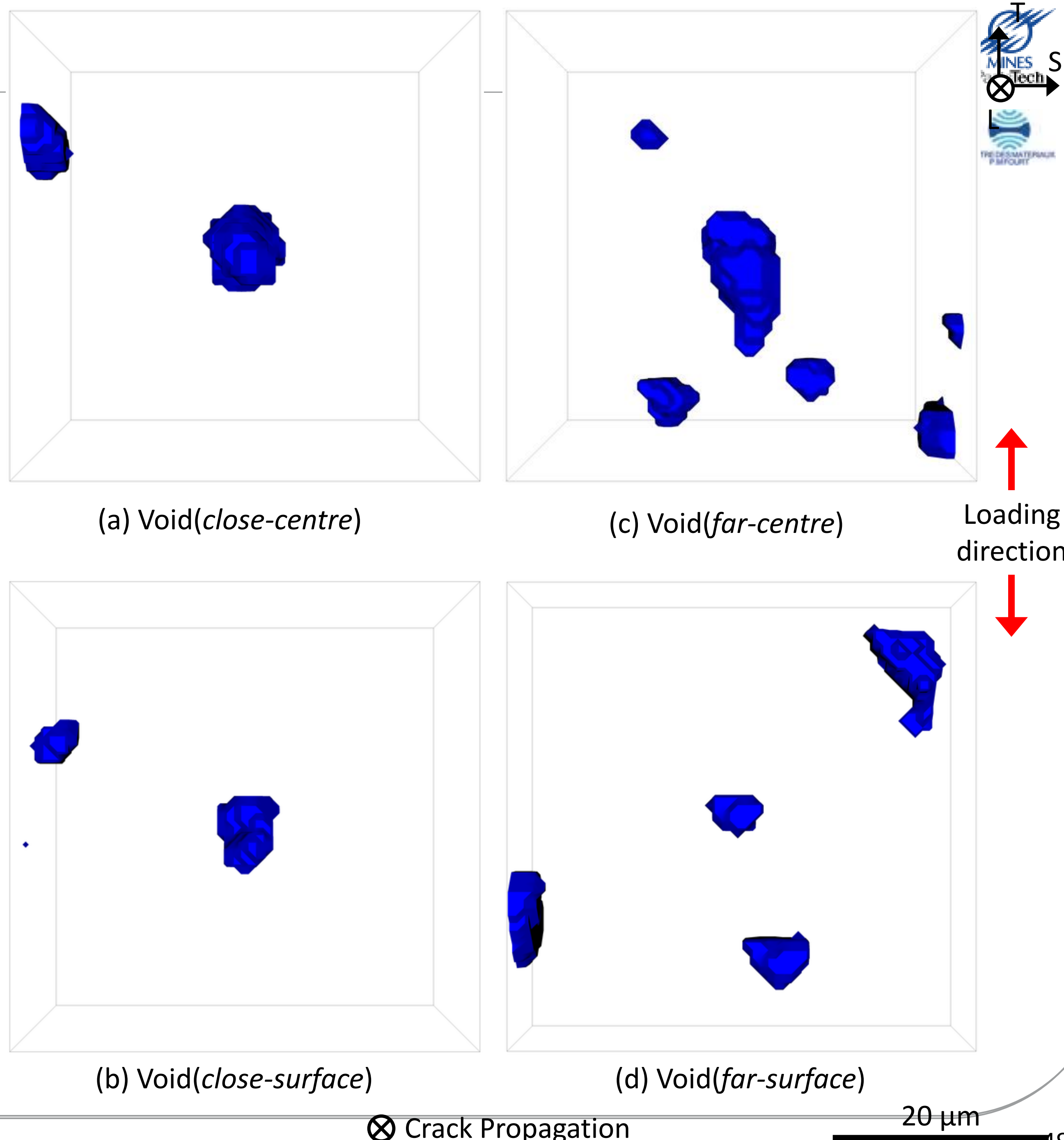

*[T. Ueda *et al.*, 2014, *Acta Mat*]

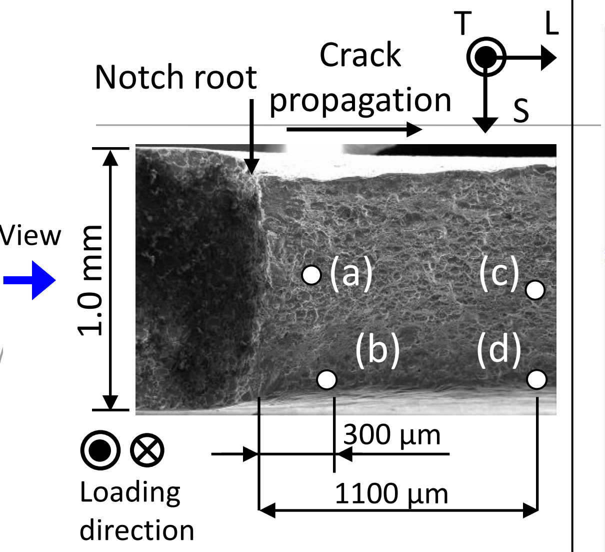

4 Voids (at different load steps) before coalescence

- Void in the flat region grows symmetrically
- Voids on slant region rotate and grow towards slant failure

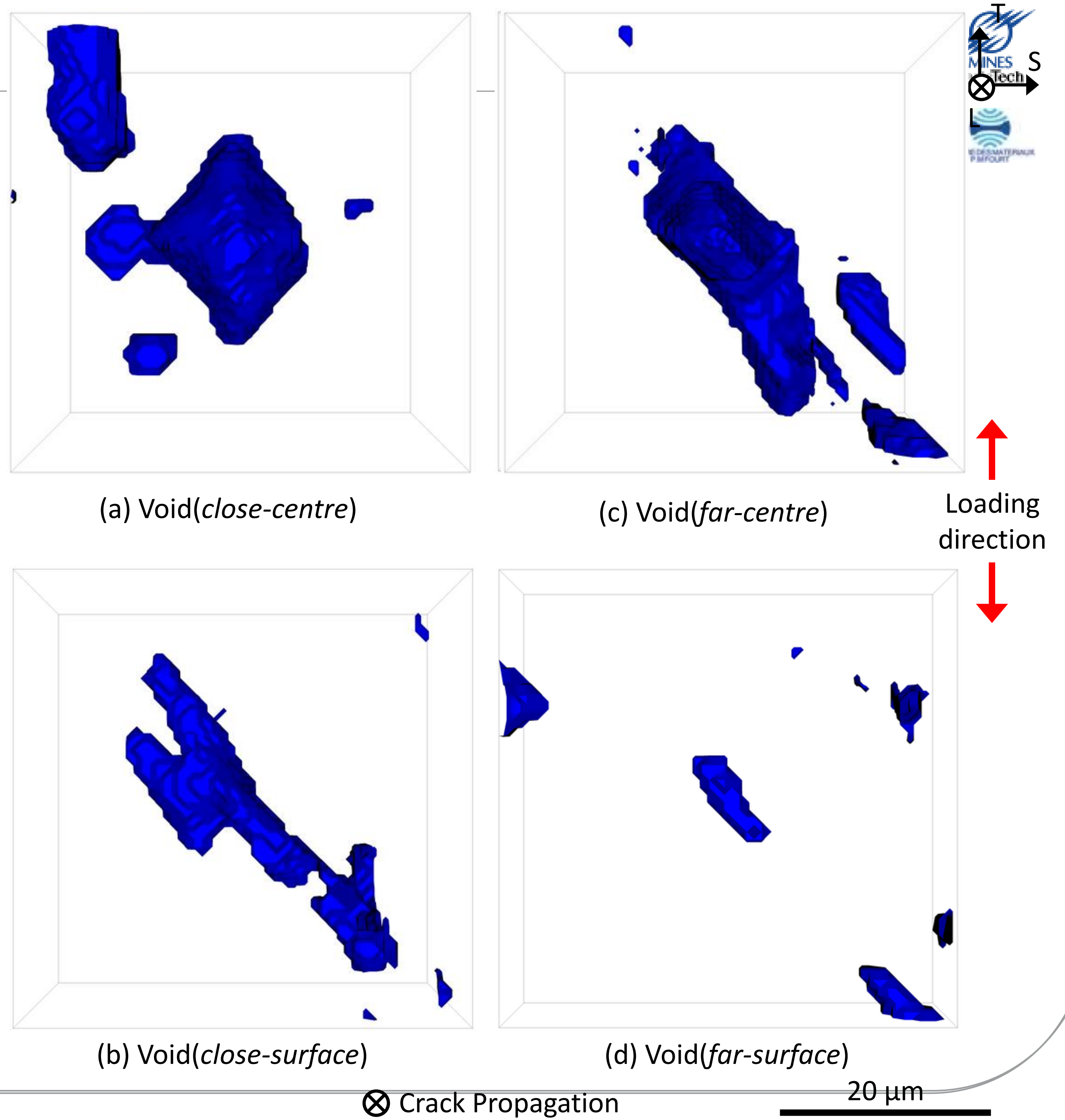

(a) Void(*close-centre*)

(c) Void(*far-centre*)

(b) Void(*close-surface*)

(d) Void(*far-surface*)

*[T. Ueda *et al.*, 2014, *Acta Mat*]

Void contribution to final fracture

2D sections of laminography data

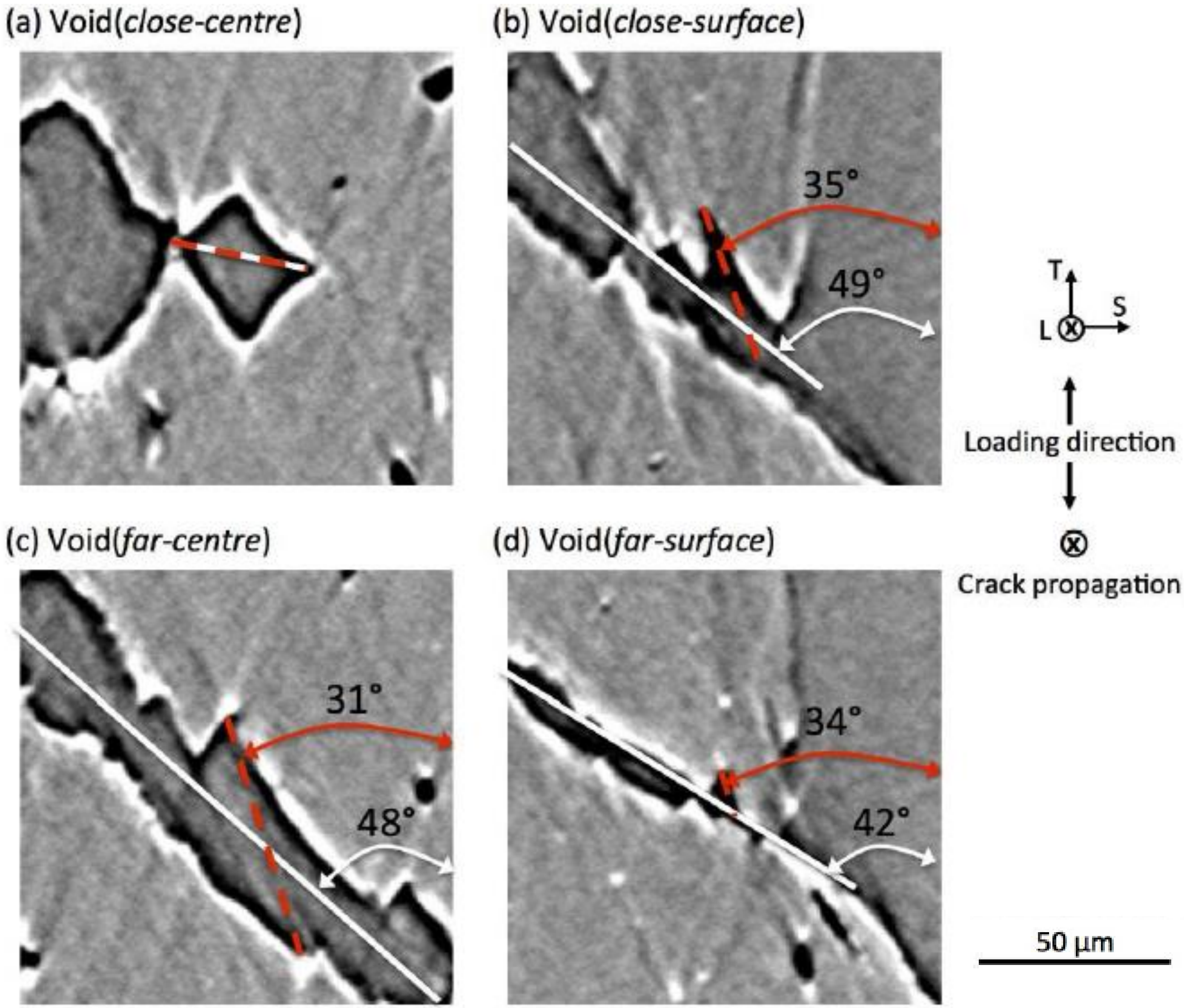

What does the strain field look like?

- Voids in the slant regions at the specimen surface do not fully contribute to the crack surface

*[T. Ueda *et al.*, 2014, *Acta Mat*]

Strain measurement

Digital (Image) Volume Correlation

- Gray level (2D or) 3D images
- Image 1: $f(\underline{x})$ image 2: $g(\underline{x})$
- Conservation of grey levels

$$f(\underline{x}) \cong g(\underline{x} + \underline{u}(\underline{x}))$$

- Measure $\underline{u}(\underline{x})$?

- Relies on 'natural' image contrast
- What if damage sets in?

Global DVC (Correli C8)

F.Hild, S.Roux [Roux et al. Comp. Part A 2008]

LMT Cachan

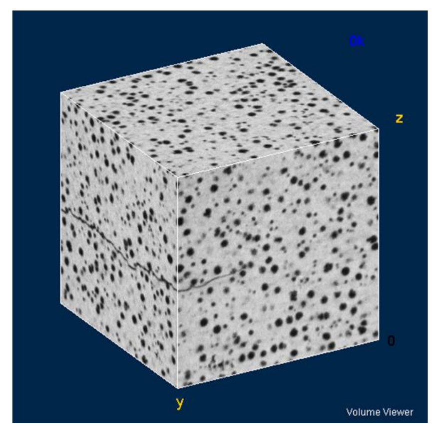

NCI

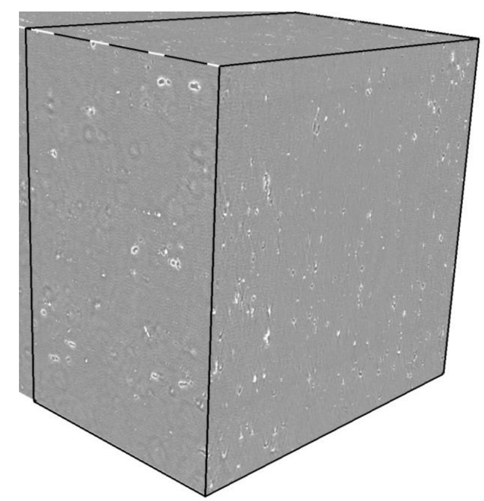

AA

PROJET FINANCÉ PAR L'ANR - PROJECT FUNDED BY THE ANR

'COMINSIDE' project:

1. Laminography imaging +
2. strain measurement +
3. microstructructural simulation (CEMEF)

Digital Volume Correlation on *in-situ* SRCLaminography data

- Performance assessment: correlation of 2 scans of undeformed material of the same ROI: rigid body motion
- scan centre shifted

The same ROI

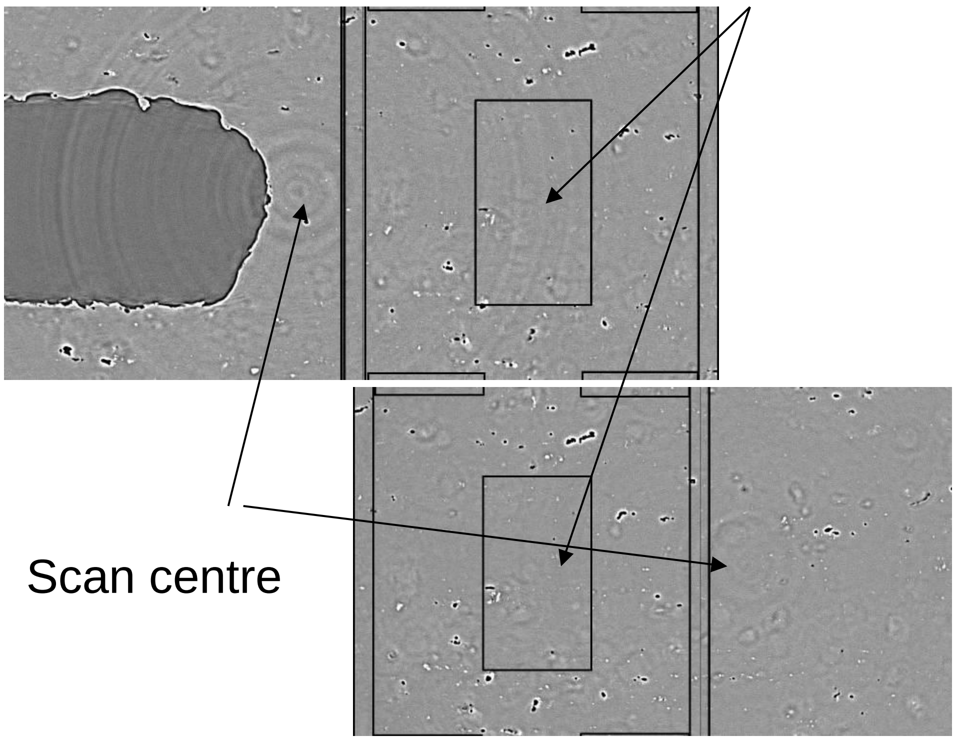

Scan centre

Measurement uncertainty below 1 %
For AA2139 elements 32 voxels

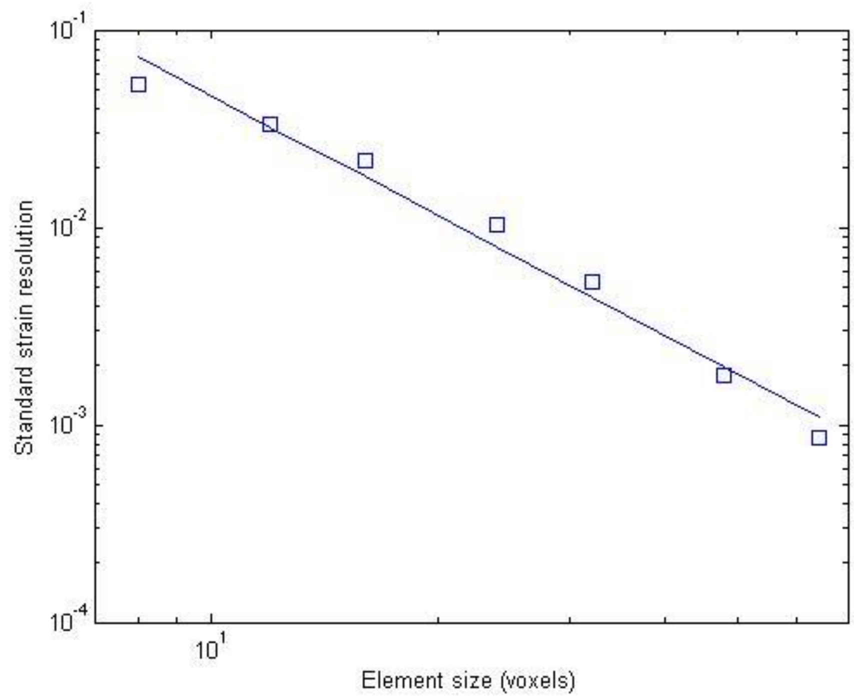

[Morgeneyer *et al.*, 2013, *Exp. Mech*]

Microstructure: aluminium alloy AA 2198-T8

Grain structure (by gallium wetting):

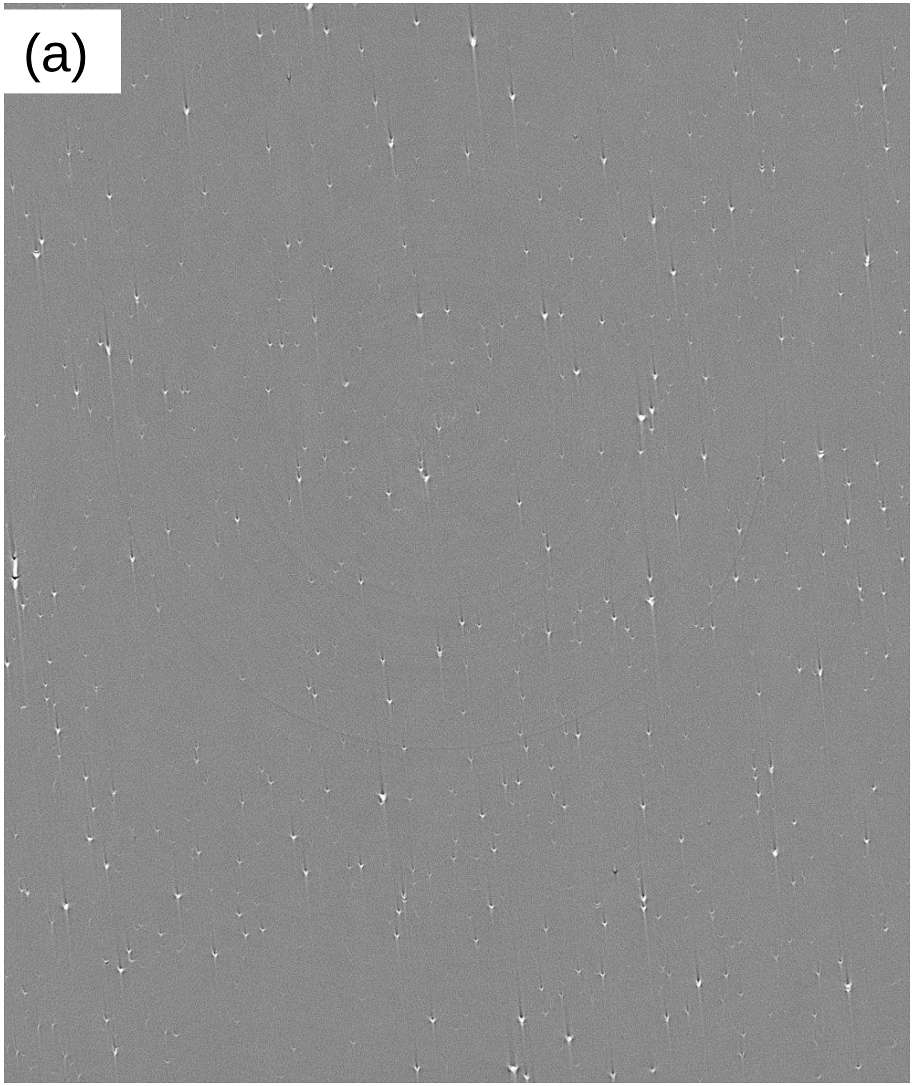

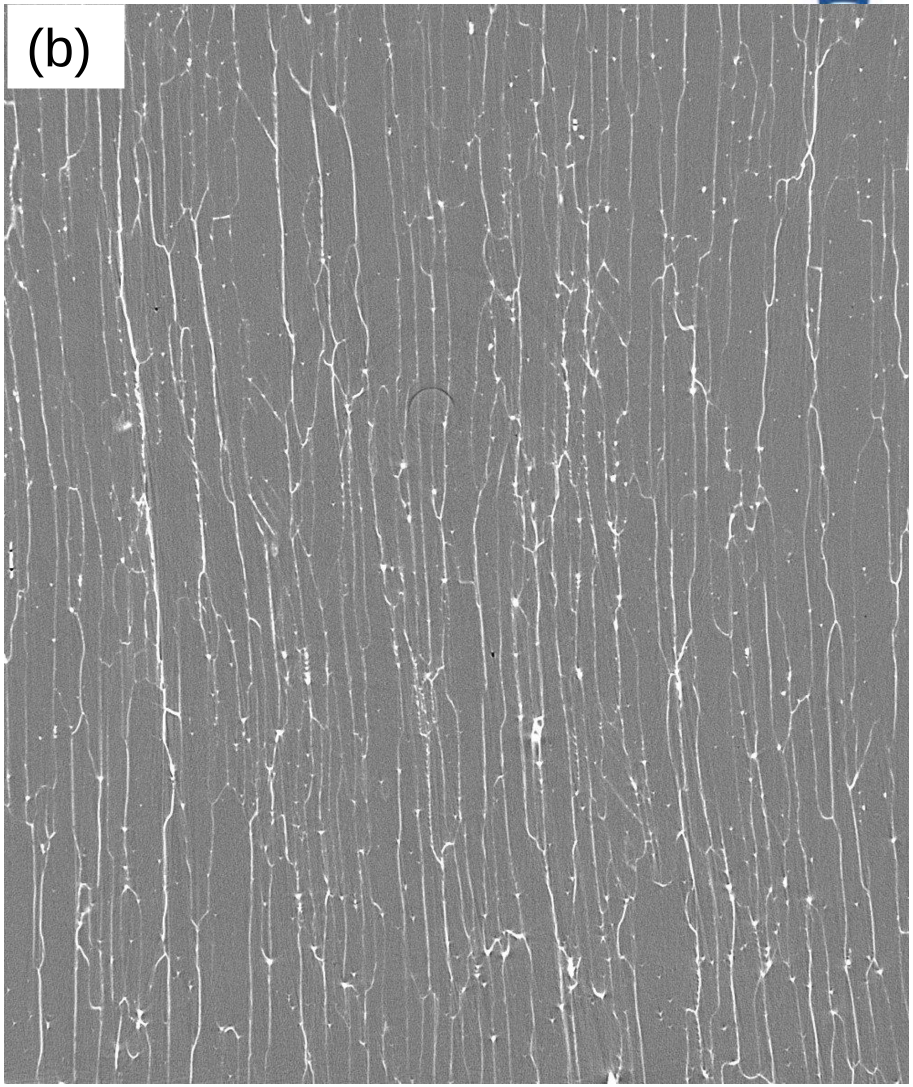

Particle volume fraction: 0.34%
Void volume fraction: < 0.03%

AA 2198 T8

- Al-Cu-Li alloy

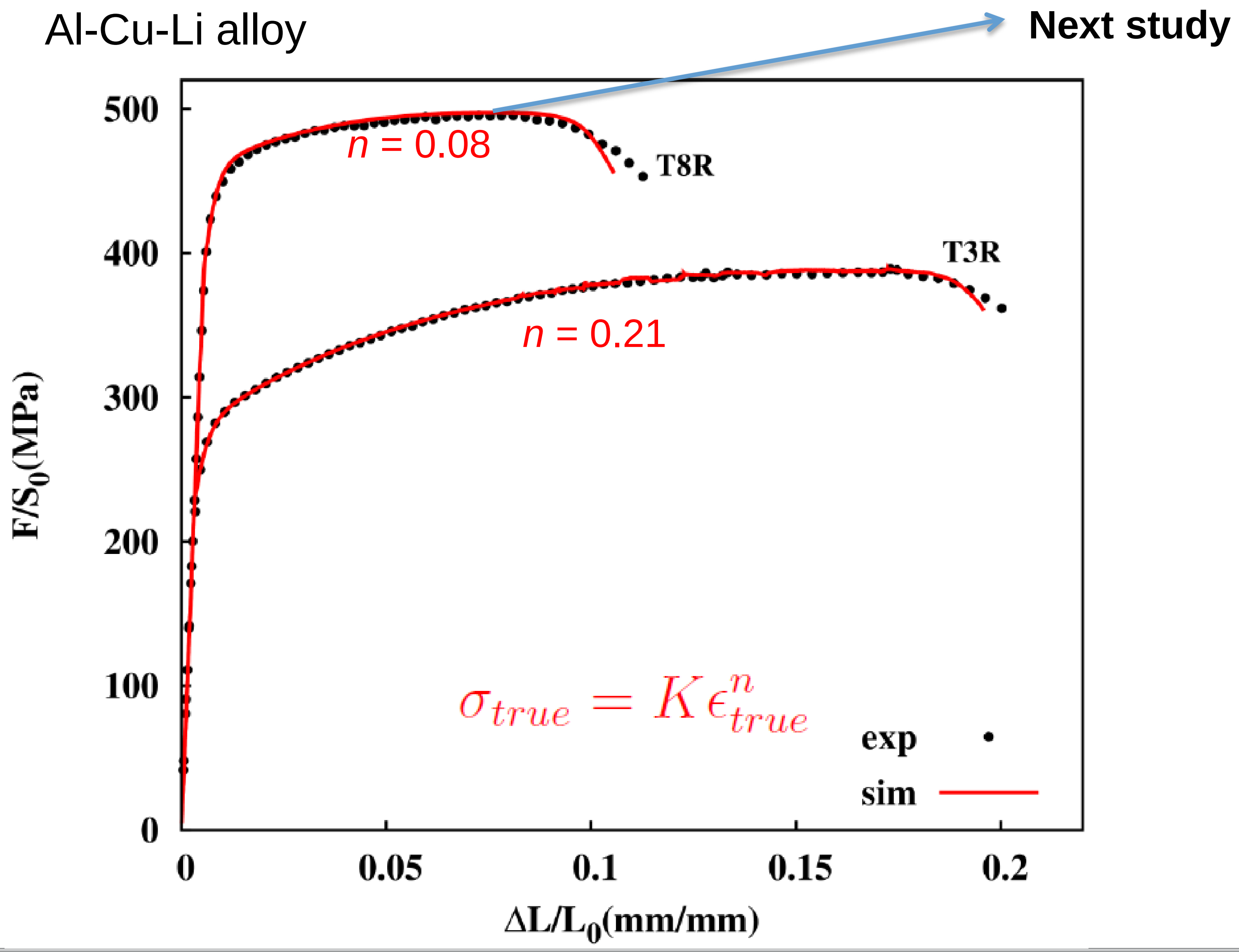

Mechanical experiment + laminography

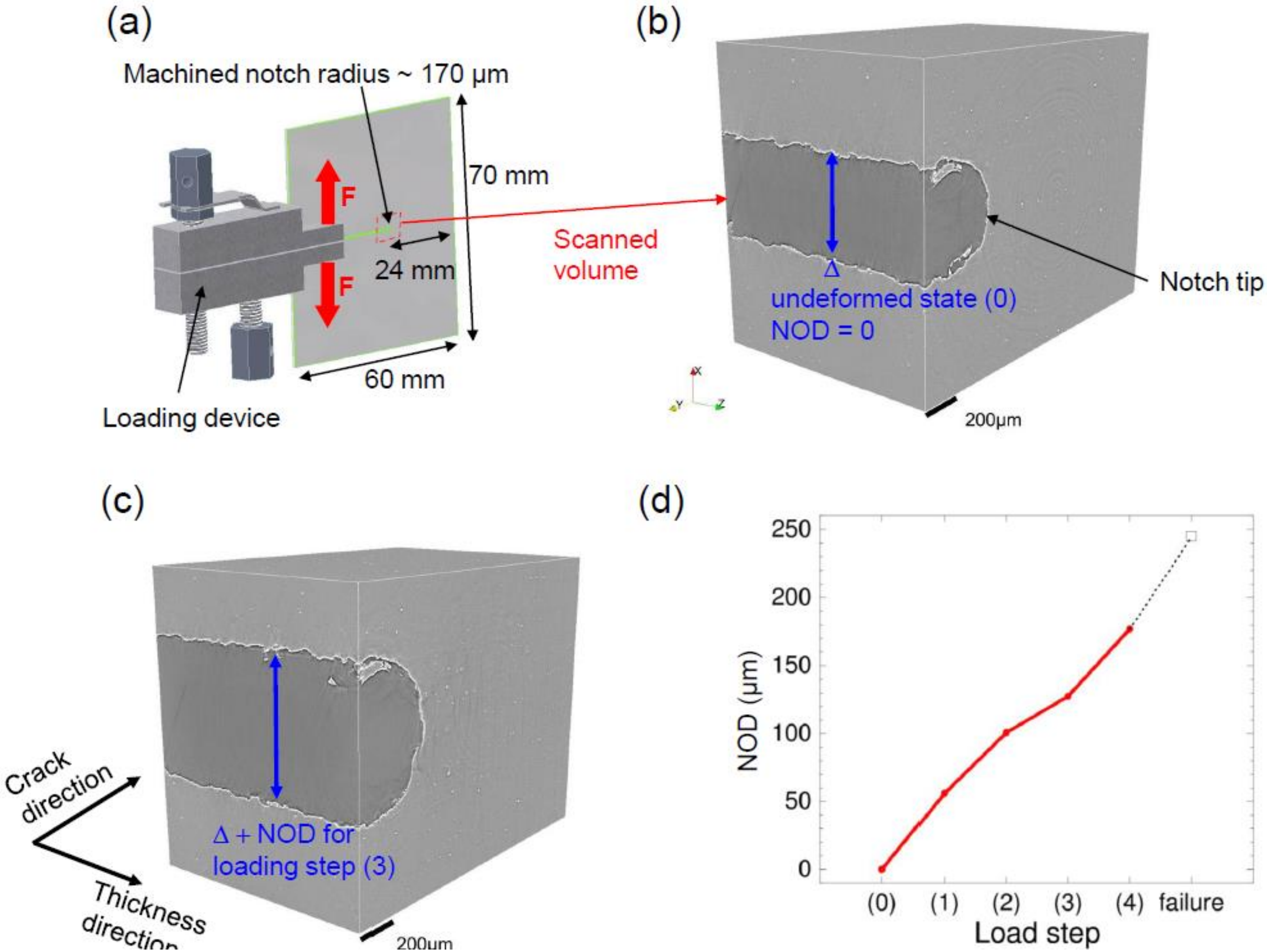

Digital volume correlation

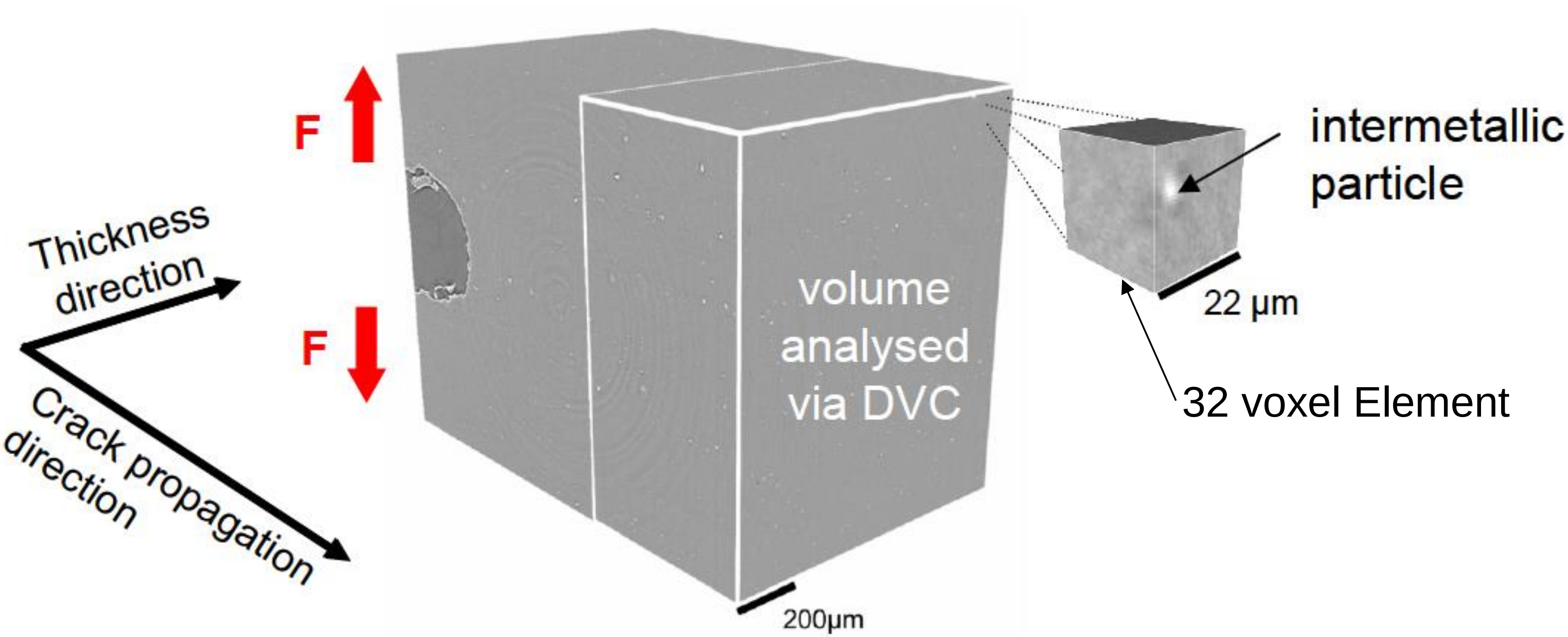

Size of the ROI: 1184 x 512 x 992 voxels (830 µm x 360 µm x 700 µm)

32-voxel elements:
Less than 0.1% of strain uncertainty

Spatial resolution:
Twice the element size:
2 x 32 voxel = 45 µm

Voxel length: 0.7 µm

Comparison: damage and strain evolution

*[Morgeneyer *et al.*, 2014, *Acta Mat.* 69 pp. 78-91]
Master Thesis: T. Taillandier-Thomas

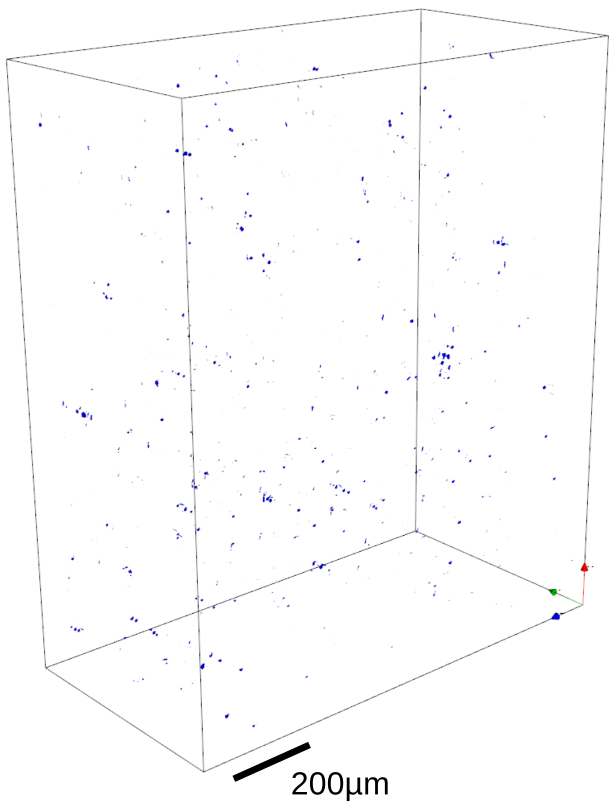

Rendered voids in:
Loadstep (0)

Comparison: damage and strain evolution

*[Morgeneyer *et al.*, 2014, *Acta Mat.* 69 pp. 78-91]
Master Thesis: T. Taillandier-Thomas

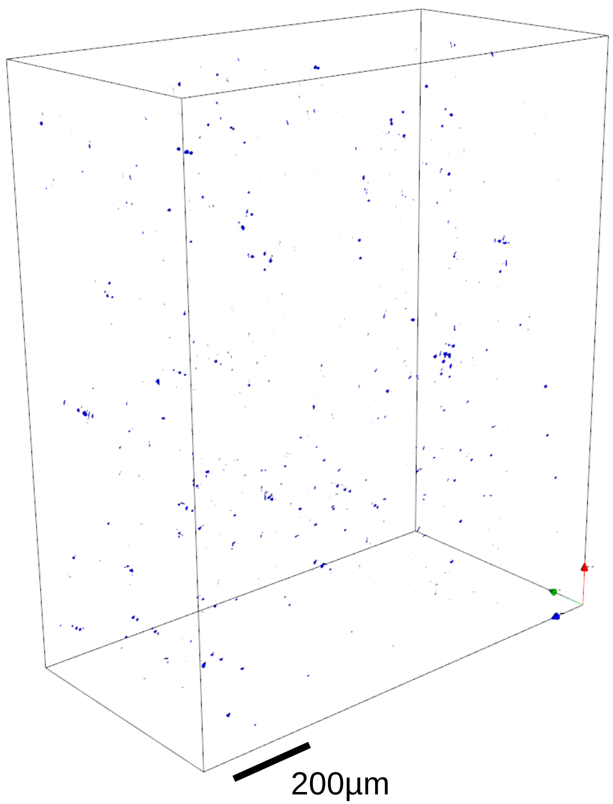

Rendered voids in:
Loadstep (1)

Comparison: damage and strain evolution

*[Morgeneyer *et al.*, 2014, *Acta Mat.* 69 pp. 78-91]
Master Thesis: T. Taillandier-Thomas

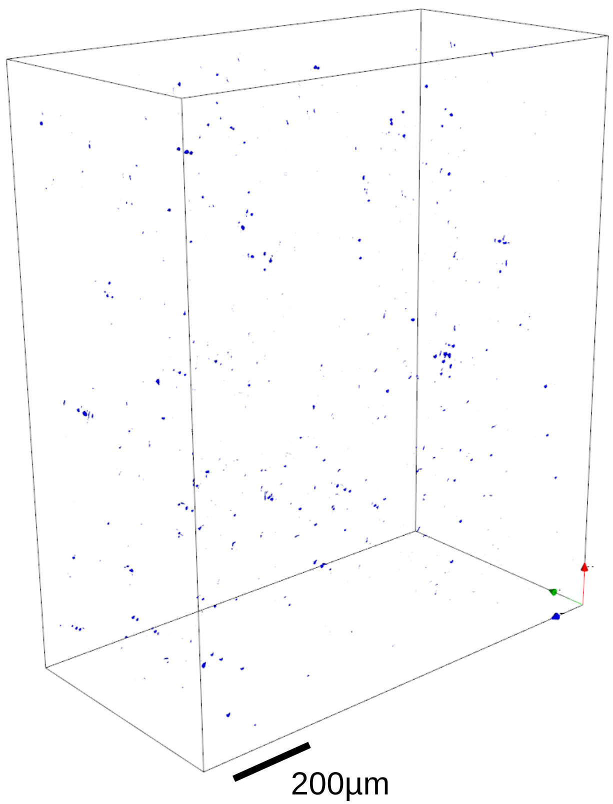

Rendered voids in:
Loadstep (1)

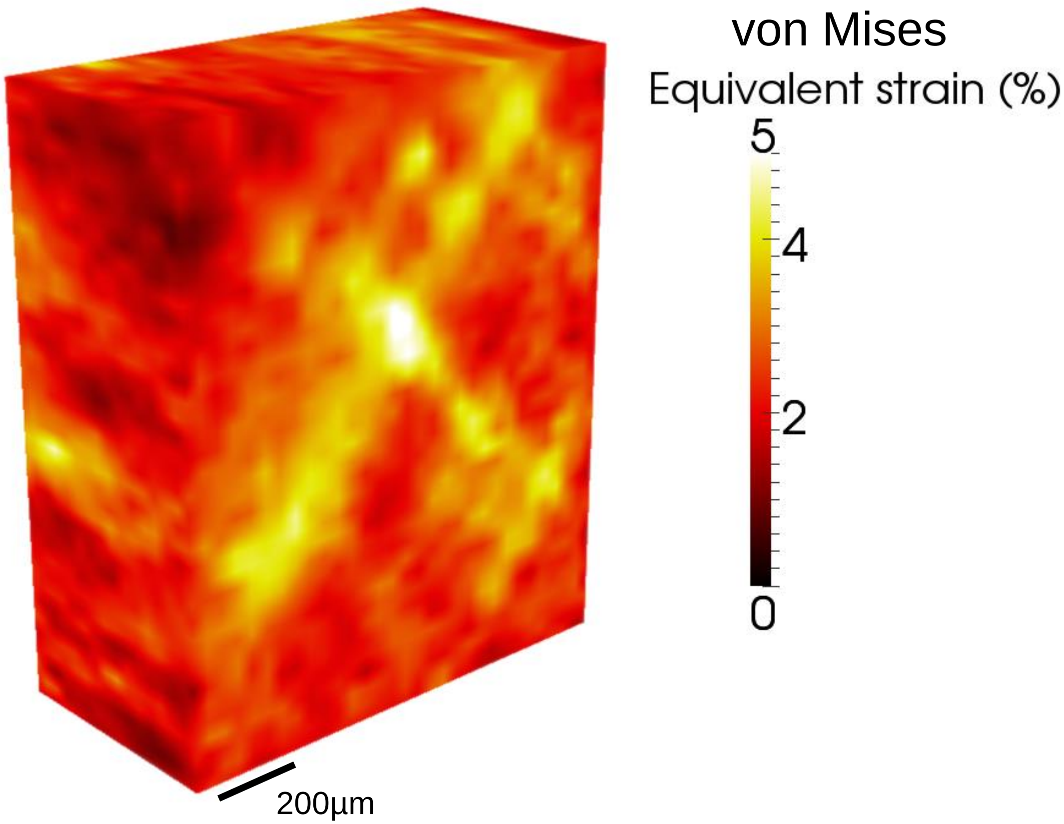

Equivalent strain between:
Loadstep (0) - loadstep (1)

Comparison: damage and strain evolution

*[Morgeneyer *et al.*, 2014, *Acta Mat.* 69 pp. 78-91]
Master Thesis: T. Taillandier-Thomas

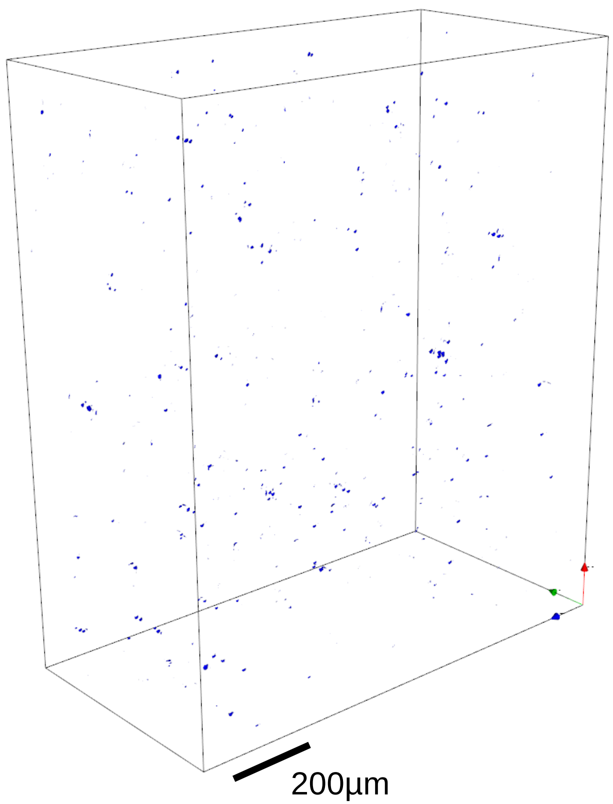

Rendered voids in:
Loadstep (2)

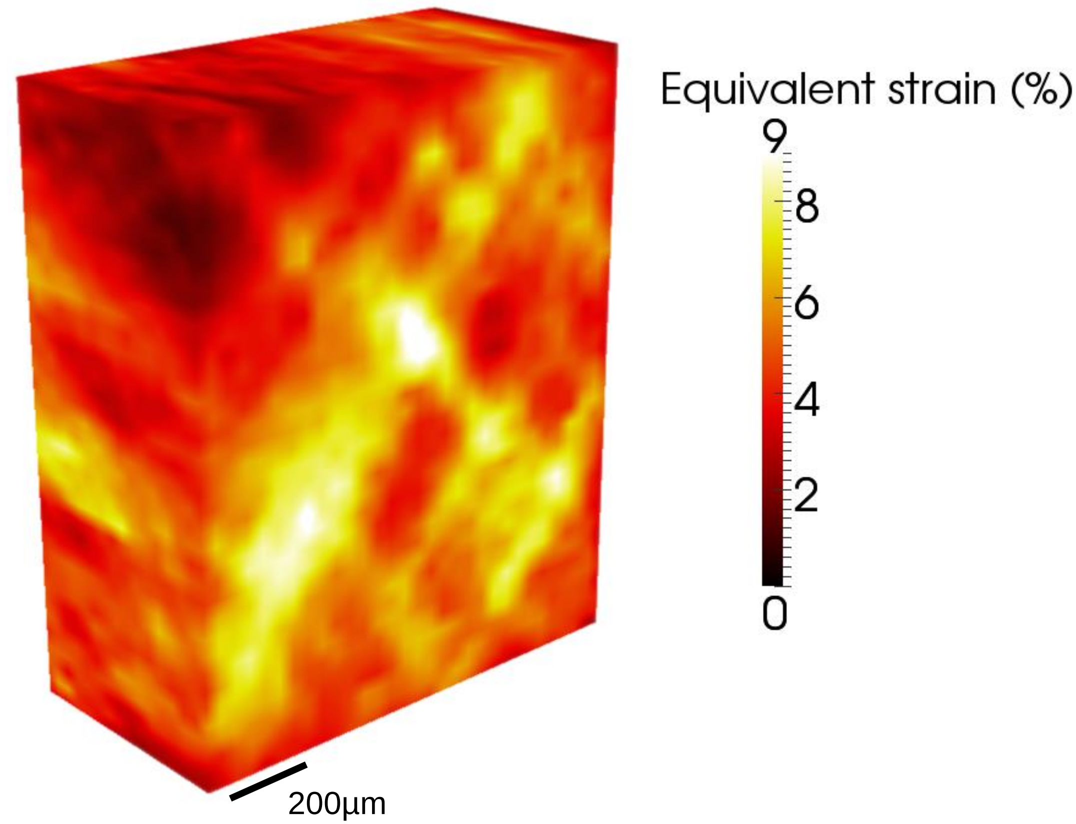

Equivalent strain between:
Loadstep (0) - loadstep (2)

Comparison: damage and strain evolution

*[Morgeneyer *et al.*, 2014, *Acta Mat.* 69 pp. 78-91]
Master Thesis: T. Taillandier-Thomas

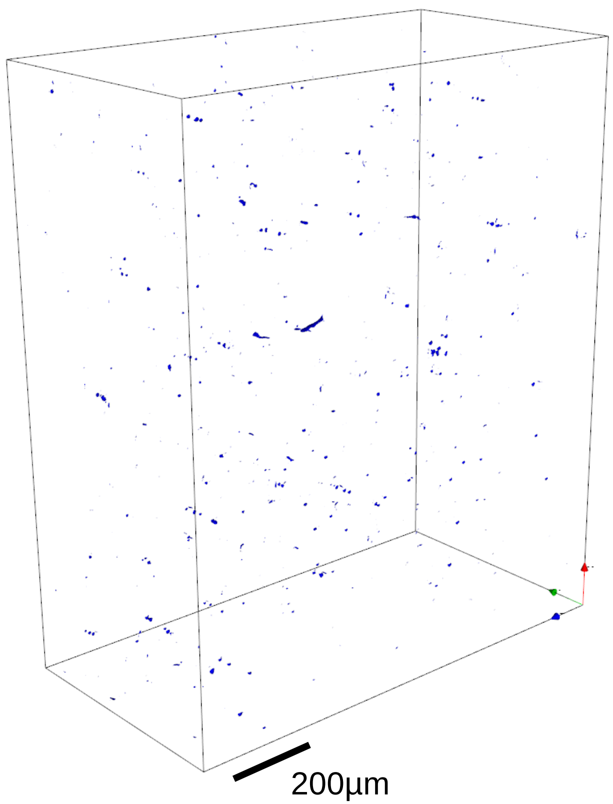

Rendered voids in:
Loadstep (3)

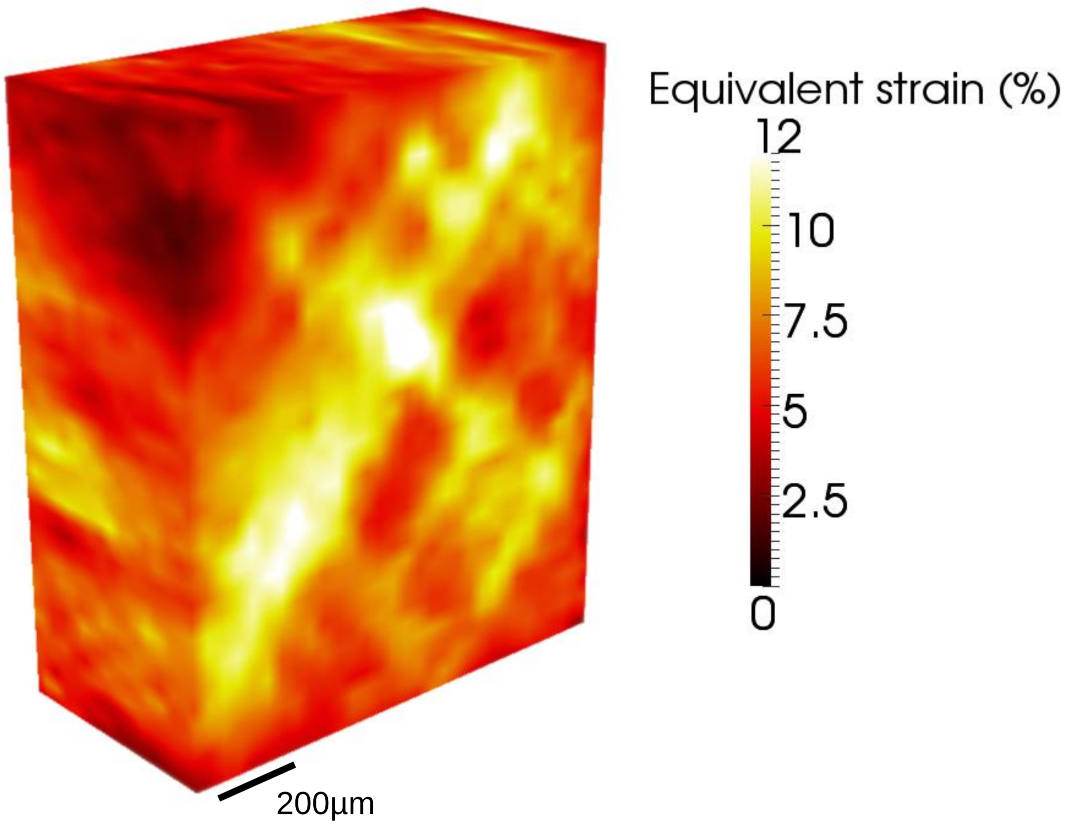

Equivalent strain between:
Loadstep (0) - loadstep (3)

Comparison: damage and strain evolution

*[Morgeneyer *et al.*, 2014, *Acta Mat.* 69 pp. 78-91]
Master Thesis: T. Taillandier-Thomas

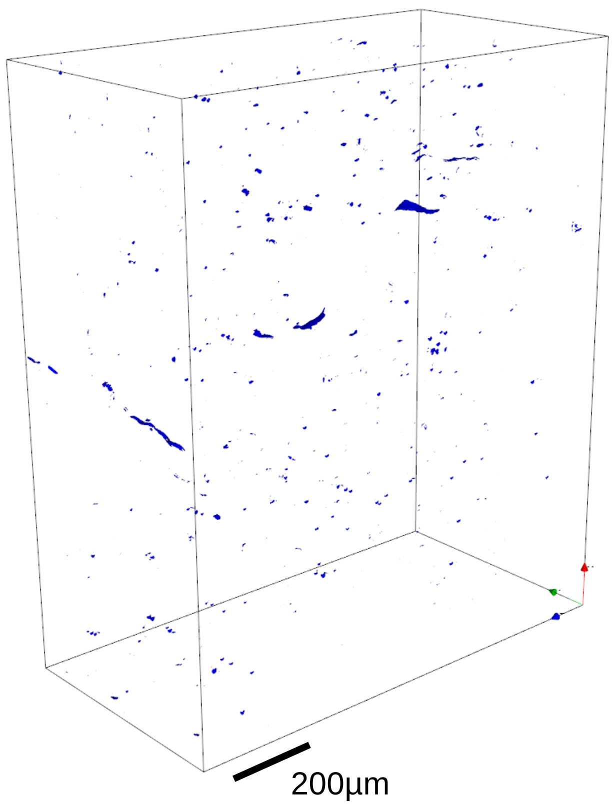

Rendered voids in:
Loadstep (4)

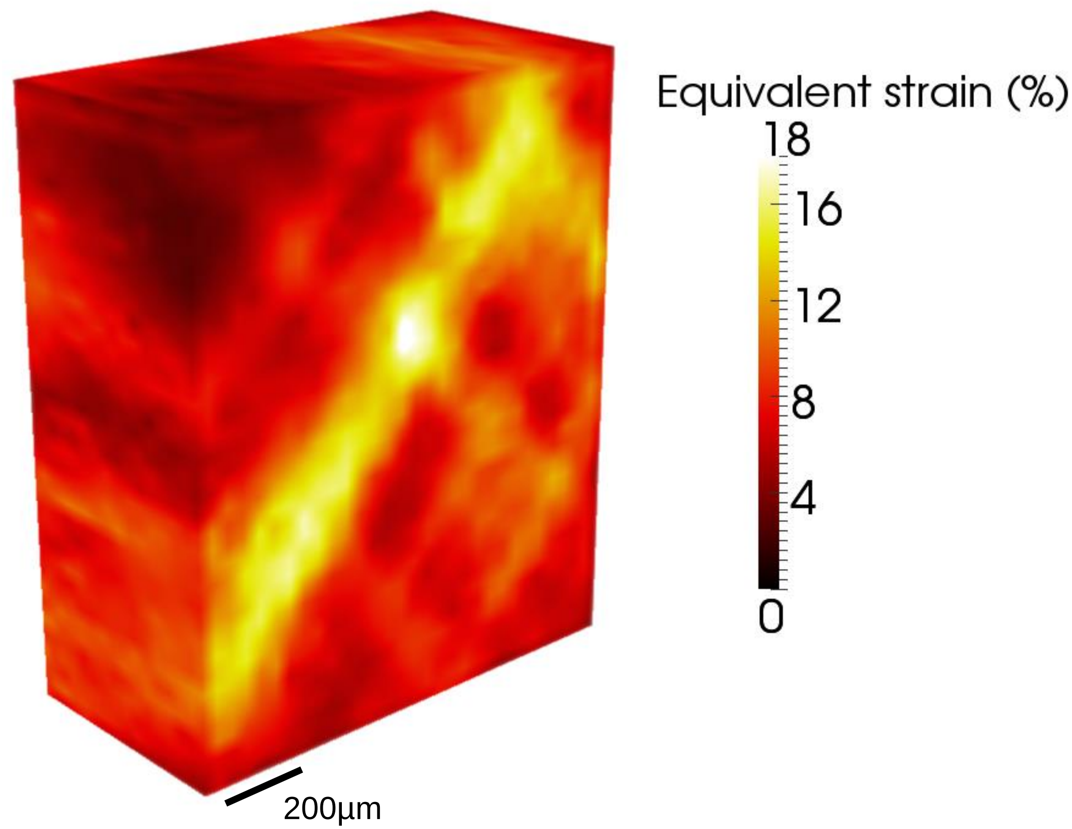

Equivalent strain between:
Loadstep (0) - loadstep (4)

Comparison: damage and strain evolution

*[Morgeneyer *et al.*, 2014, *Acta Mat.* 69 pp. 78-91]
Master Thesis: T. Taillandier-Thomas

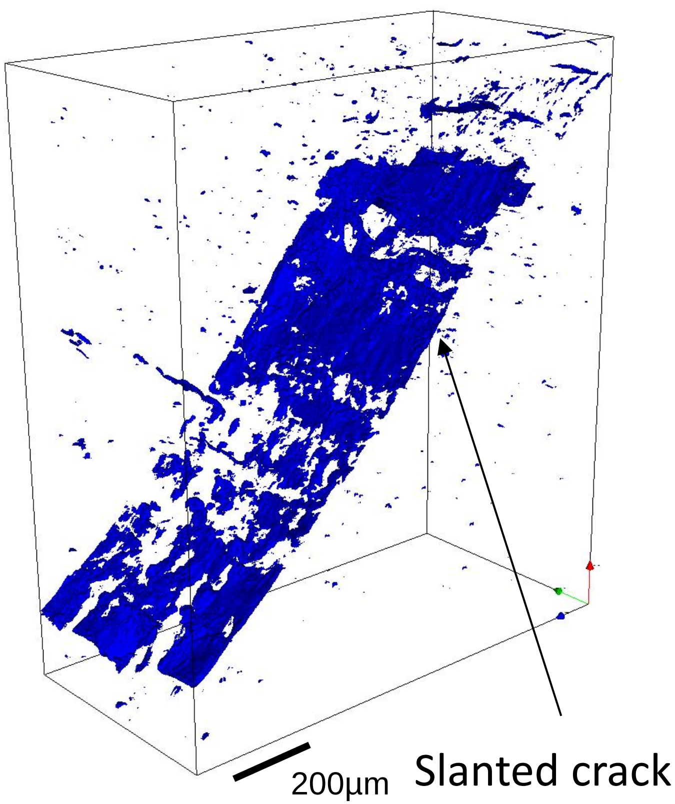

Rendered crack/damage
at failure

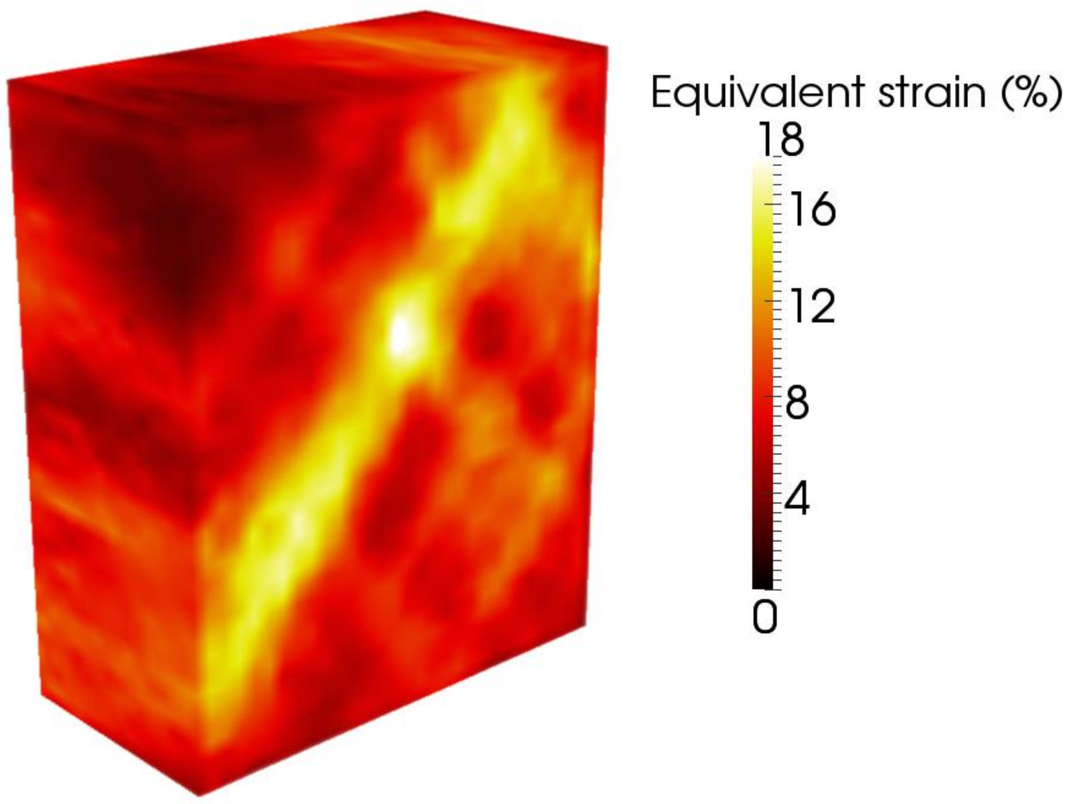

Equivalent strain between:
Loadstep (0) - loadstep (4)

Strain evolution

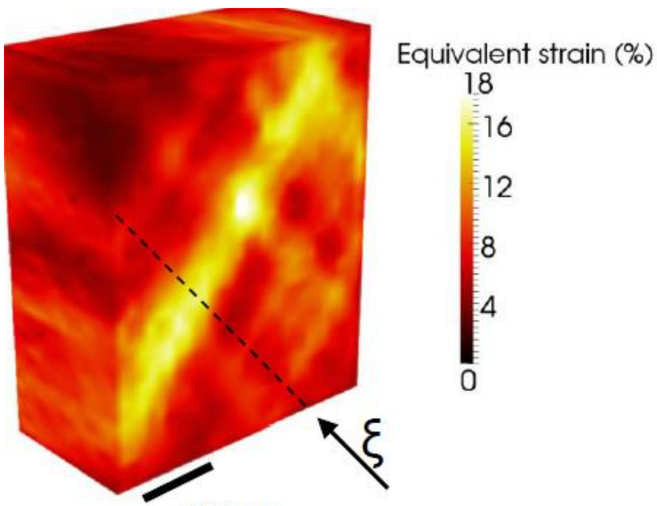

Location of straight line for Figure 6

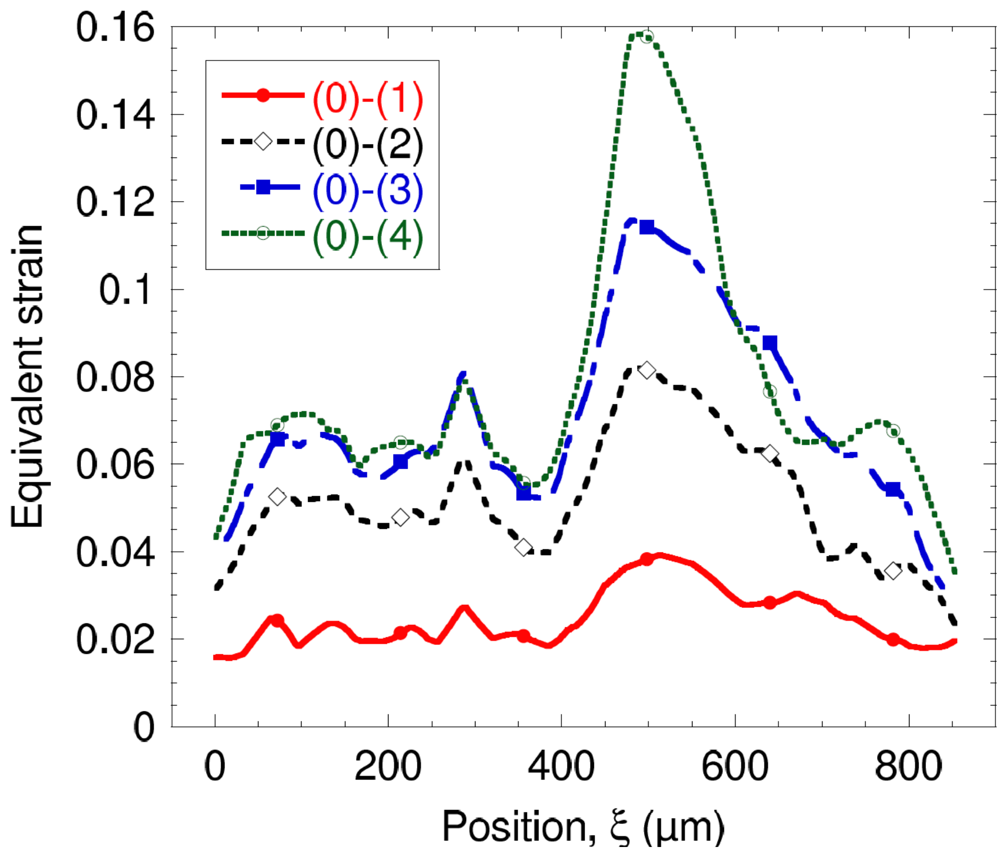

FE field?

Measured vs. simulated field

AA2198

*[Morgeneyer *et al.*, 2014, *Acta Mat.* 69 pp. 78-91]
Master Thesis: T. Taillandier-Thomas

- Result from 3D FE simulation with ideal bounday conditions using:
  - 1. von Mises plasticity
  - or 2. GTN model
  - *(or 3. macroscopic anisotropic model)*

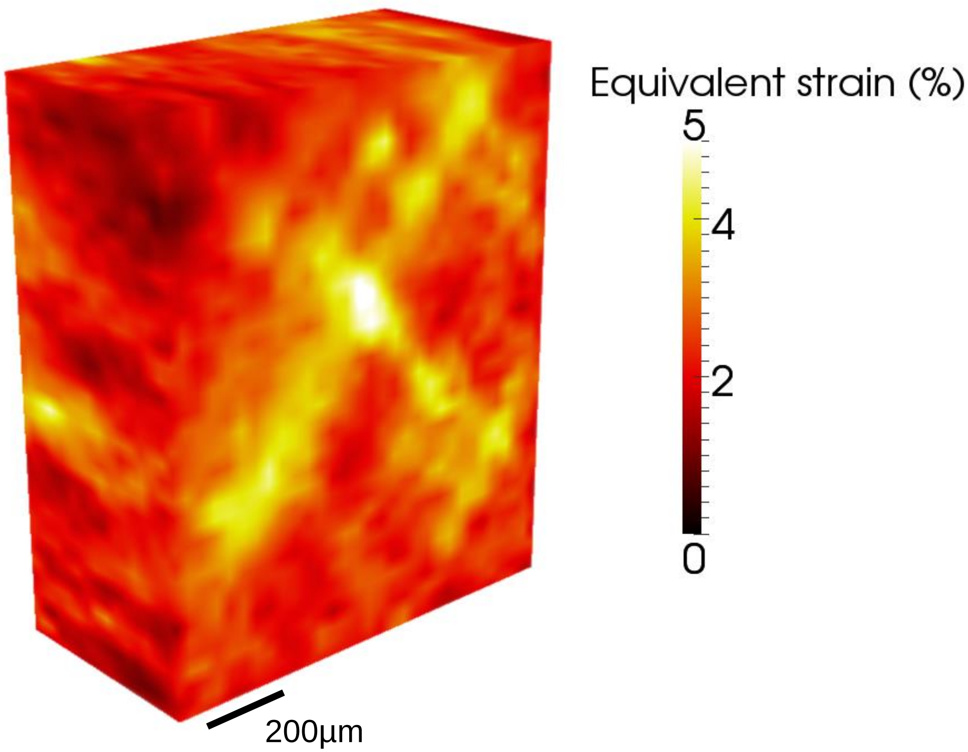

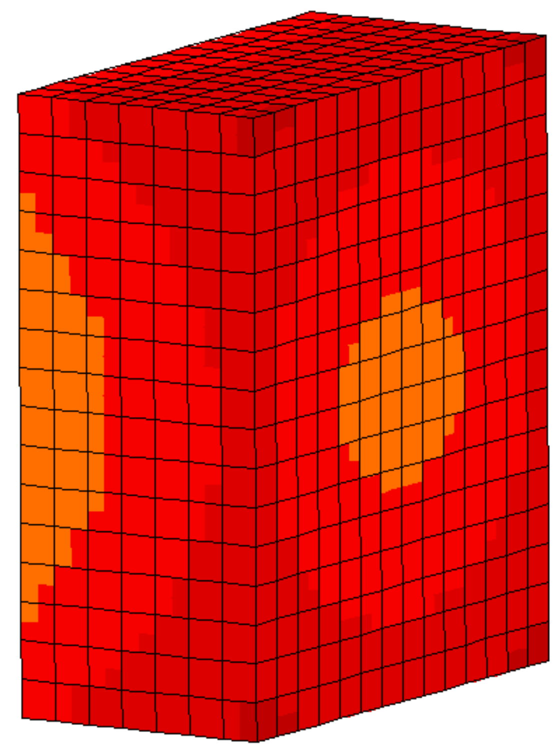

Different ROI : closer to the notch

- Getting closer to the notch*
- Assess other strain components

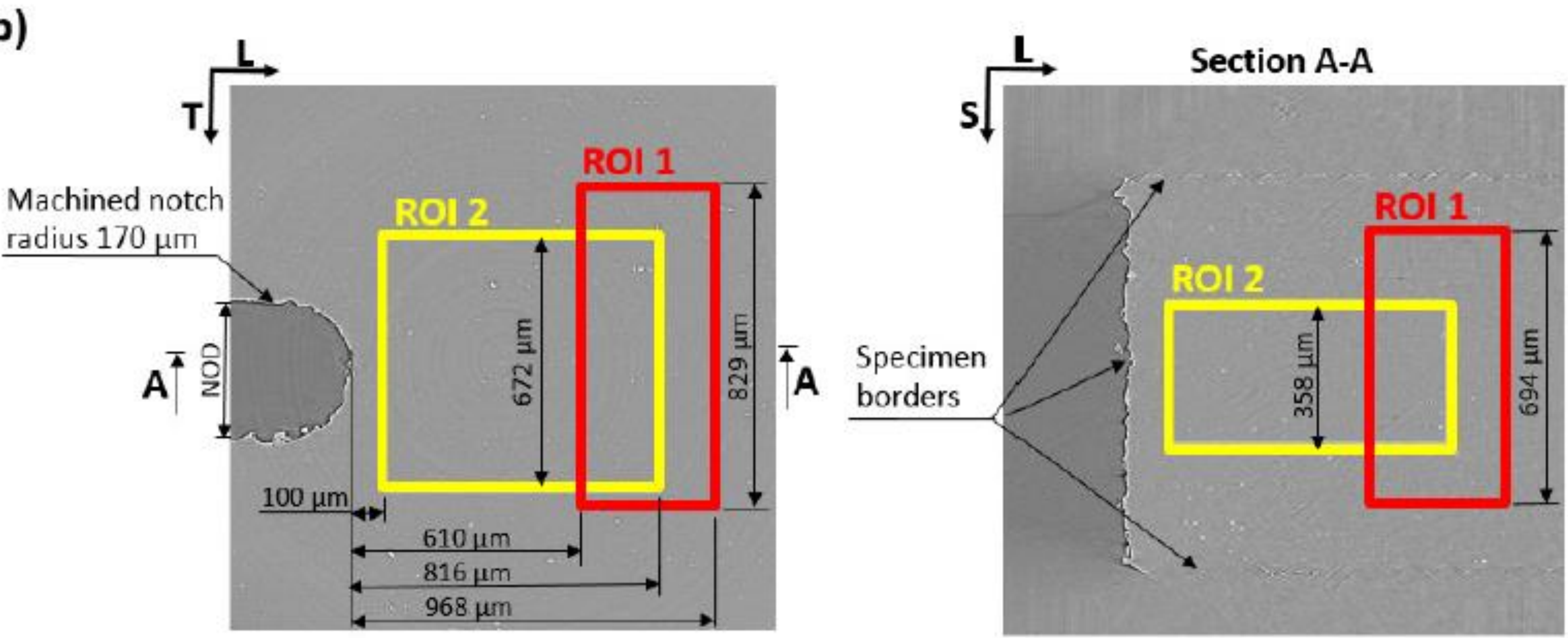

*[Buljac *et al.*, 2016, Int. J. Fracture]

Strains fields close to the notch

Plane strain in propagation direction,

as strain in propagation direction $\varepsilon_{LL} = 0$!

*[Buljac *et al.*, 2016, Int. J. Fracture]

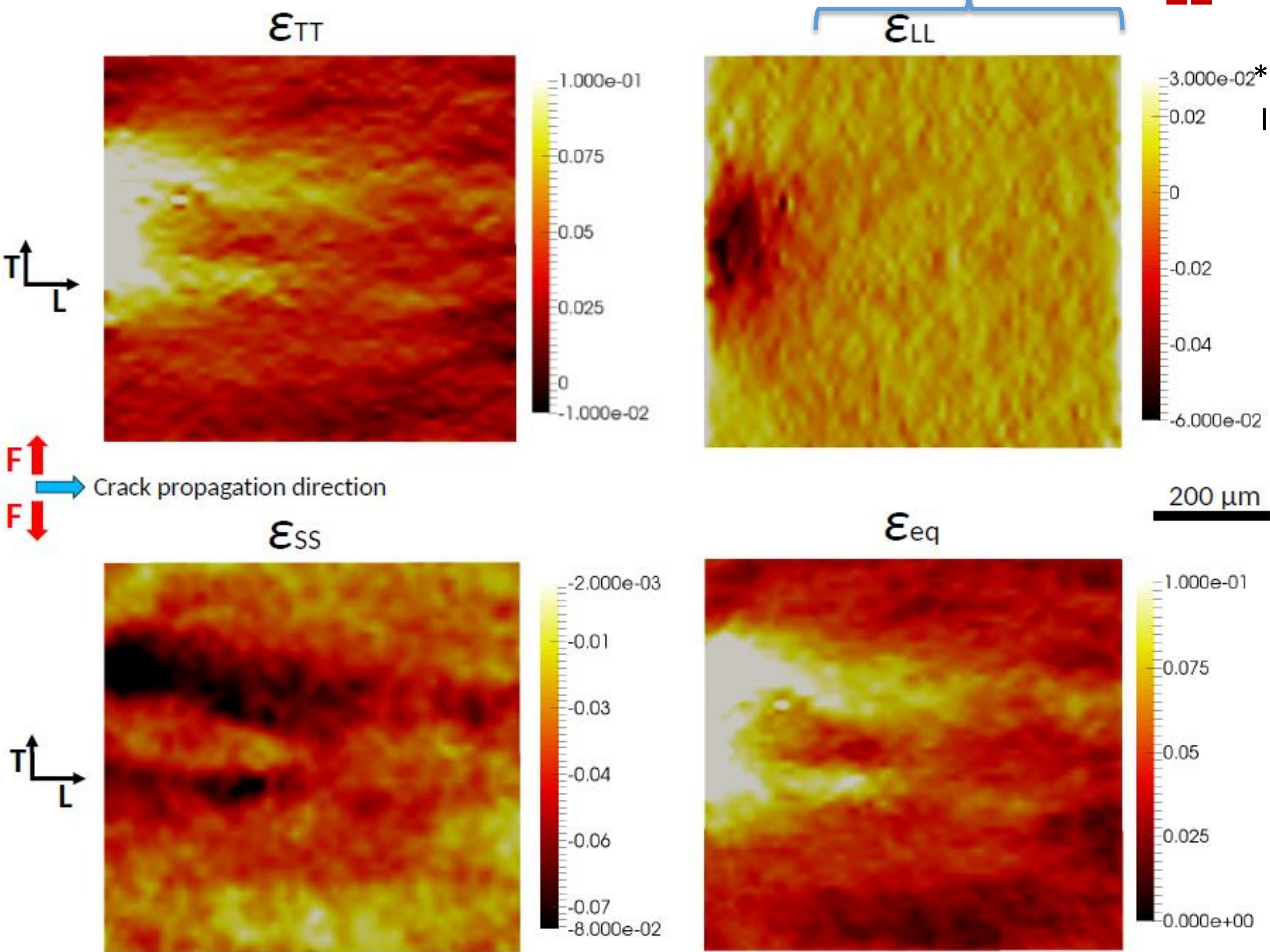

Reminder

- Plane strain direction in a thick sample: thickness direction!

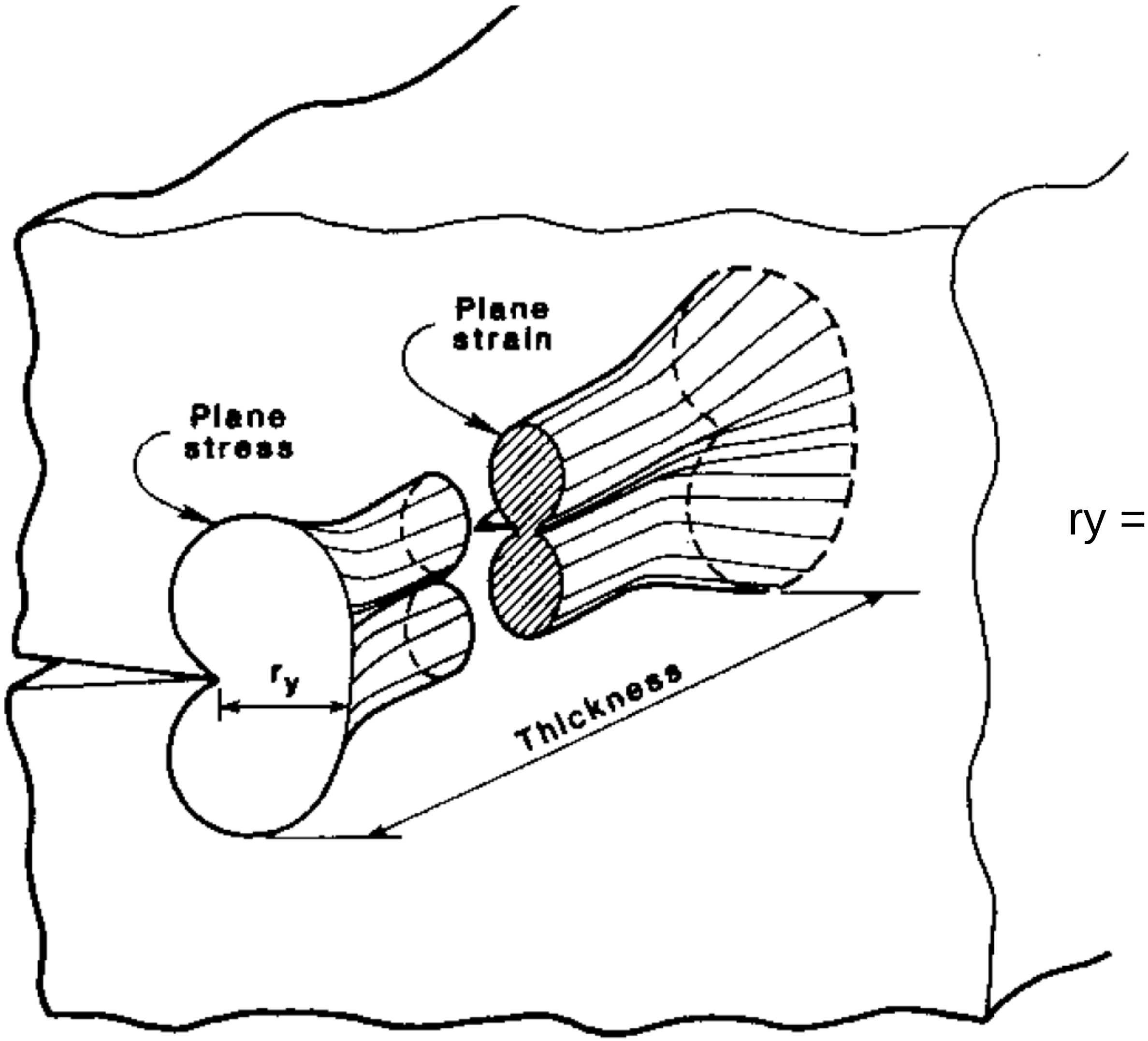

ry = plastic zone size

Cuts normal to propagation direction

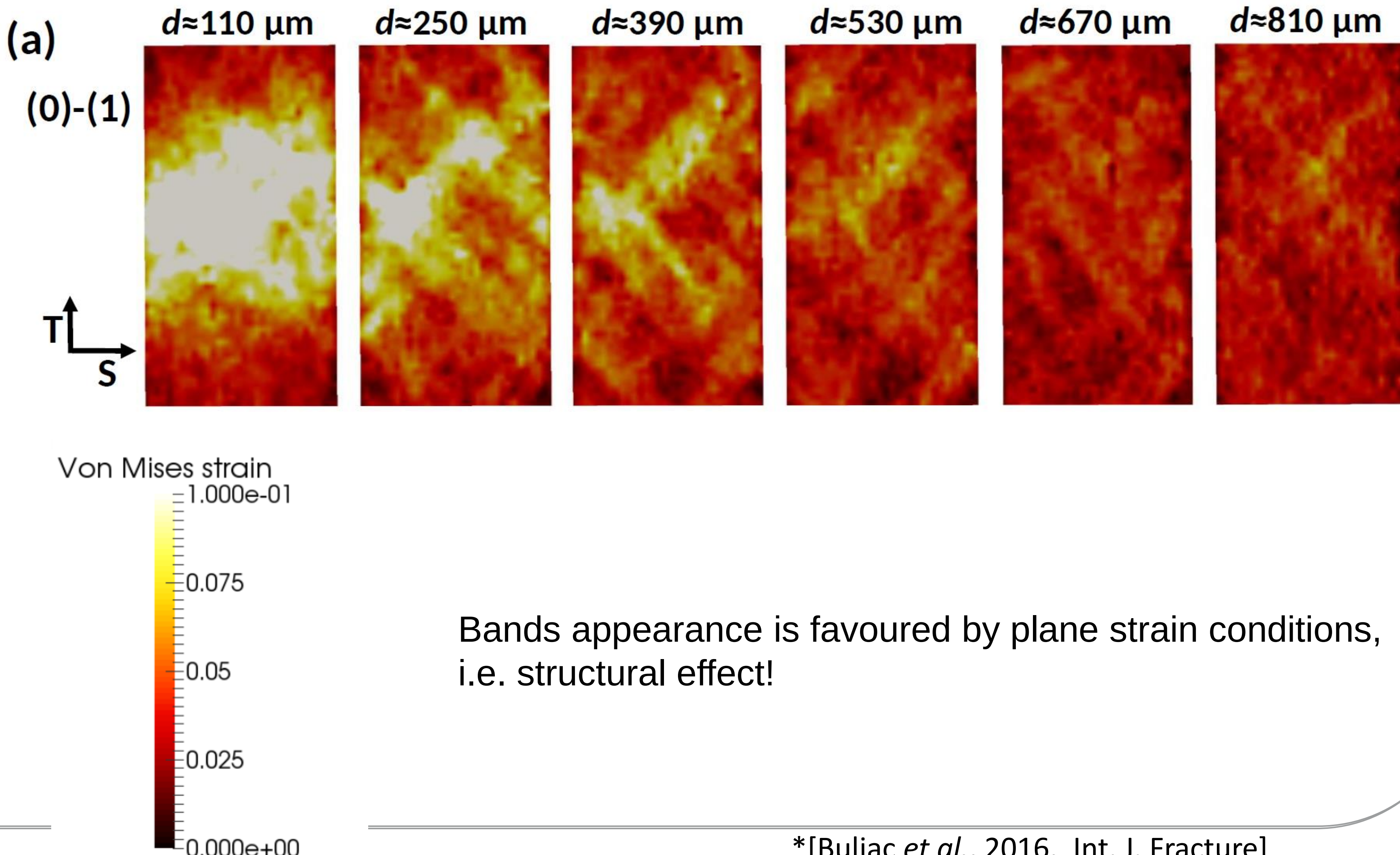

Bands appearance is favoured by plane strain conditions, i.e. structural effect!

*[Buljac *et al.*, 2016, Int. J. Fracture]

some conclusions

- *In situ* observations at micrometre scale of notch-microstructure interactions are possible via *in situ* synchrotron laminography

- Evolution of (pre-existing) voids can be observed and measured:
  - Symmetric void growth on the flat crack
  - Void reorientation on the slant crack

- For materials with initial image contrast simultaneous strain and damage measurement are possible
  - Uncertainty about 1% strain for AA

- Strain concentration in the slant bands precedes the onset of damage
  - The bands cannot be reproduced with von Mises plasticity or the Gurson model

- Do other materials show a similar slant strain concentration bands ?

AA 2198 T3

- Al-Cu-Li alloy

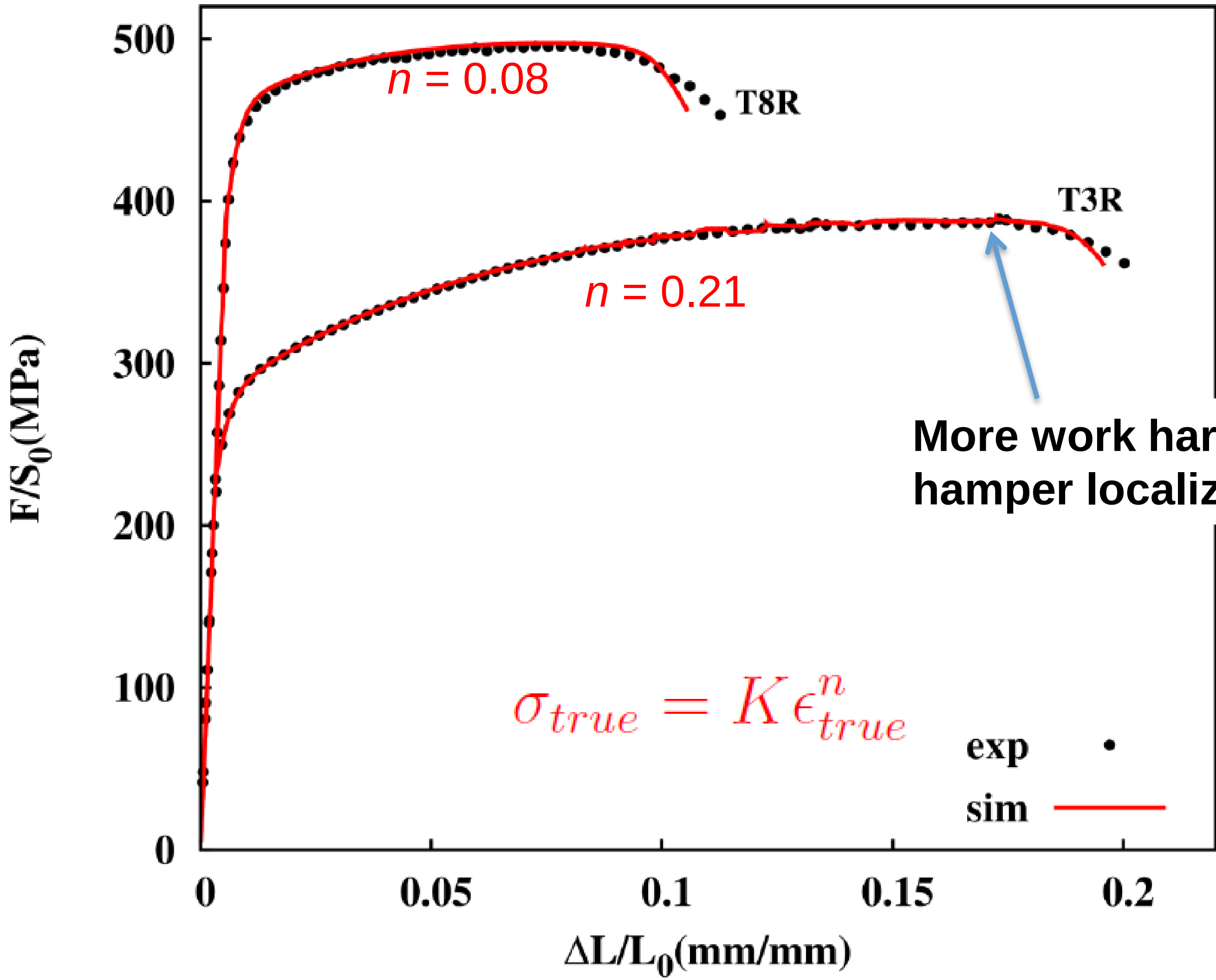

More work hardening should hamper localization (Rice 1976)!

Strain field far ahead of notch for 2198 T3

Cumulated von Mises strain

(0) - (3)

Direct correlations

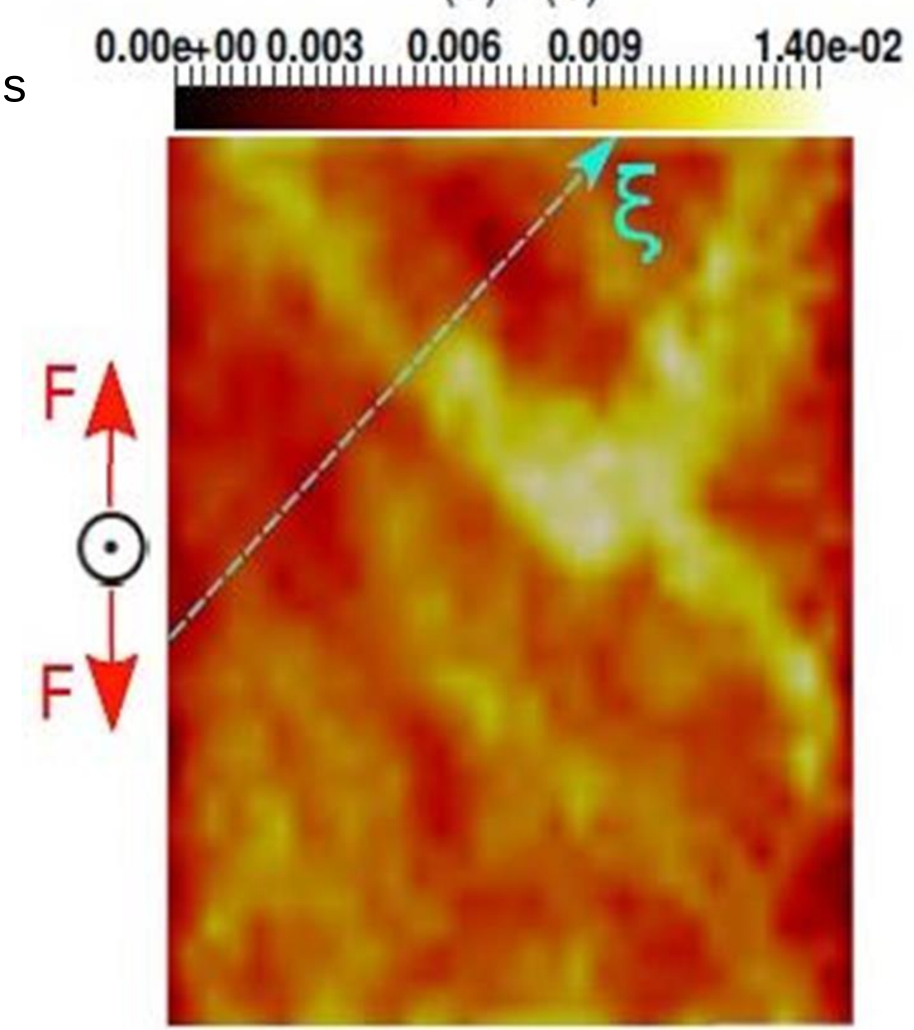

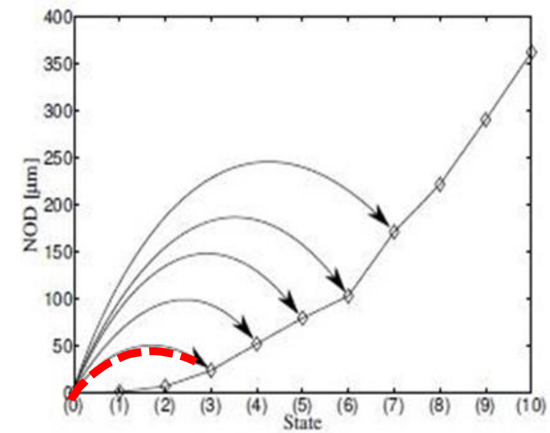

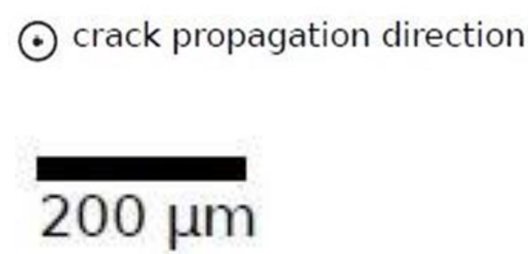

- early strained band despite high work hardening

Buljac et al Acta Mat 2018

Strain field far ahead of notch for 2198 T3

Cumulated von Mises strain

Direct correlations

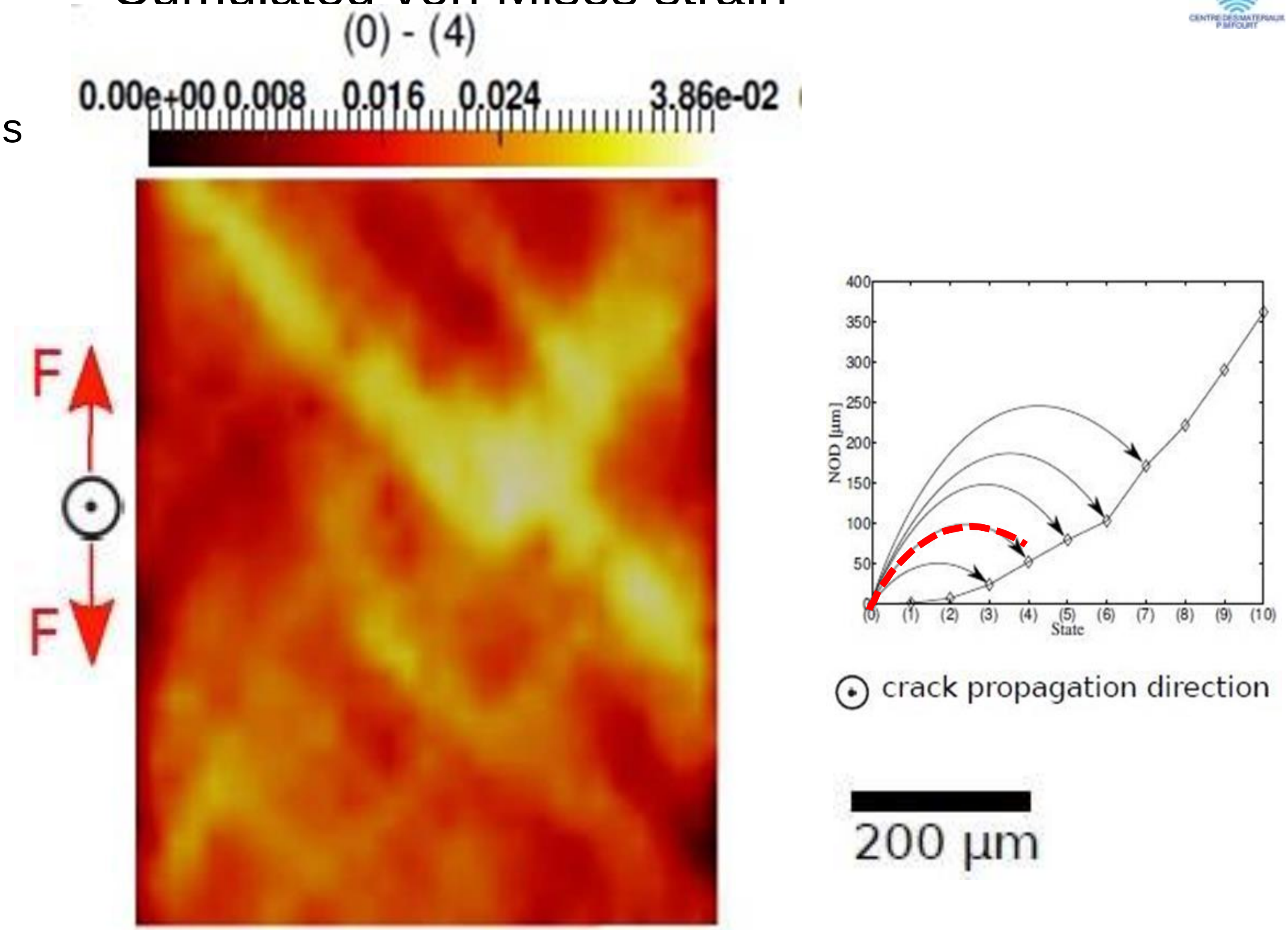

- early strained band despite high work hardening

Buljac et al Acta Mat 2018

Strain field far ahead of notch for 2198 T3

Cumulated von Mises strain

(0) - (5)

Direct correlations

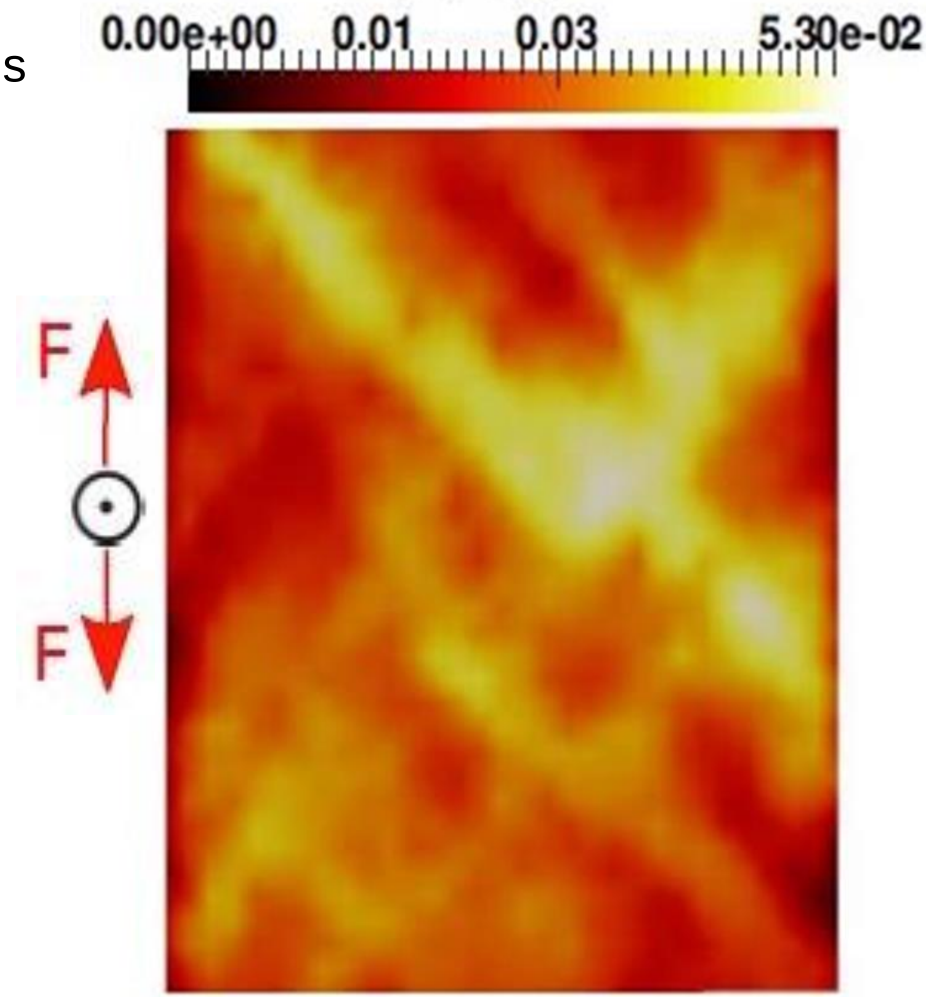

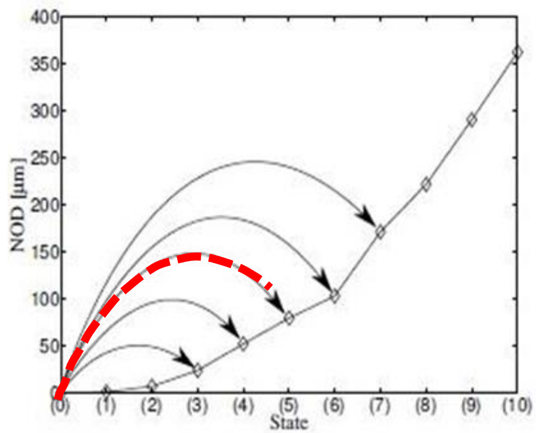

⊙ crack propagation direction

200 µm

- early strained band despite high work hardening

Buljac et al Acta Mat 2018

Strain field far ahead of notch for 2198 T3

Cumulated von Mises strain

(0) - (6)

Direct correlations

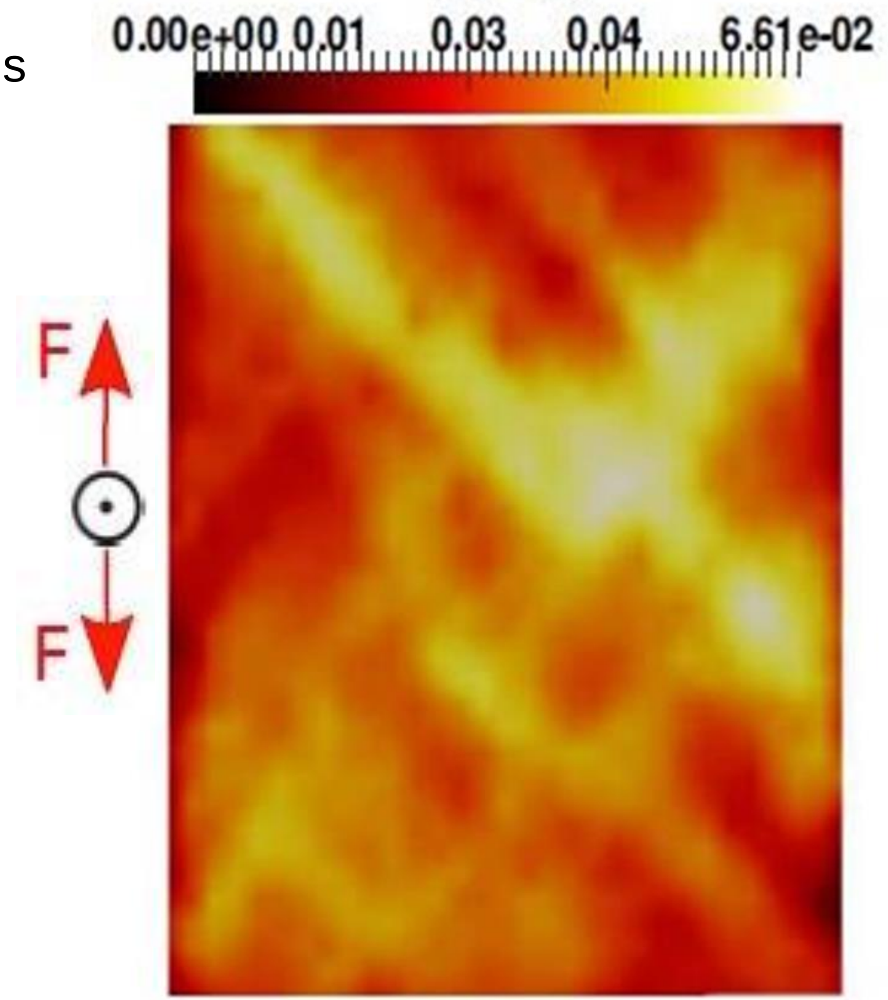

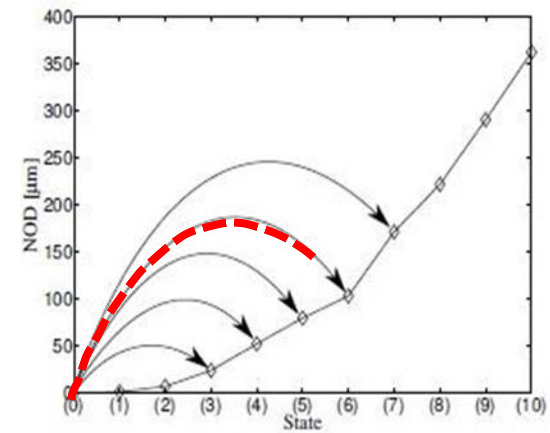

⊙ crack propagation direction

200 µm

- early strained band despite high work hardening

Strain field far ahead of notch for 2198 T3

Cumulated von Mises strain

Direct correlations

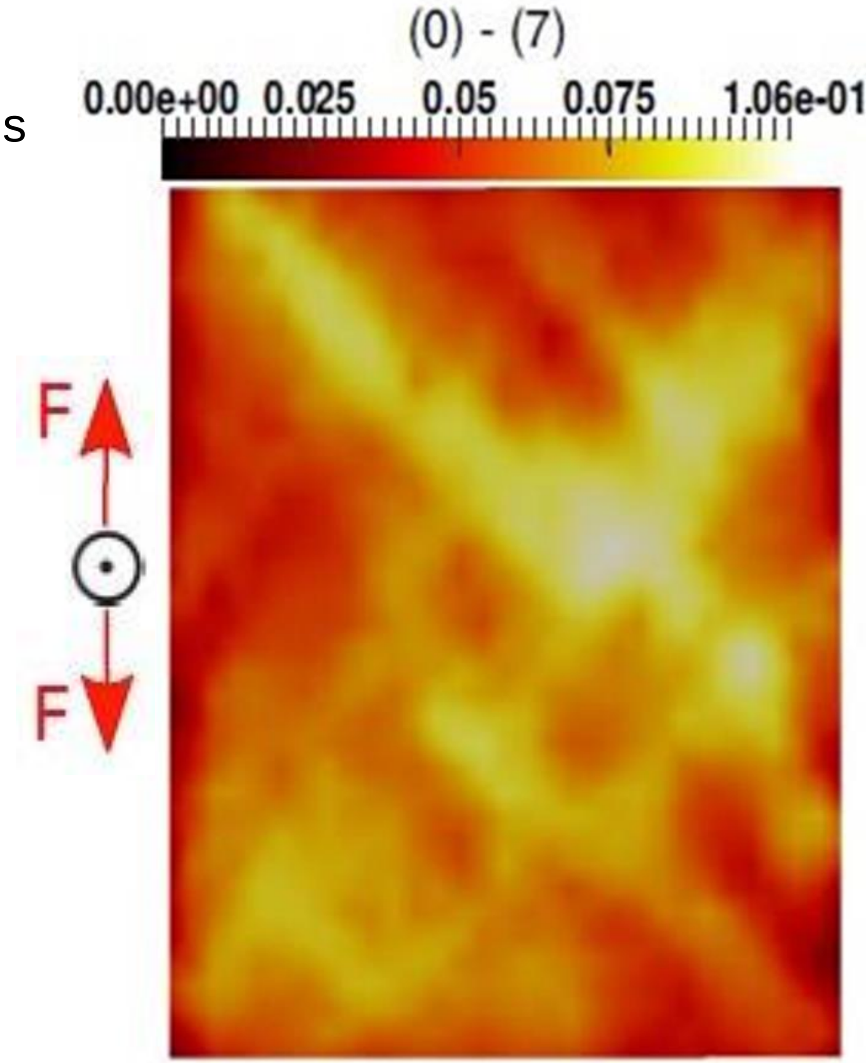

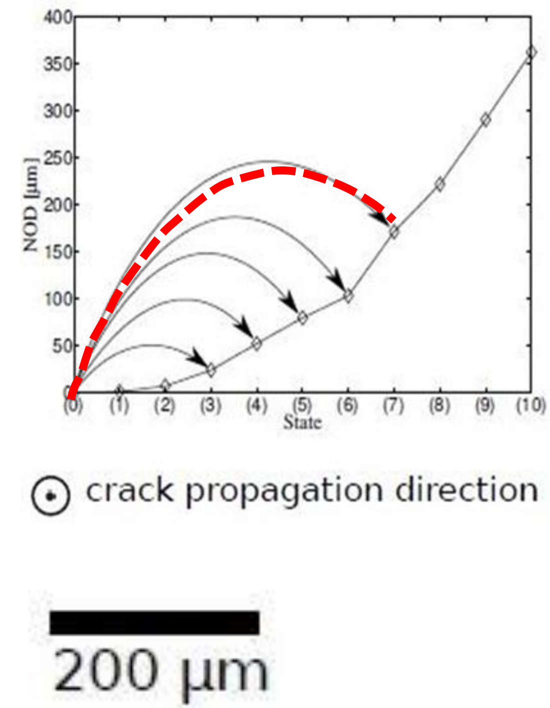

- early strained band despite high work hardening

Buljac et al Acta Mat 2018

Strain field far ahead of notch for 2198 T3

Final fracture

Direct correlations

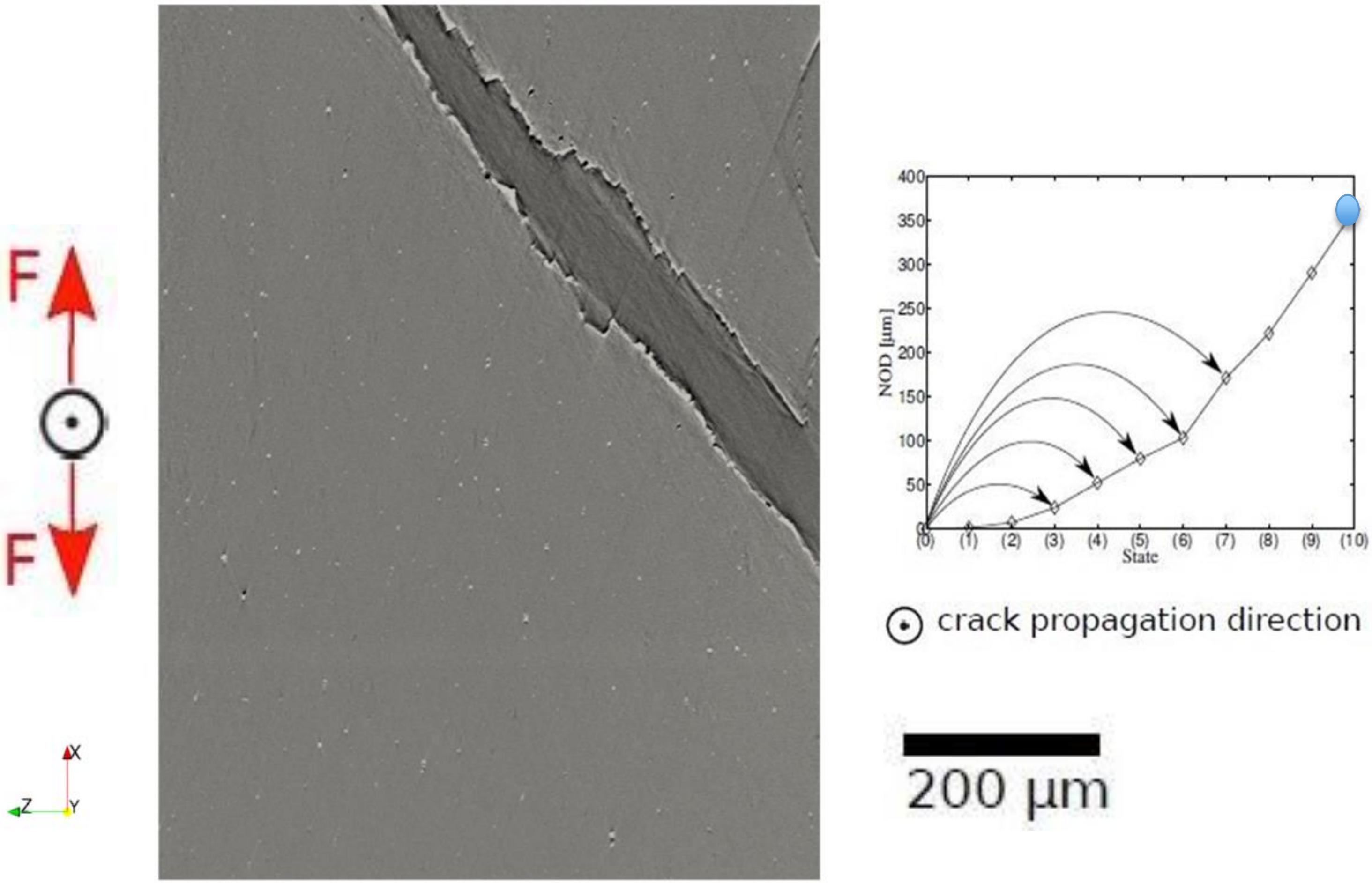

- early strained band despite high work hardening

Buljac et al Acta Mat 2018

Strain field for AA2139 T3

Perspectives: Effect of material (2139 T3)

- Effect of **strain hardening** and **initial porosity**
  - Initial microstructure and incremental strain field

ROI: 864 x 608 x 992 voxels or 520 Mo
DOF ~ 54,000

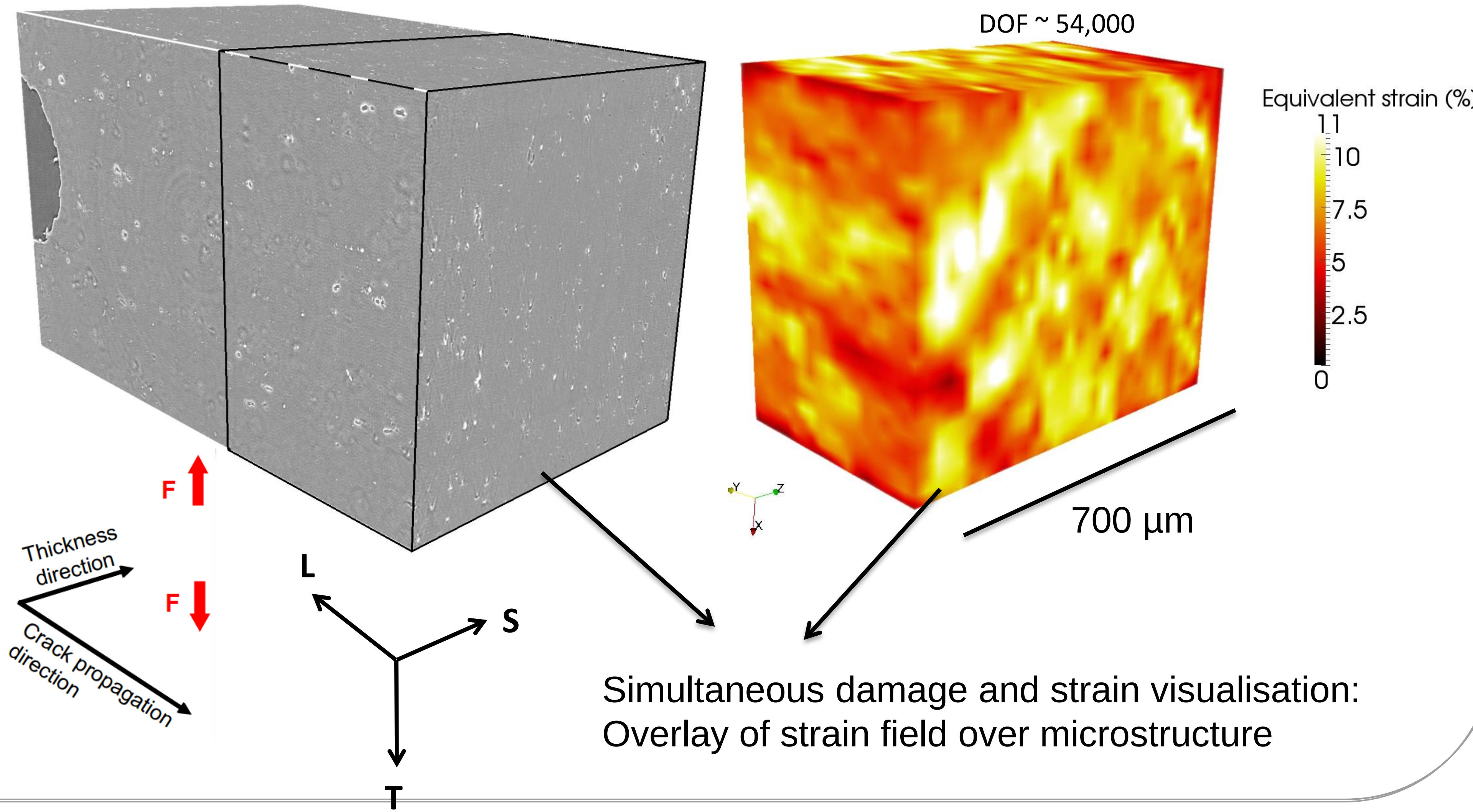

Simultaneous damage and strain visualisation:
Overlay of strain field over microstructure

2139 T3: overlay strain + microstructure

Incremental von Mises equivalent strain: $p_{eq}(u_{b\text{-}i})$

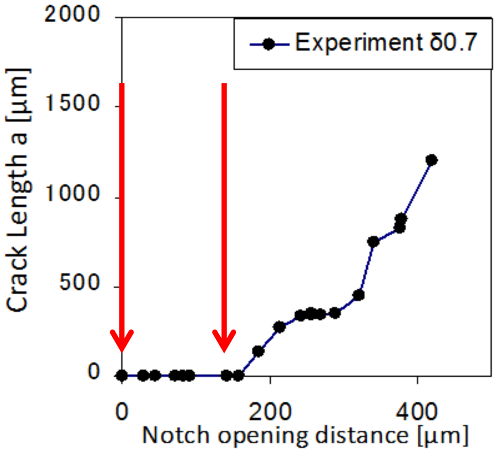

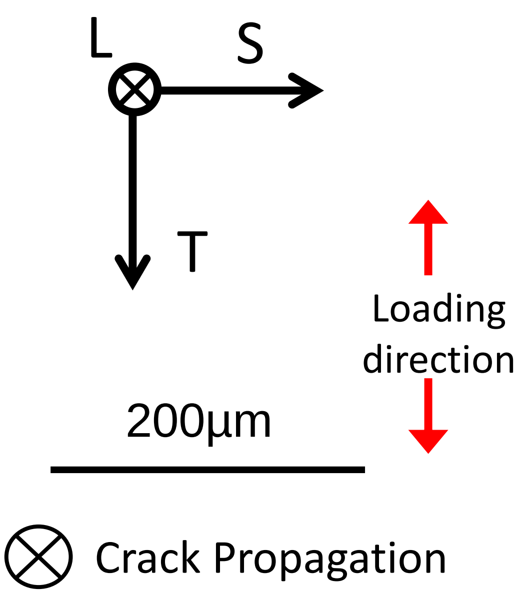

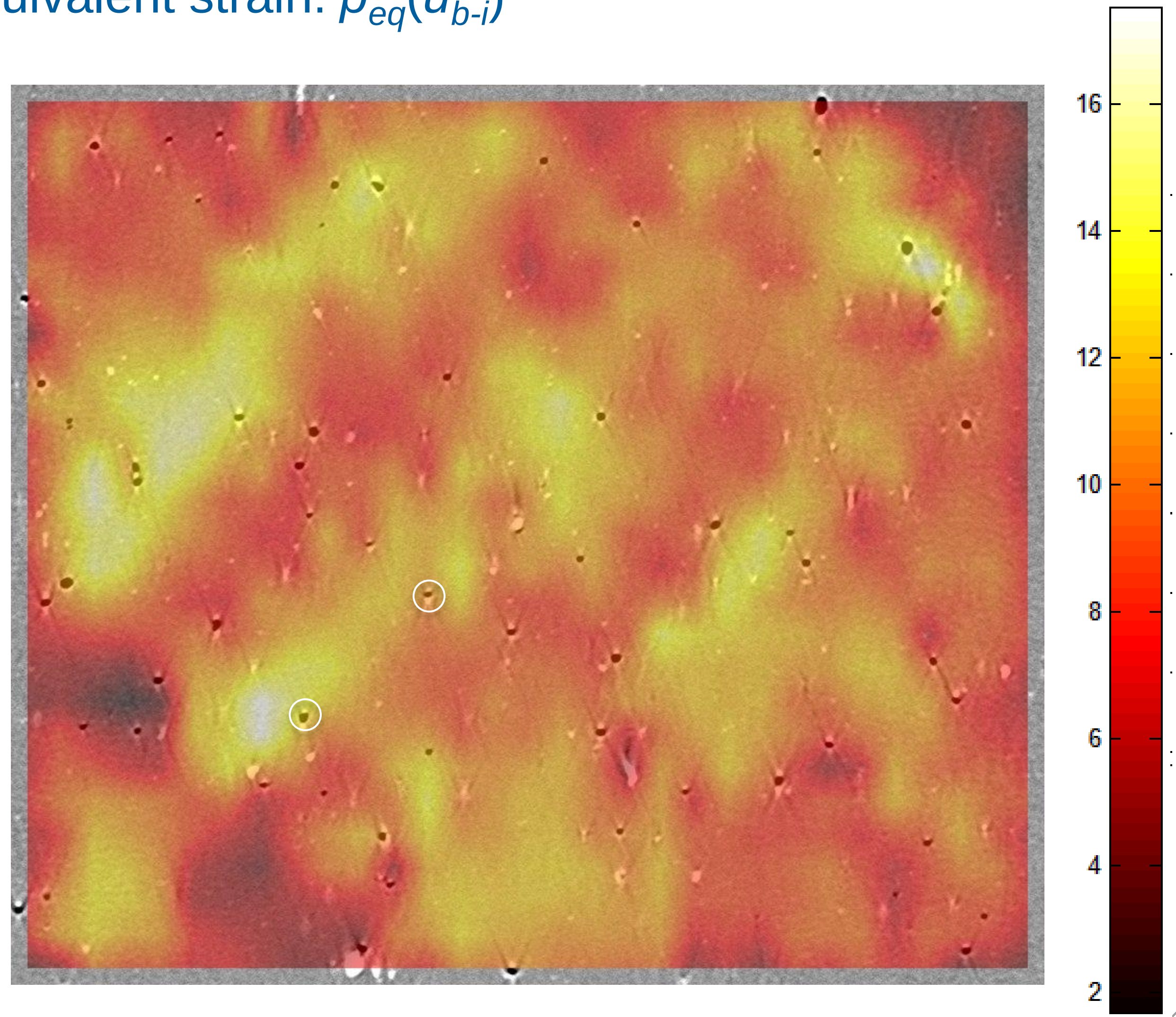

2139 T3: overlay strain + microstructure

Incremental strain: $p_{eq}(u_{i\text{-}m})$

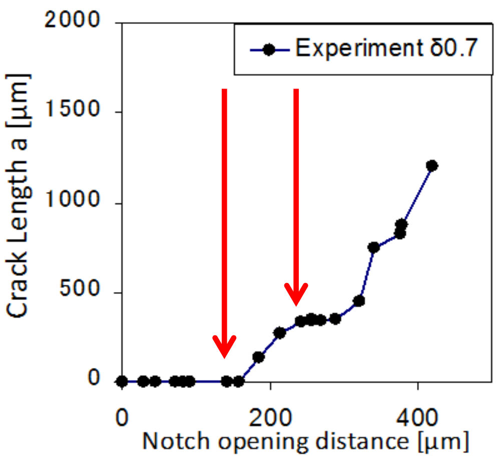

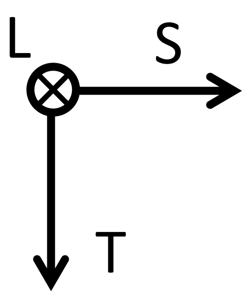

Loading direction

200µm

⊗ Crack Propagation

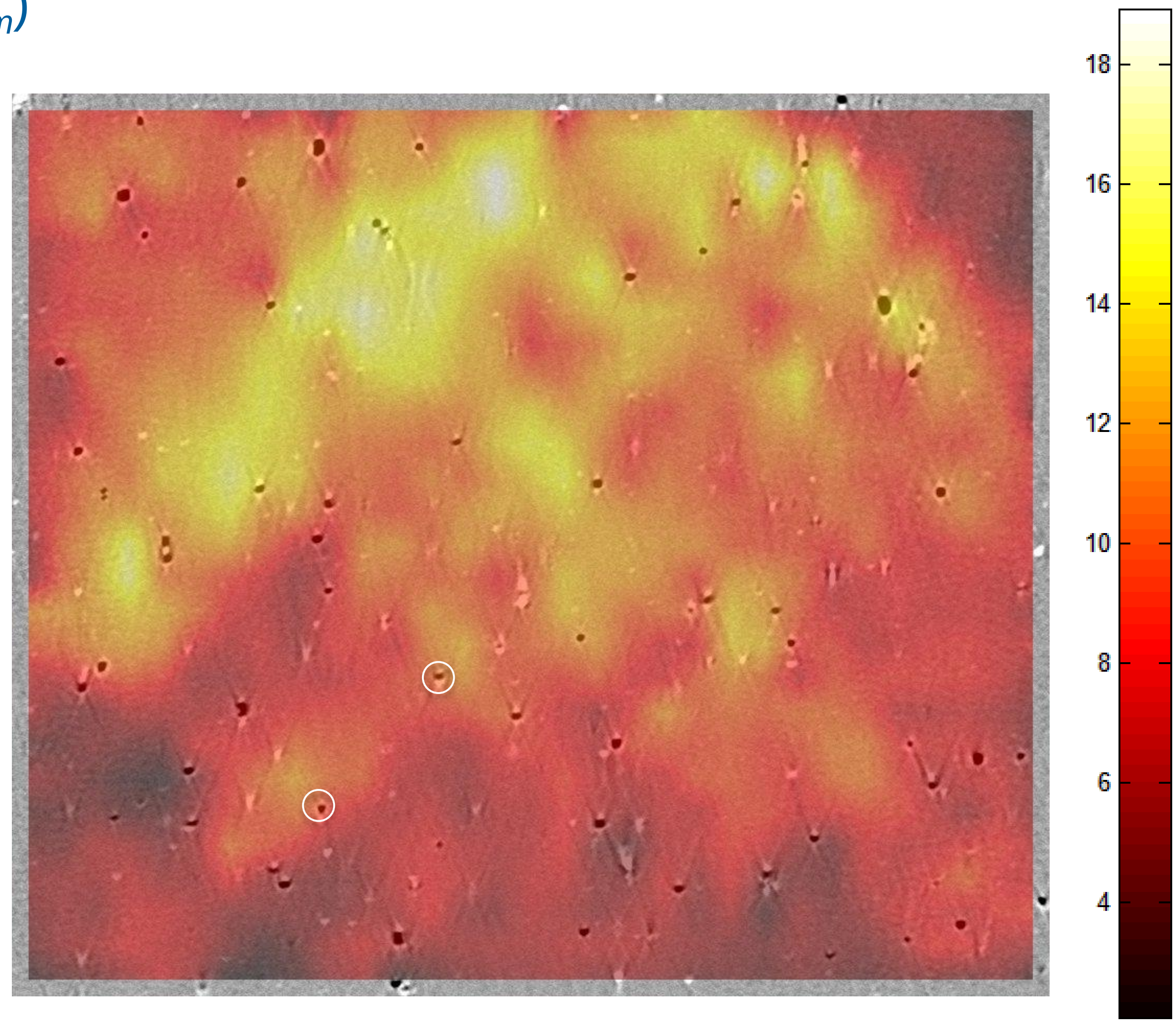

2139 T3: overlay strain + microstructure

Incremental strain: $p_{eq}(u_{m\text{-}r})$

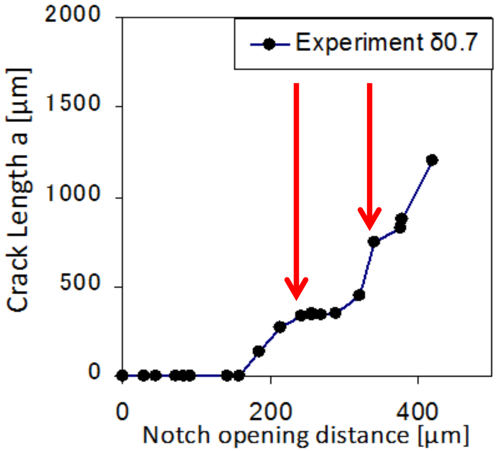

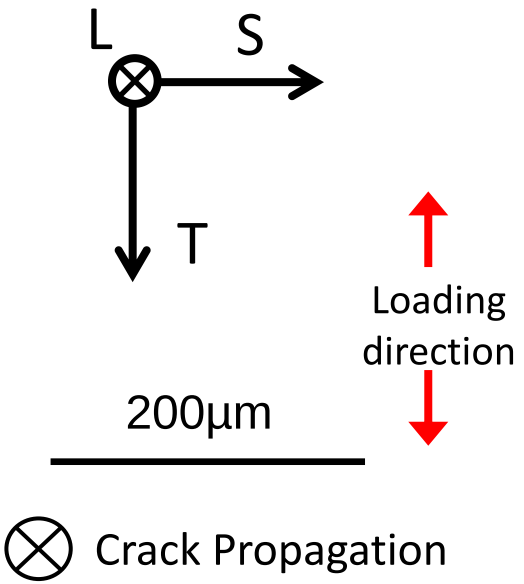

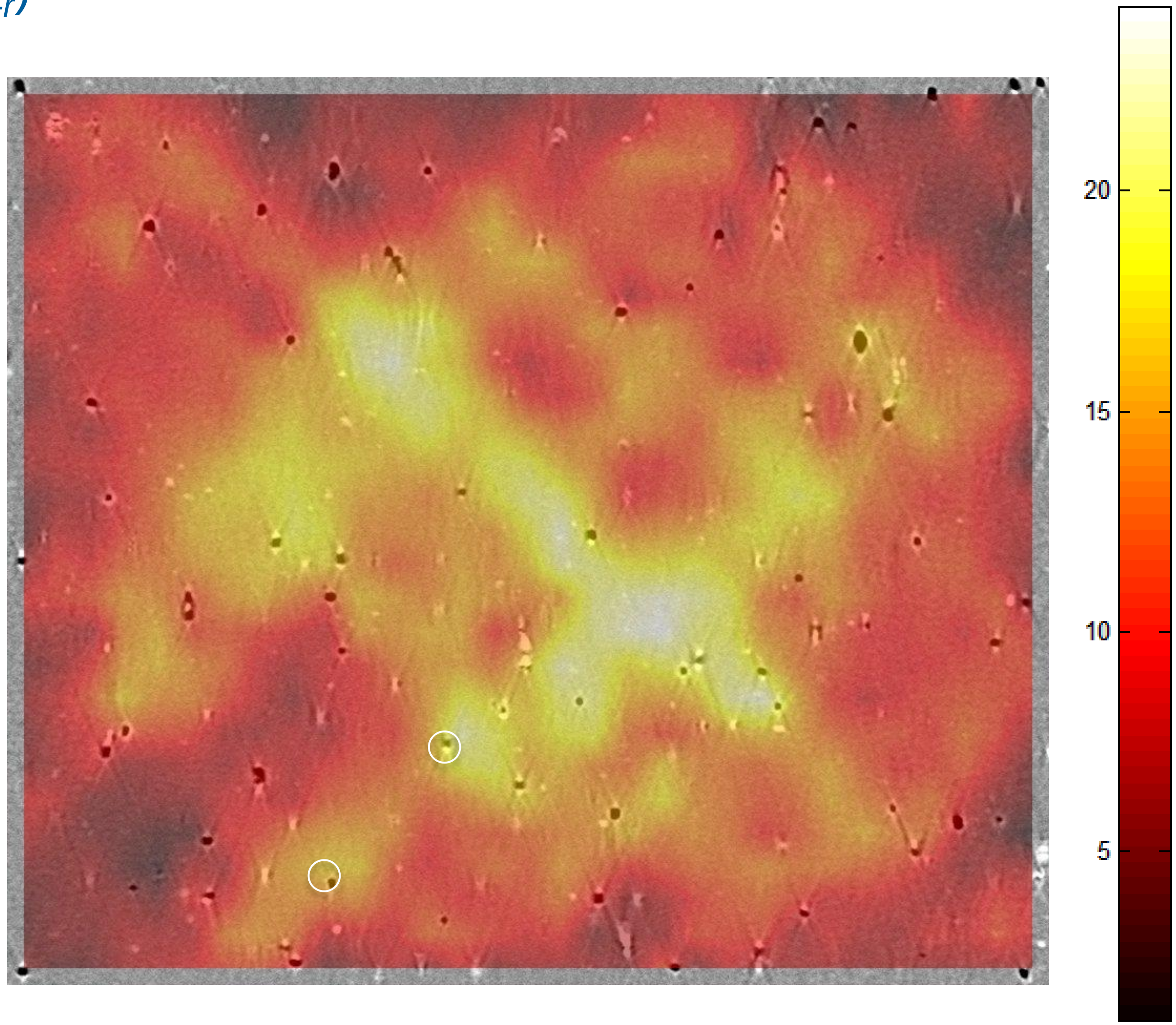

2139 T3: overlay strain + microstructure

Incremental strain: $p_{eq}(u_{r\text{-}s})$

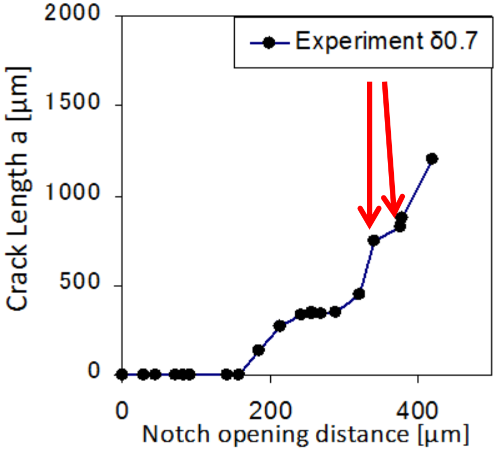

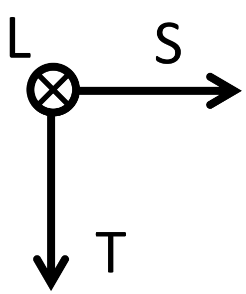

Loading direction

200µm

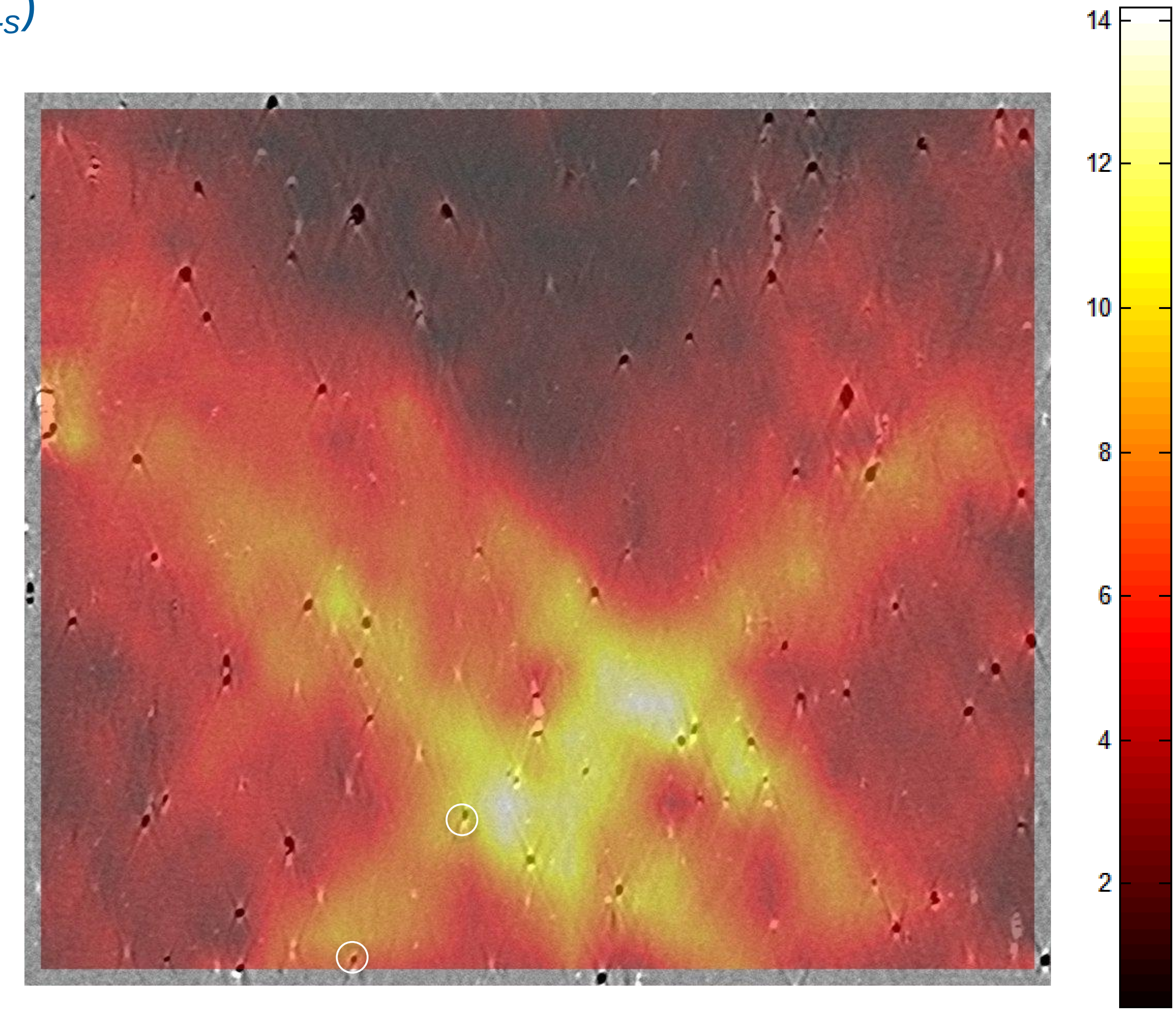

⊗ Crack Propagation

2139 T3: overlay strain + microstructure

Incremental strain: $p_{eq}(u_{s\text{-}t})$

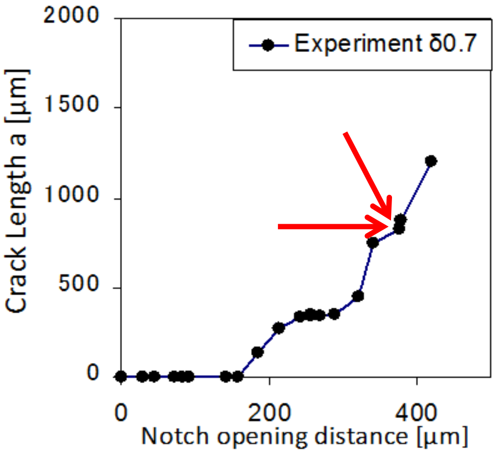

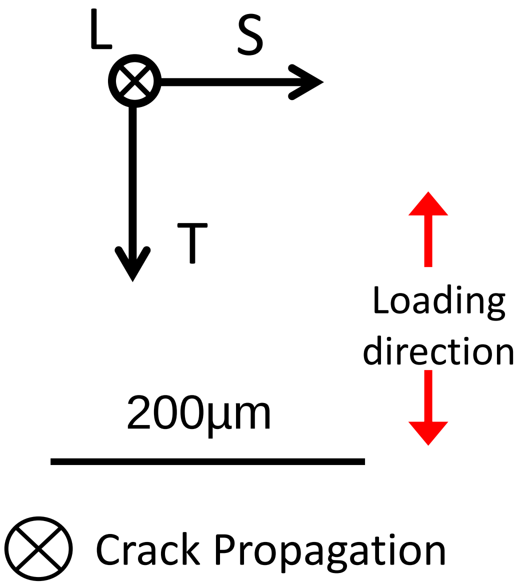

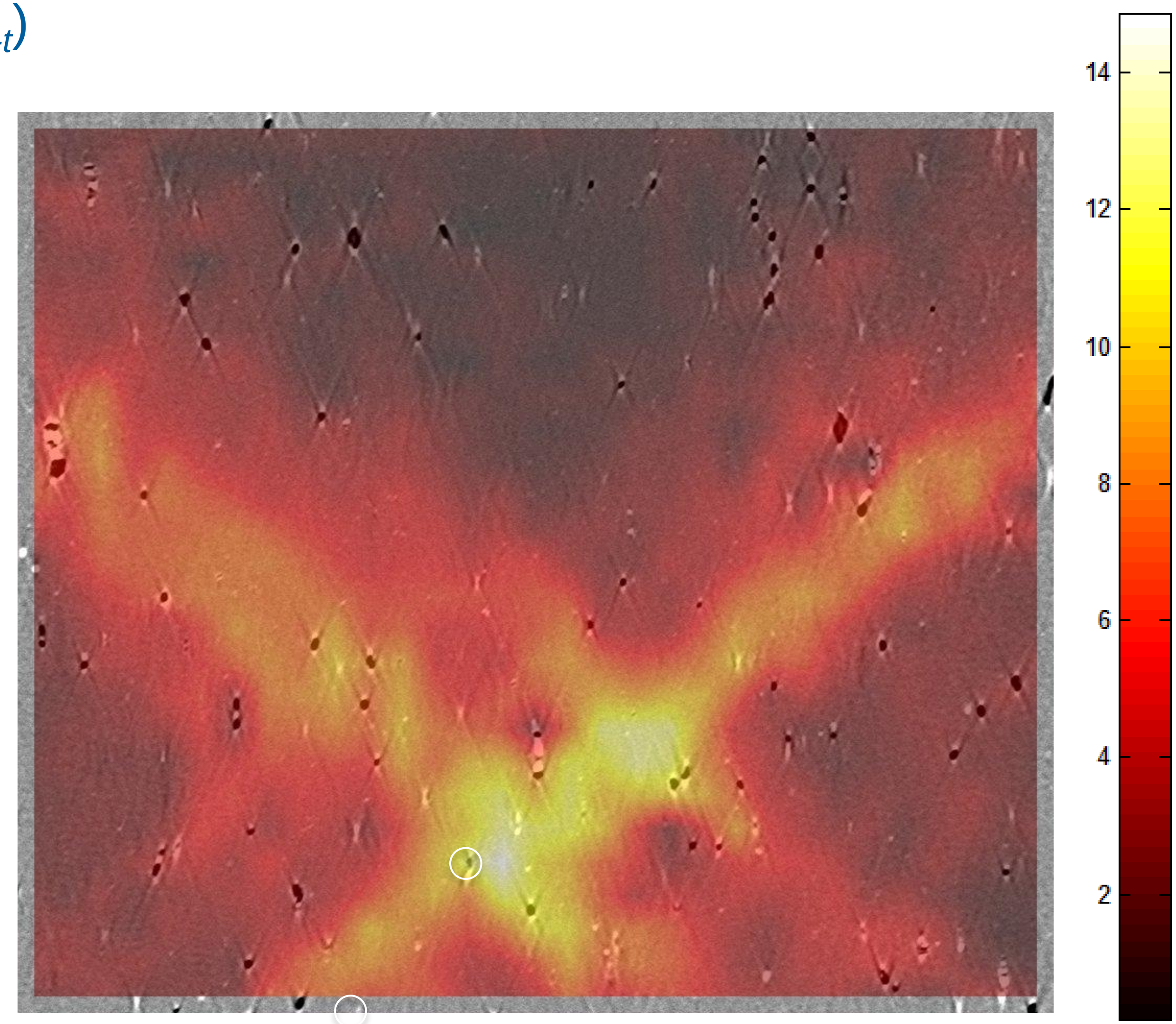

2139 T3: overlay strain + microstructure

Incremental strain: $p_{eq}(u_{t\text{-}u})$

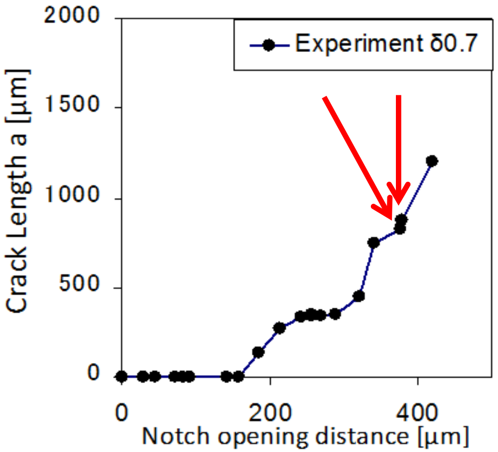

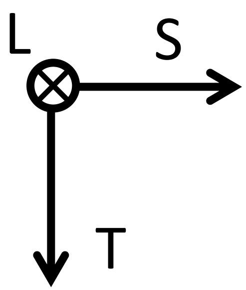

Loading direction

200µm

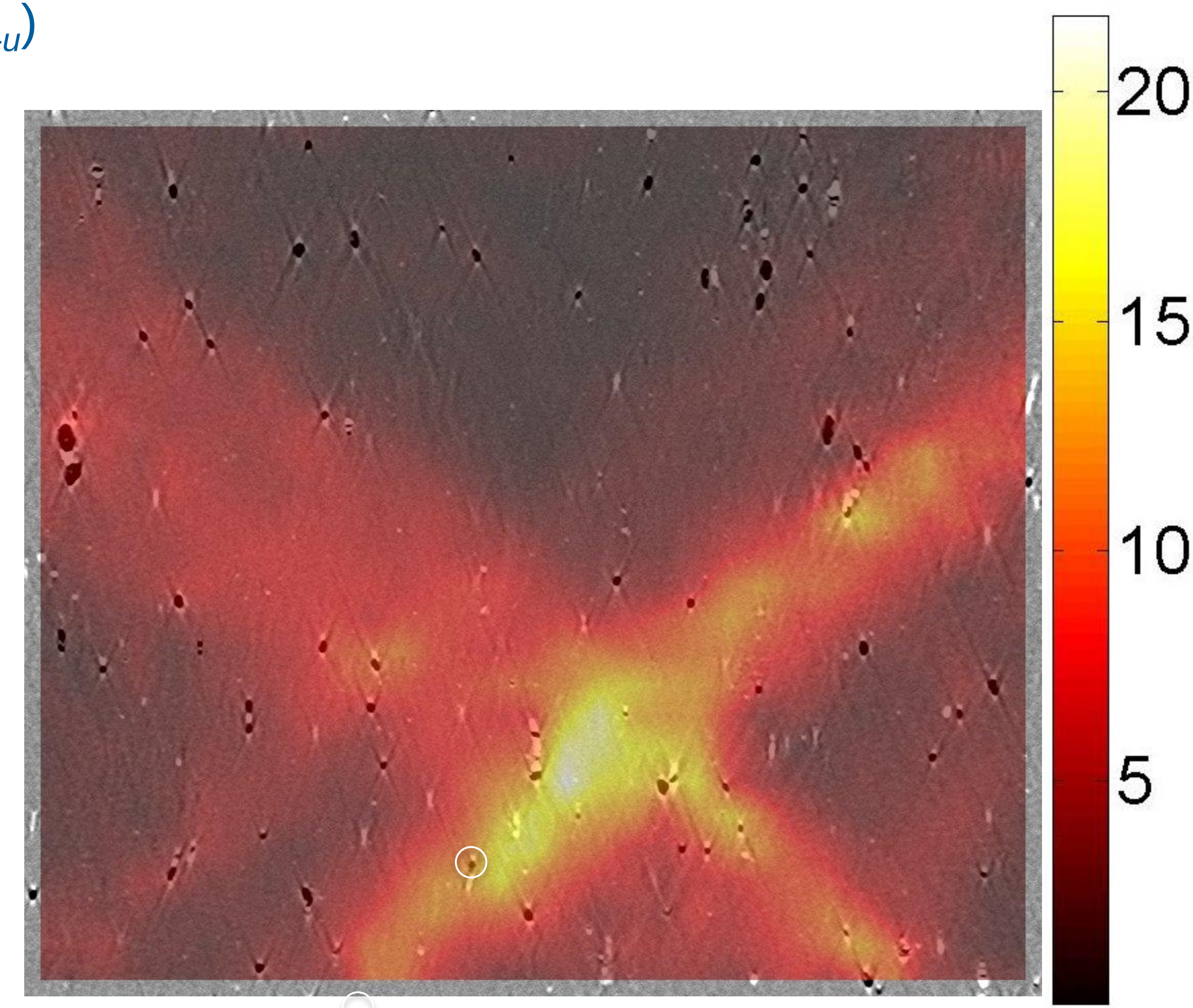

⊗ Crack Propagation

2139 T3: overlay strain + microstructure

Incremental strain: $p_{eq}(u_{u\text{-}v})$

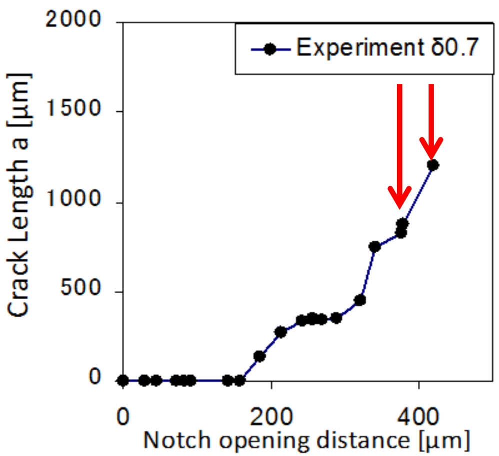

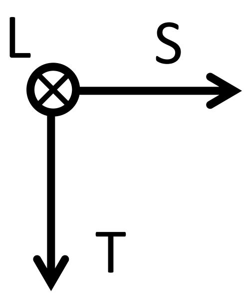

Loading direction

200µm

⊗ Crack Propagation

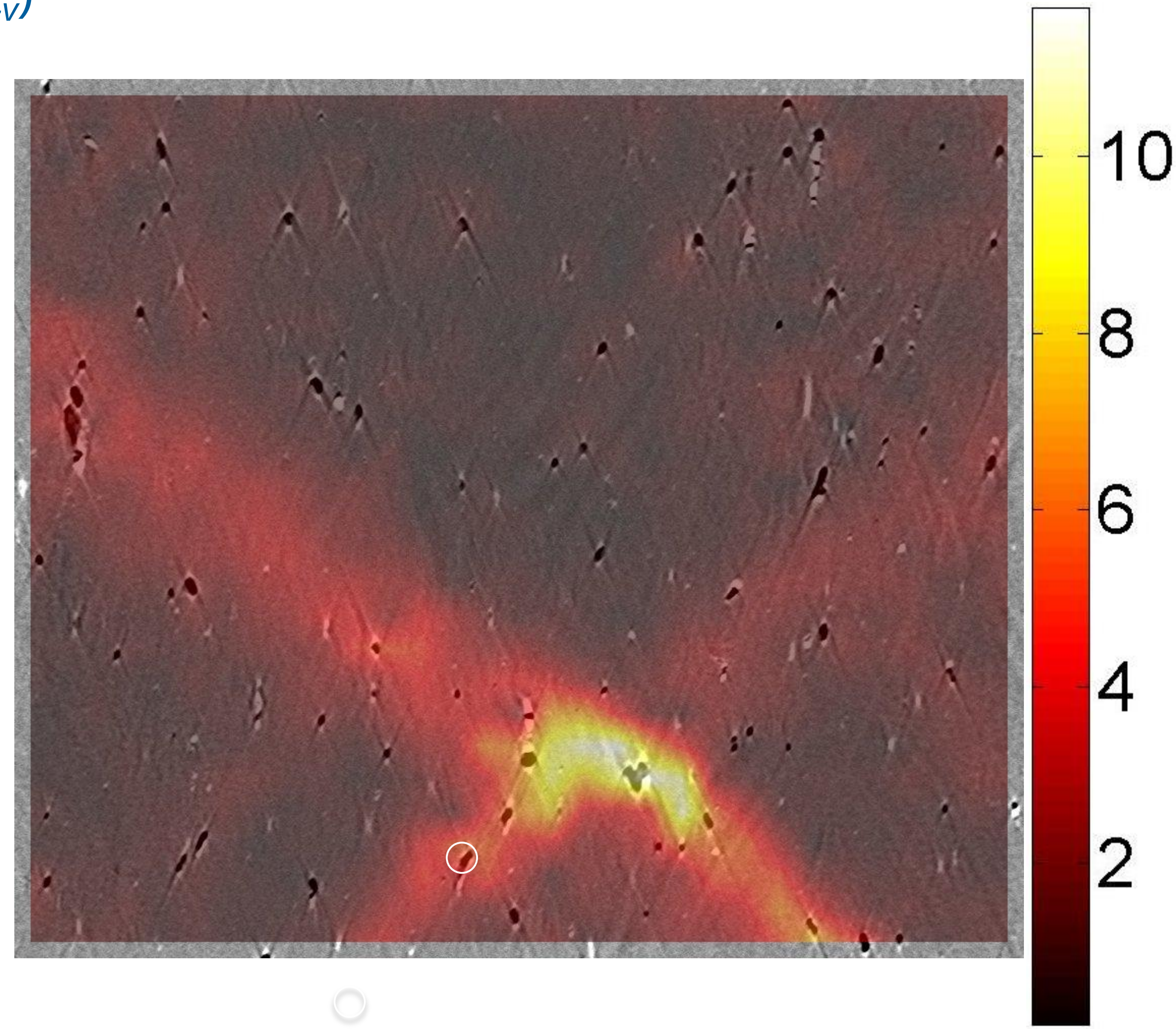

Incremental strain field: 2139 T3

Incremental strain: $p_{eq}(u_{u\text{-}v})$

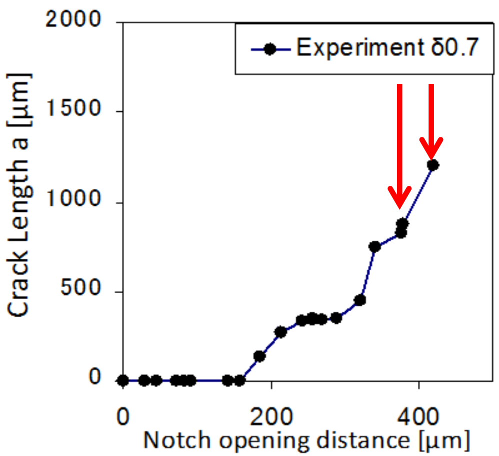

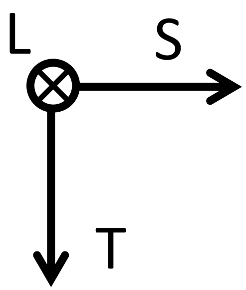

Loading direction

200µm

⊗ Crack Propagation

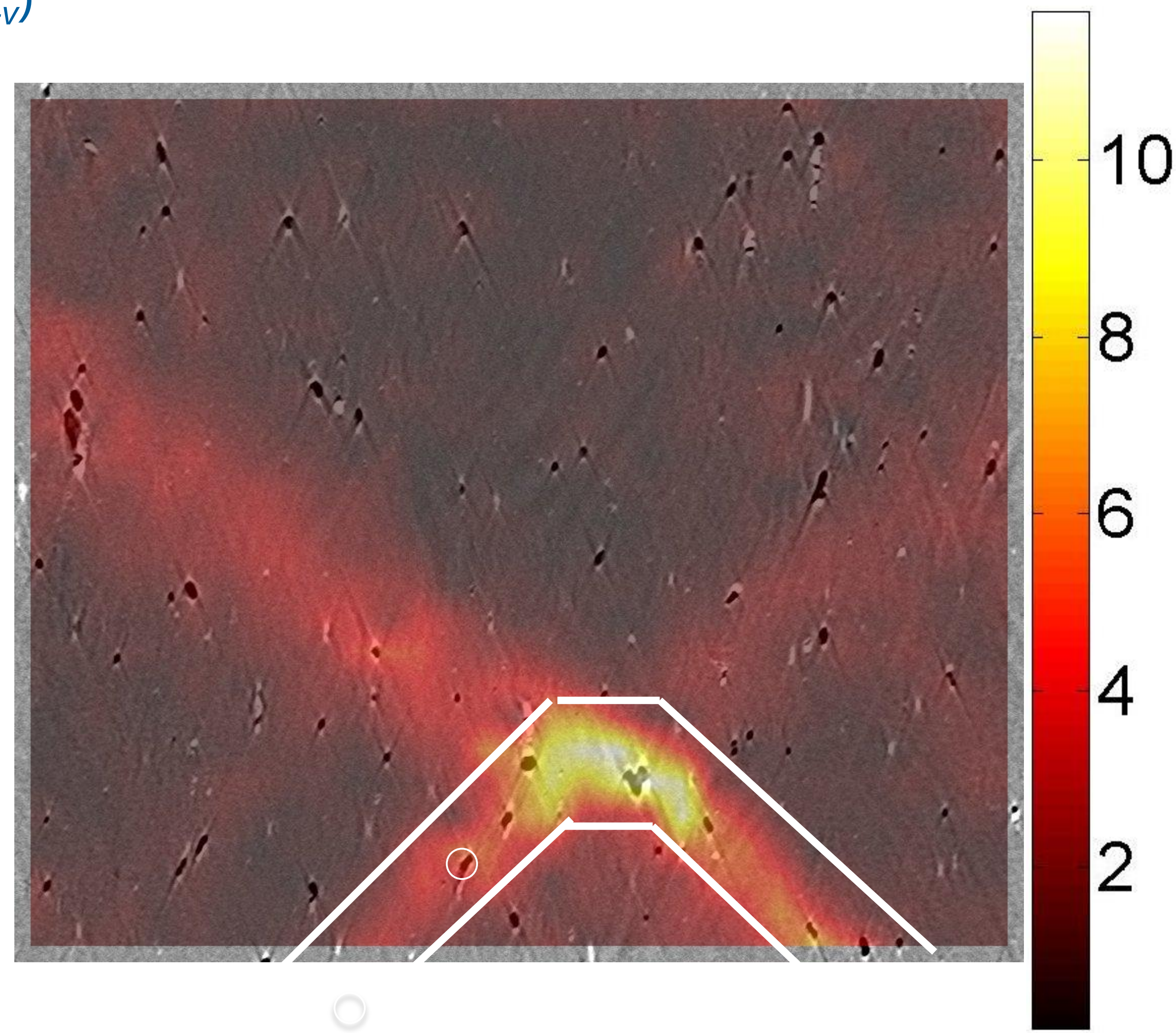

2139 T3: overlay strain + microstructure

Incremental strain: $p_{eq}(u_{v\text{-}w})$

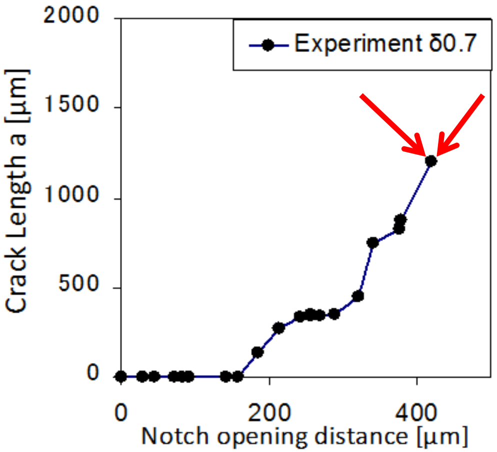

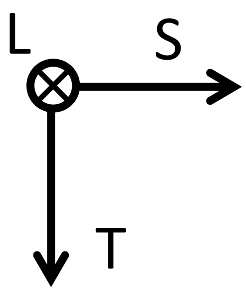

Loading direction

200µm

⊗ Crack Propagation

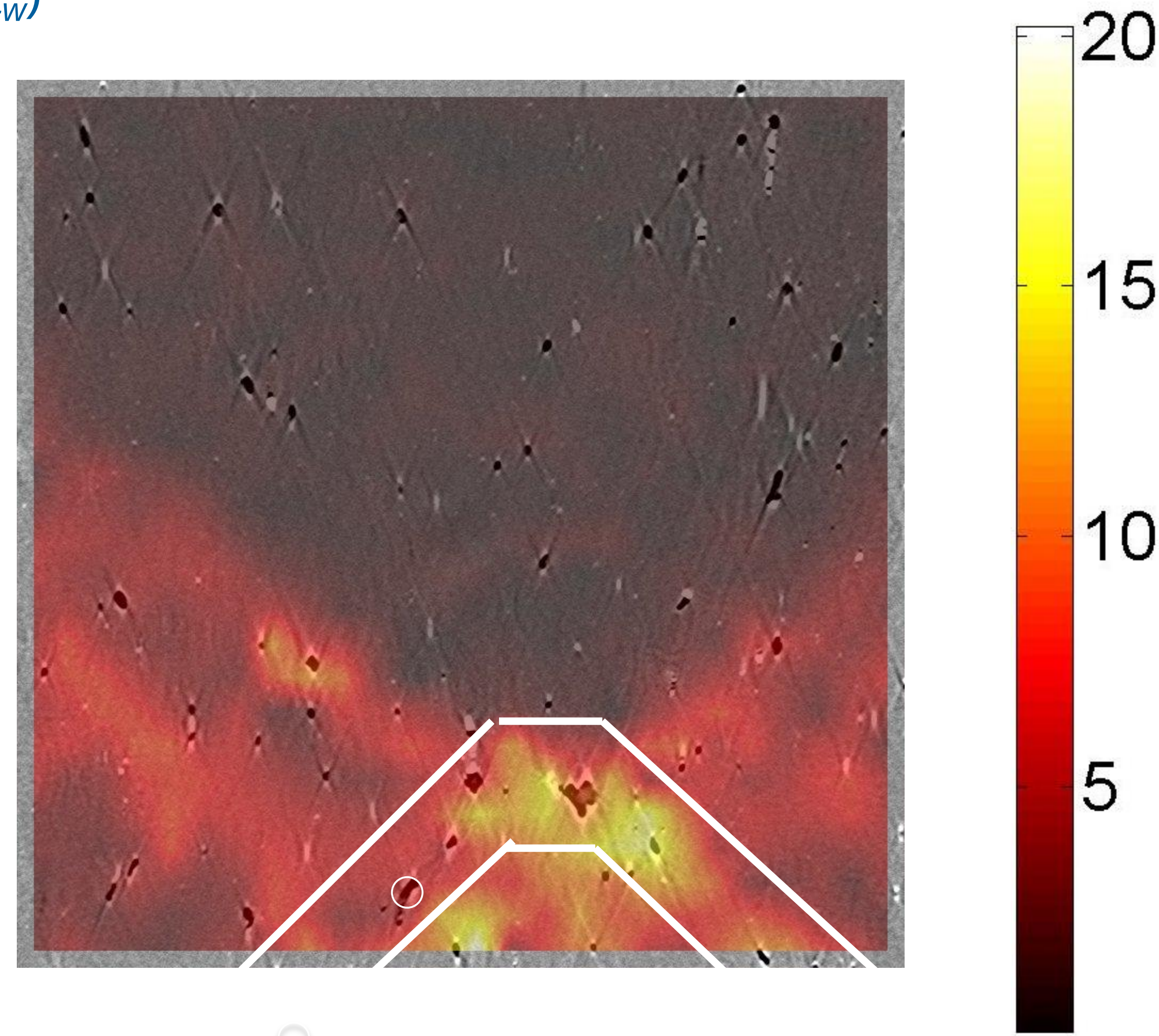

Microstructure: 2139 T3

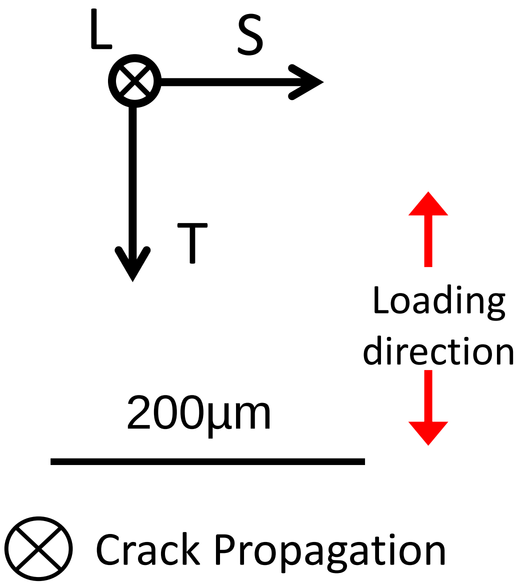

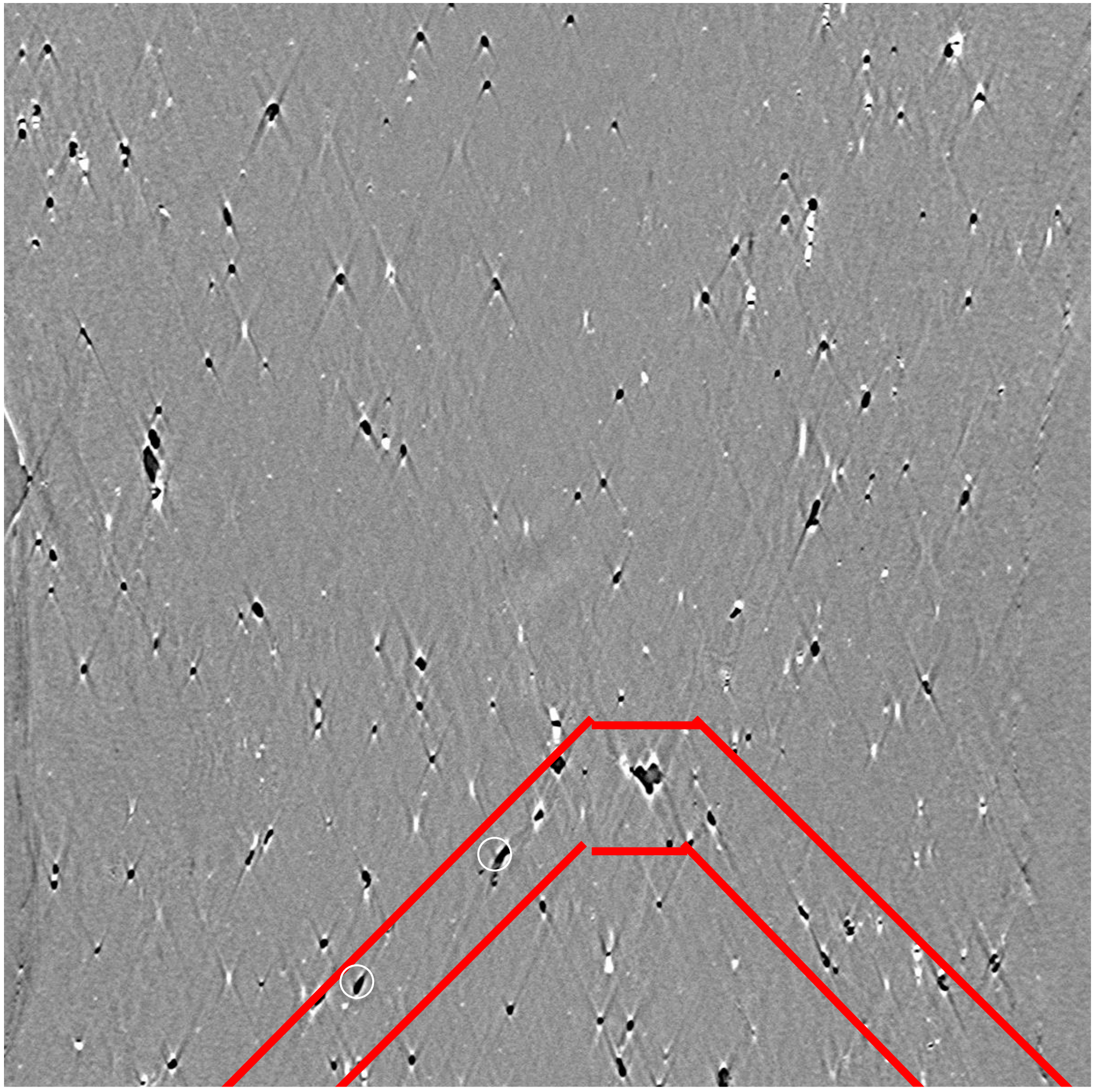

Microstructure: 2139 T3 at fracture

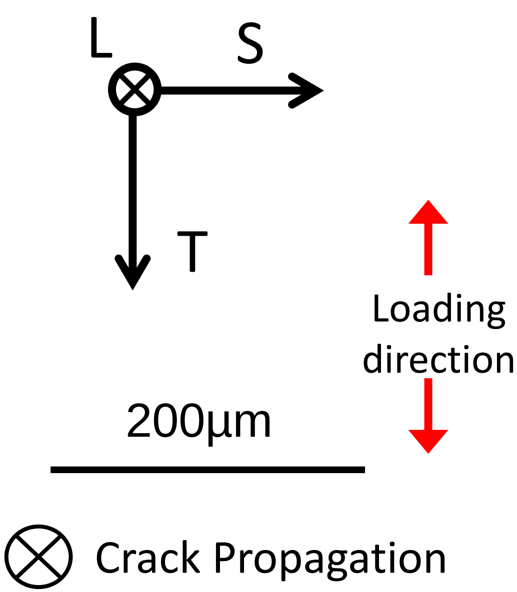

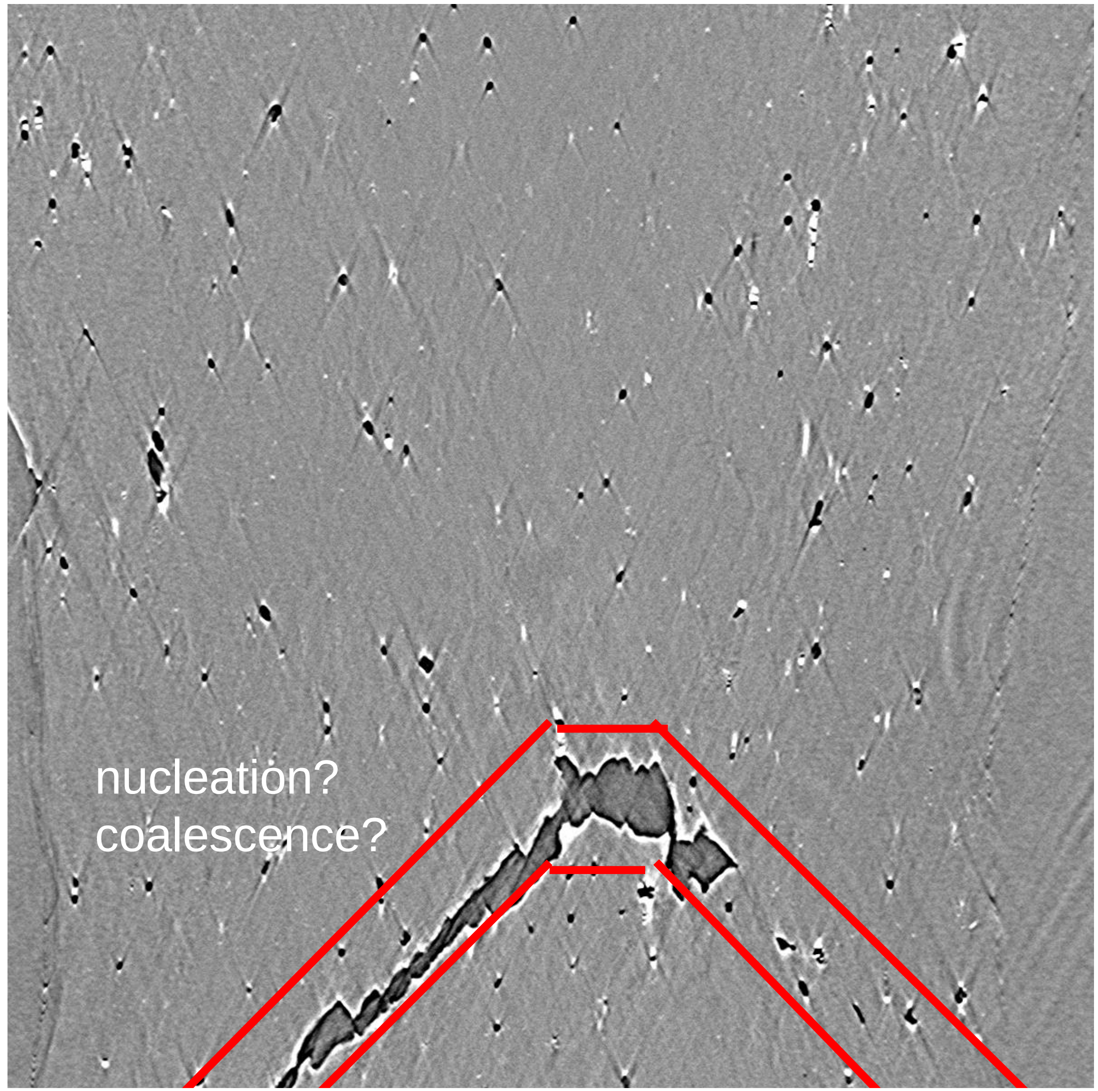

Slant strain bands with intermittent activity precede slant fracture

Strain field for AA2139 T8

AA	2139 (initial voids)		2198 recrystallized (no voids)	
T3	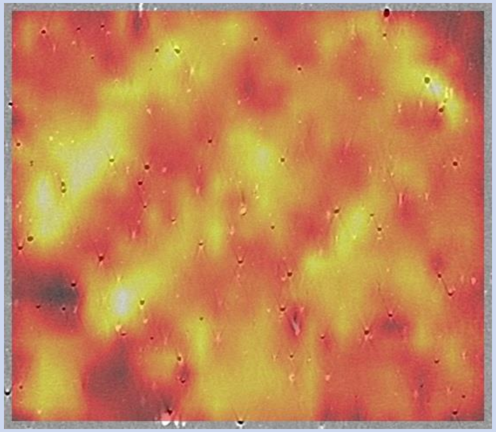 Morgeneyer et al. JMPS 2016	max 4.0 %	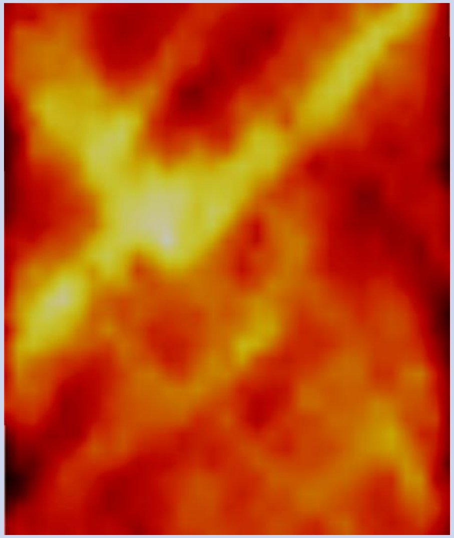	max 3.8 % Buljac et al. Acta Mat 2014
T8	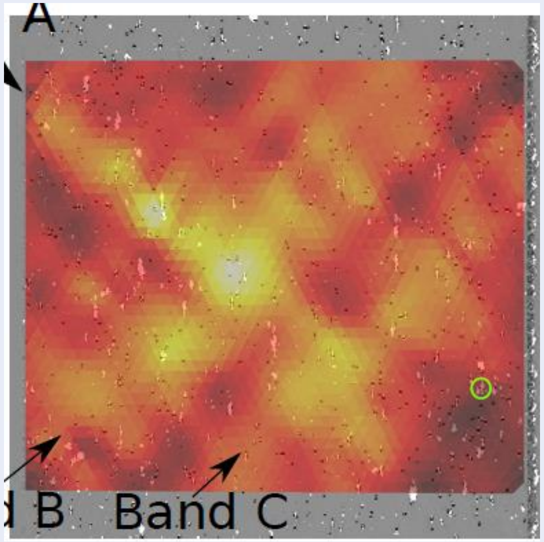 Buljac et al. EJM- A submitted	max 3.3% 1040 µm	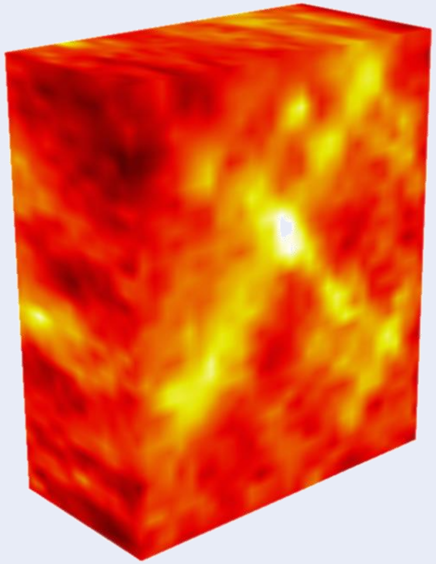 Morgeneyer et al. Acta Mat 2014	max 5 %

All four materials show early slant concentration bands in the slant fracture region

Ductile failure: Perspectives

- Plasticity needs to be reproduced numerically to predict slant fracture
  - Possible localisation origin:
    - Strain rate effects : **Portevin Le Chatelier** !
    - Crystal plasticity and texture
    - Other yield behavior / criteria (*e.g.* Mohr Coulomb)???

Portevin Le Chatelier Effect?

- Steel (Interstitial atoms: C, N), Aluminium alloy (Substitutional atoms: Cu, Li, Mg)

- Dynamic strain ageing: interaction between mobile dislocations and solute diffusion

- Macroscopic manifestation:

  - Temperature and strain rate related;

  - Negative strain rate sensitivity (nSRS);

  - Serrated yielding and localized deformation.

- Consequences

  - Unsightly surface marking;

  - Loss of toughness and ductility.

2198 T3

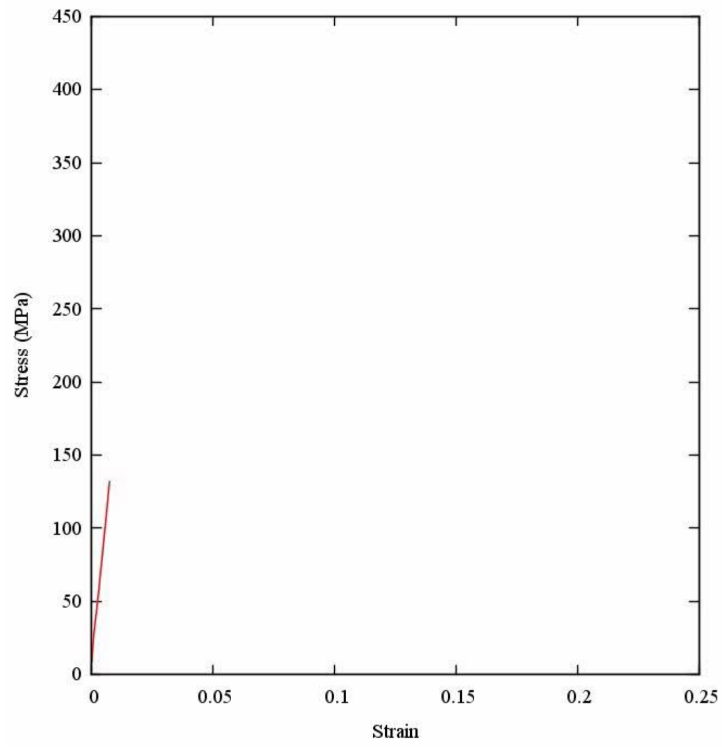

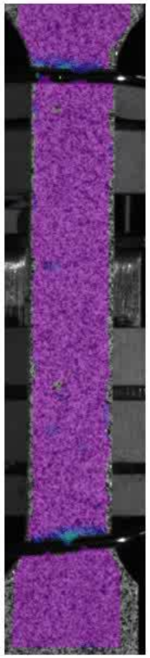

Ren et al Phil Mag. 2019

PLC effect in 2139 T3 triggered by interrupted loading

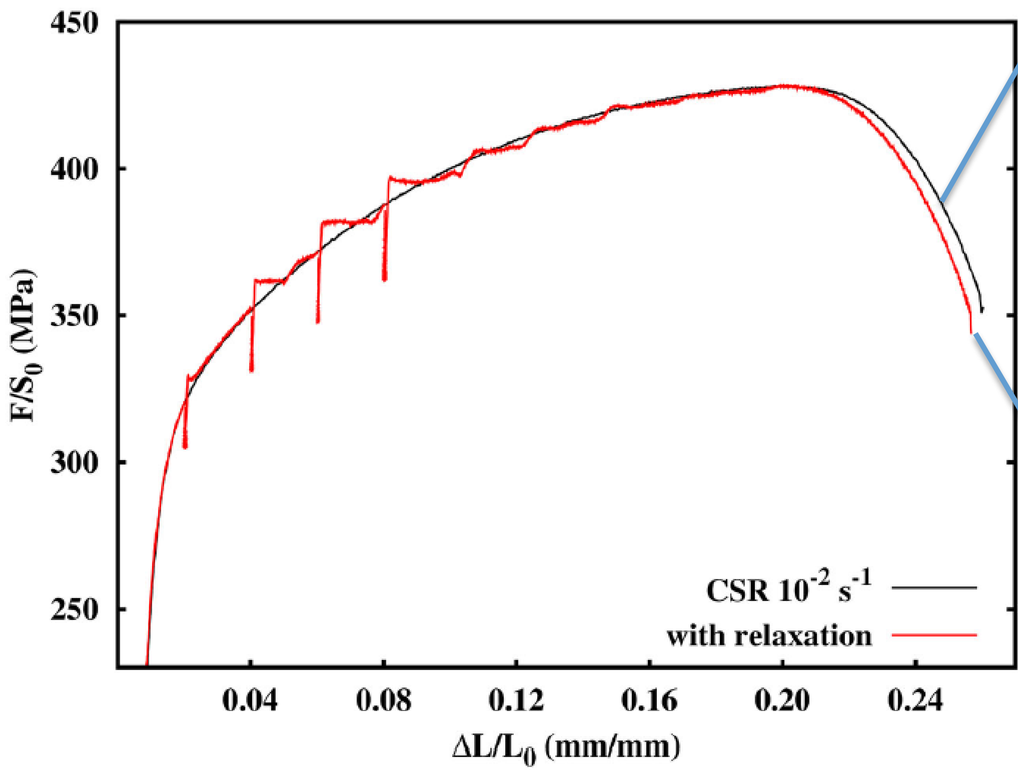

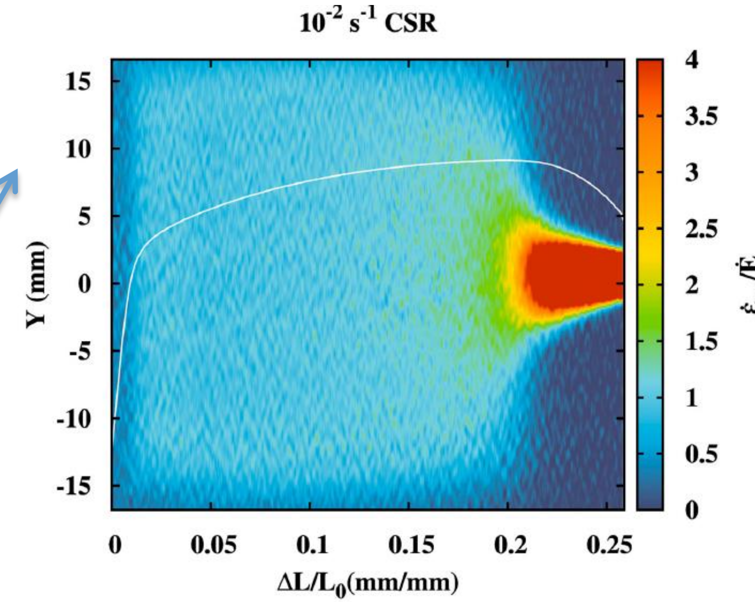

Tests with holding time

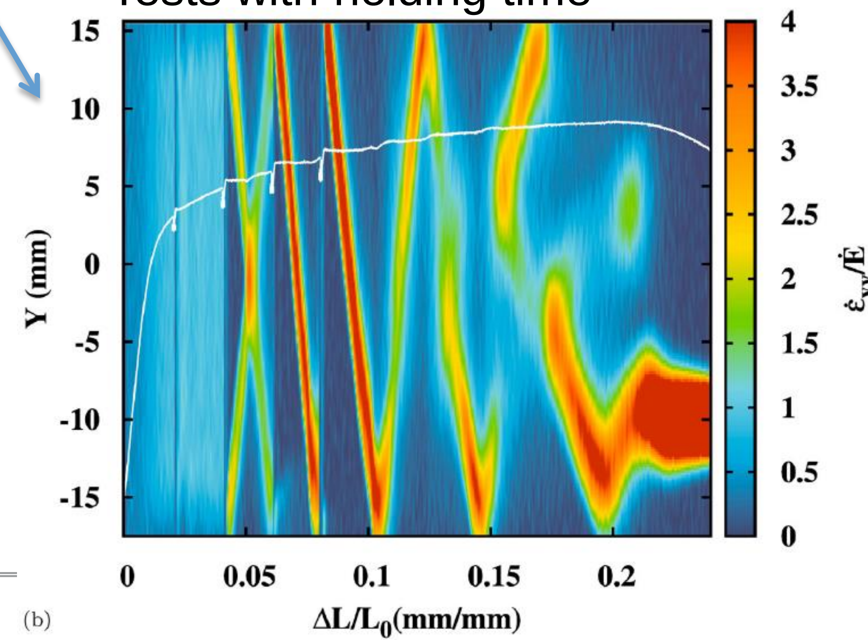

Ren et al Phil Mag. 2019

McCormick + Rousselier model simulations

- Incremental fields : experiment (equivalent strain)

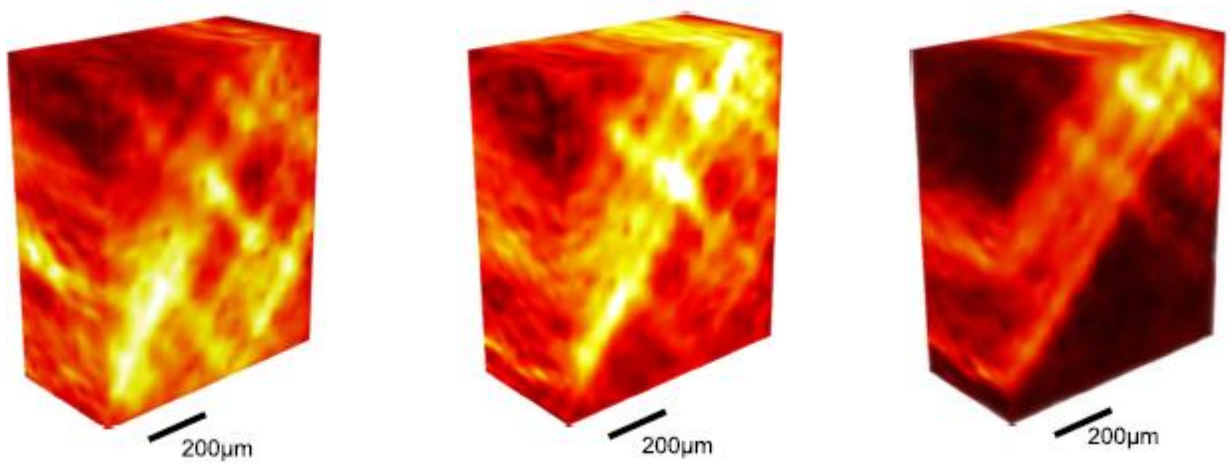

- Simulations

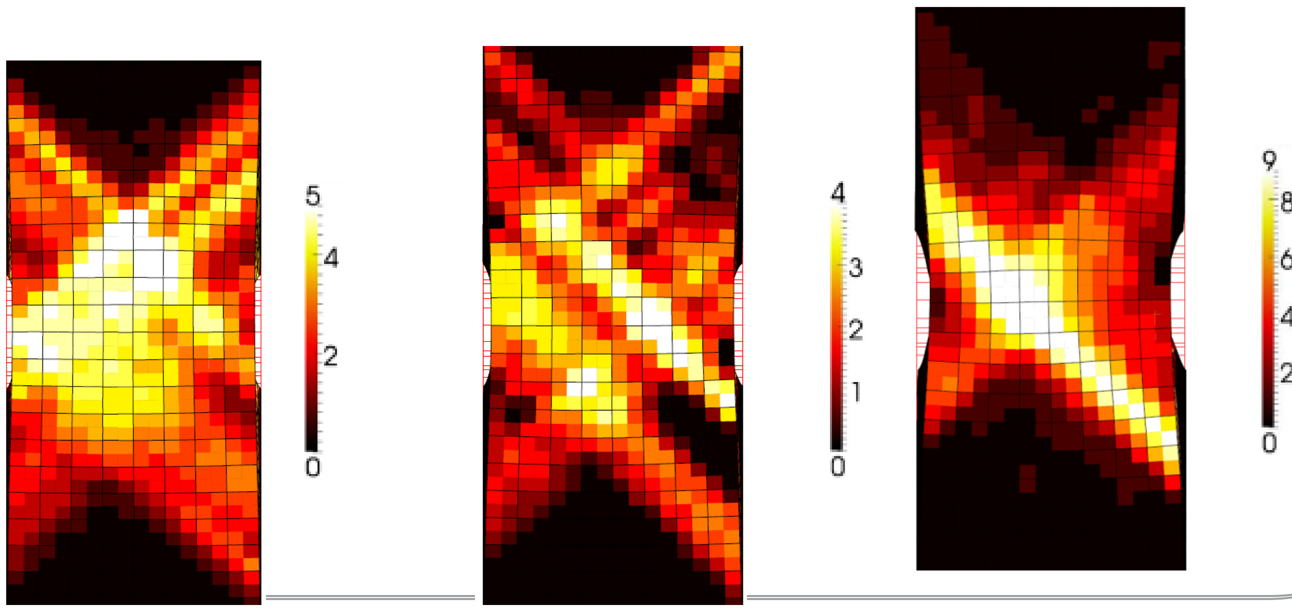

Rousselier et al IJF 2017

Changing loading conditions : shear loading

Experimental Set-up

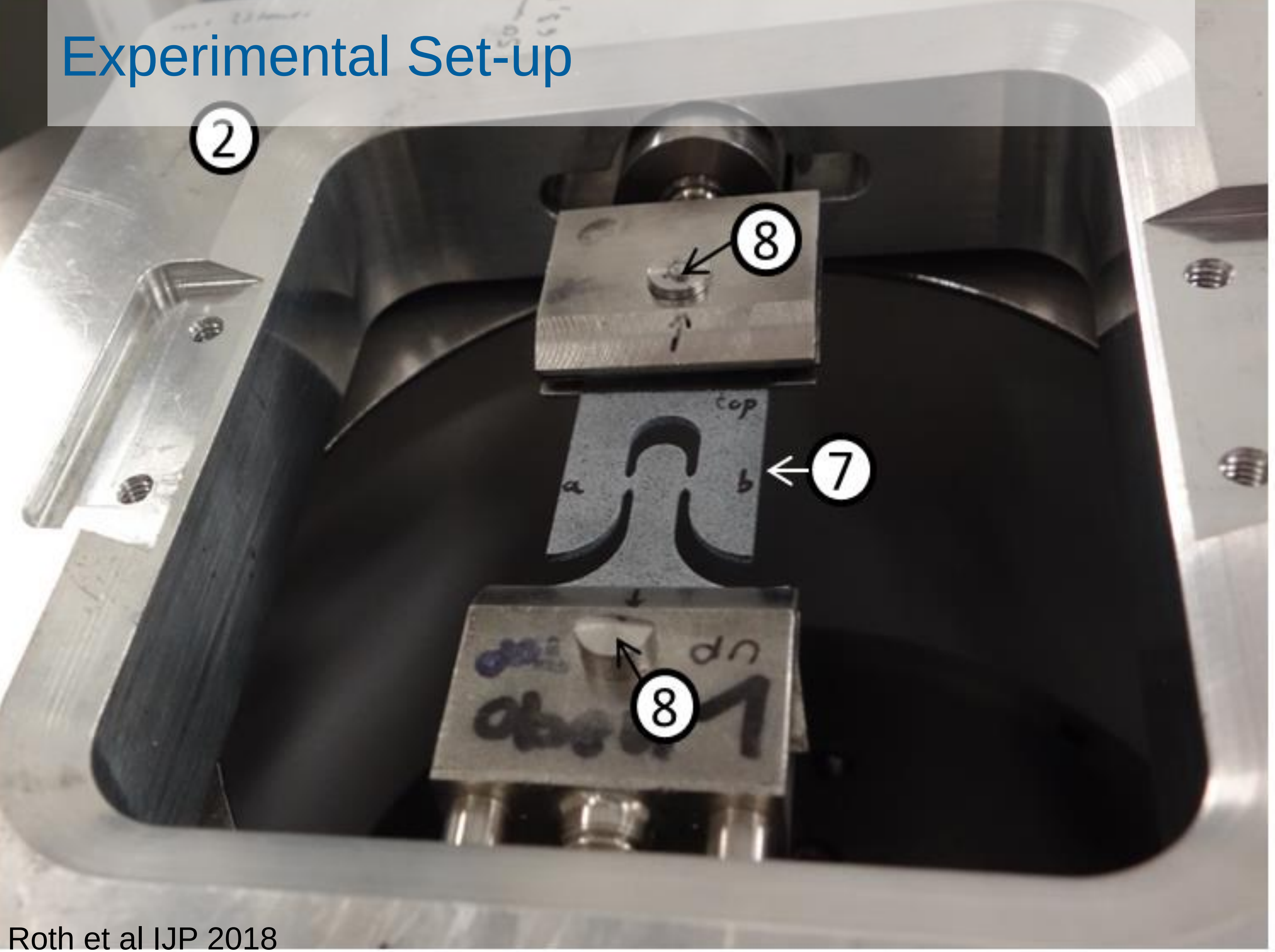

Roth et al IJP 2018

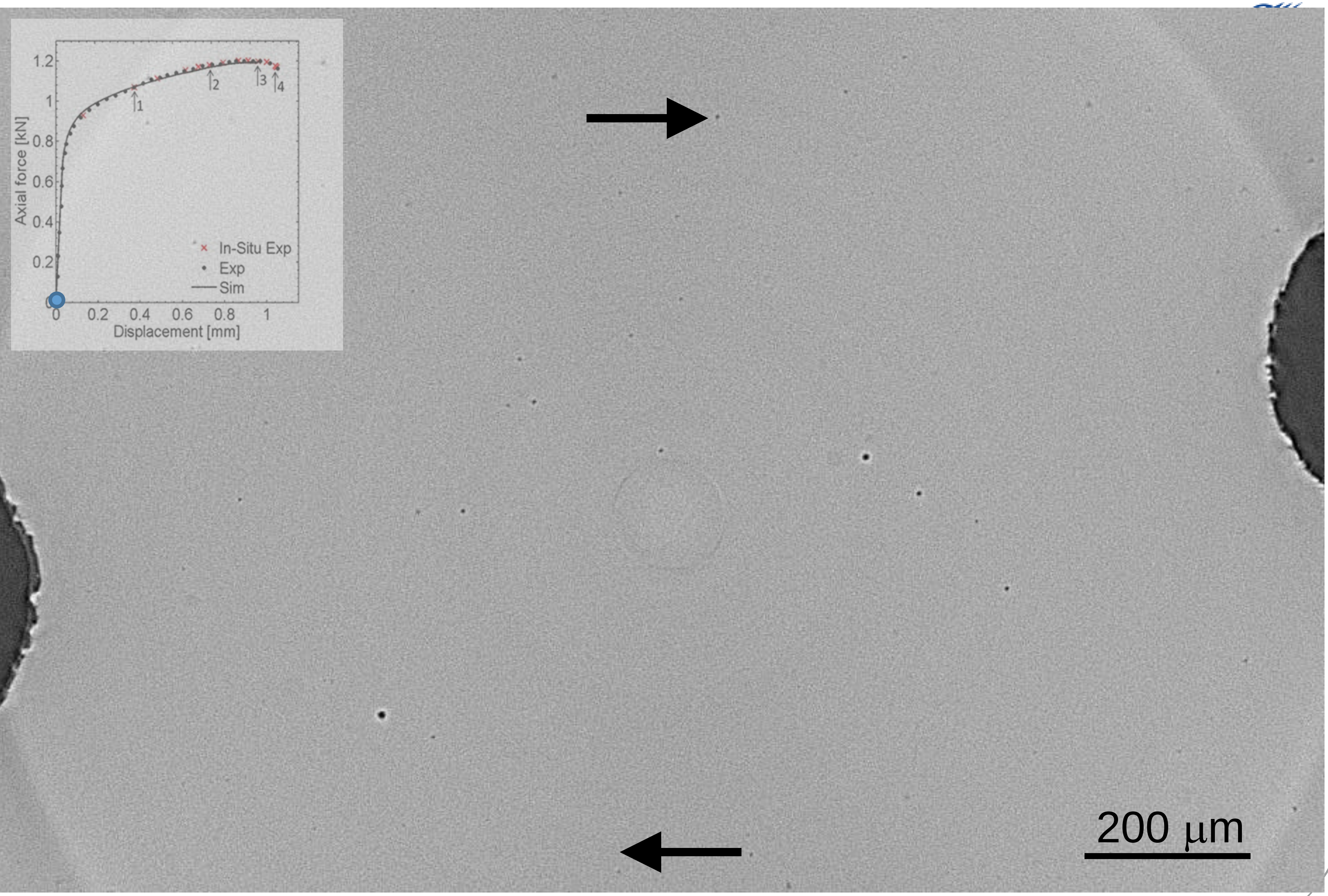

Roth et al IJP 2018

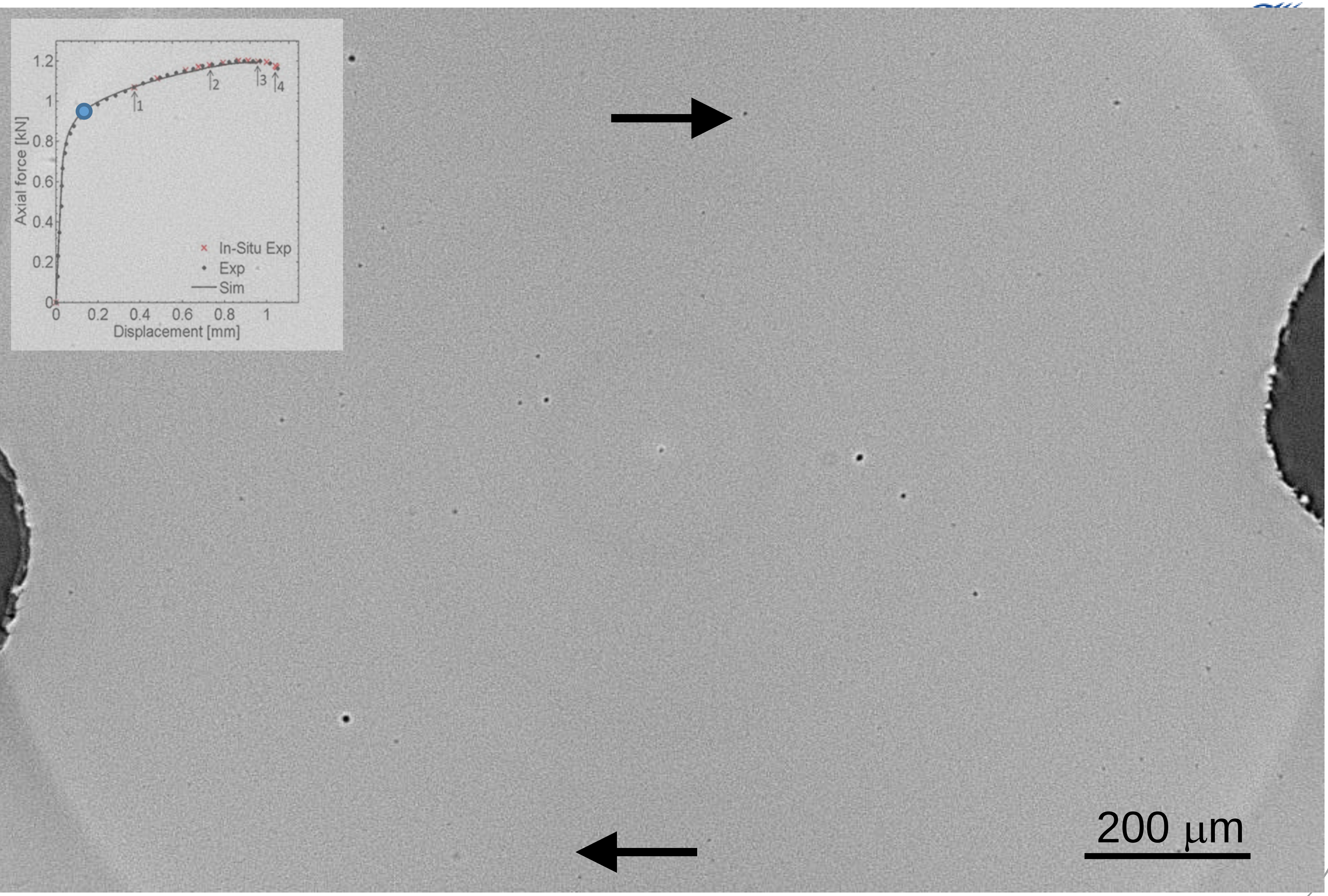

Roth et al IJP 2018

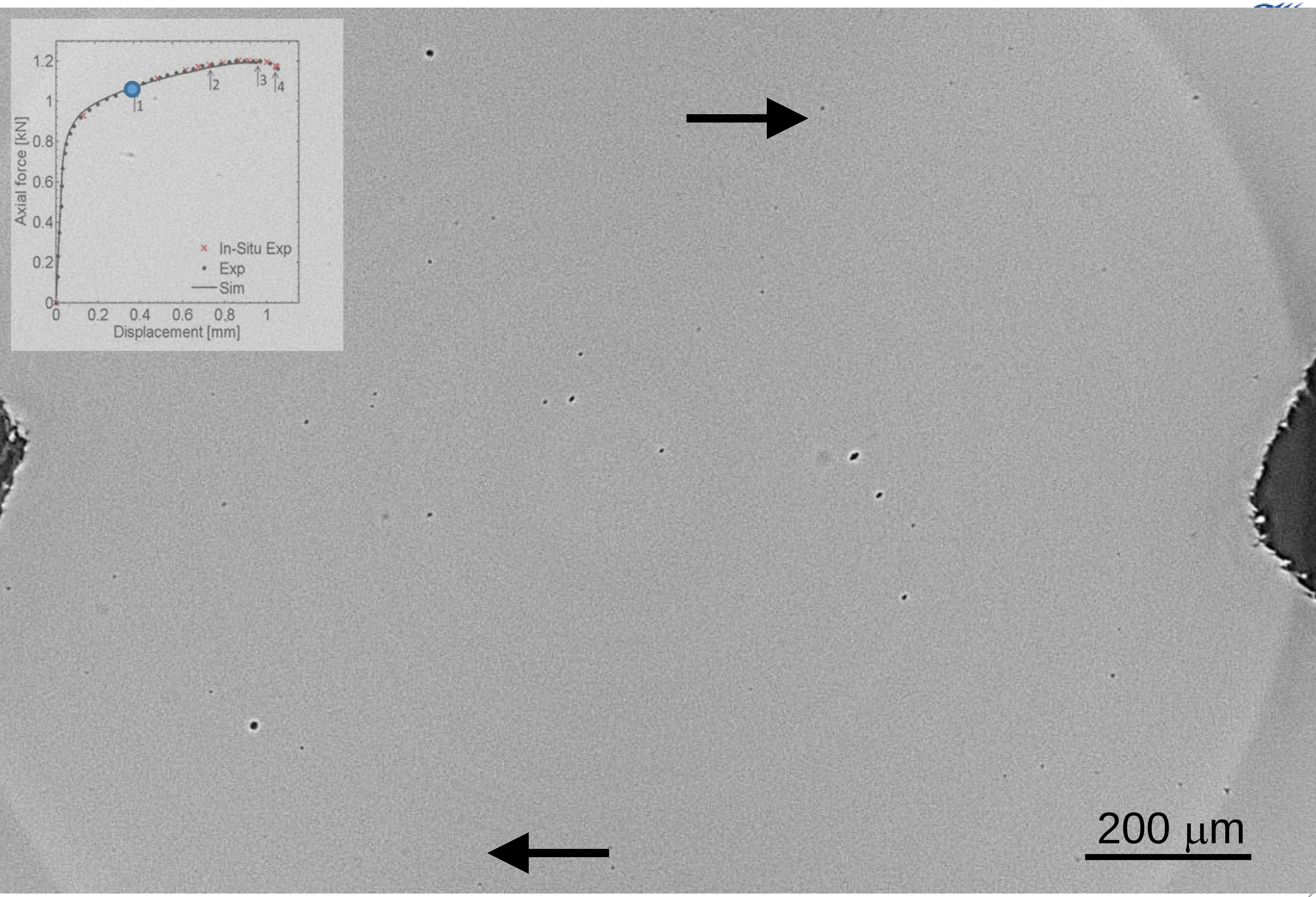

Roth et al IJP 2018

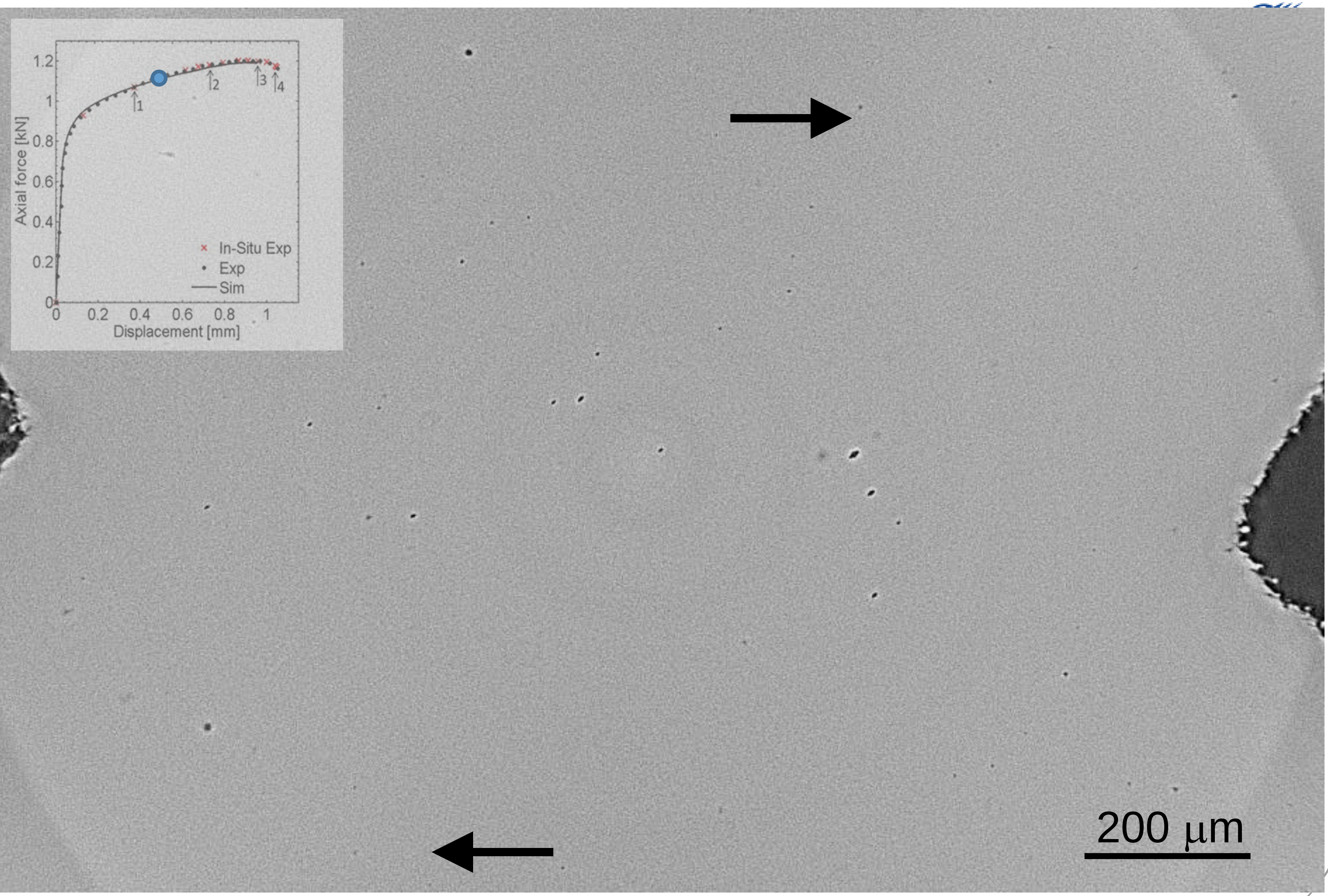

Roth et al IJP 2018

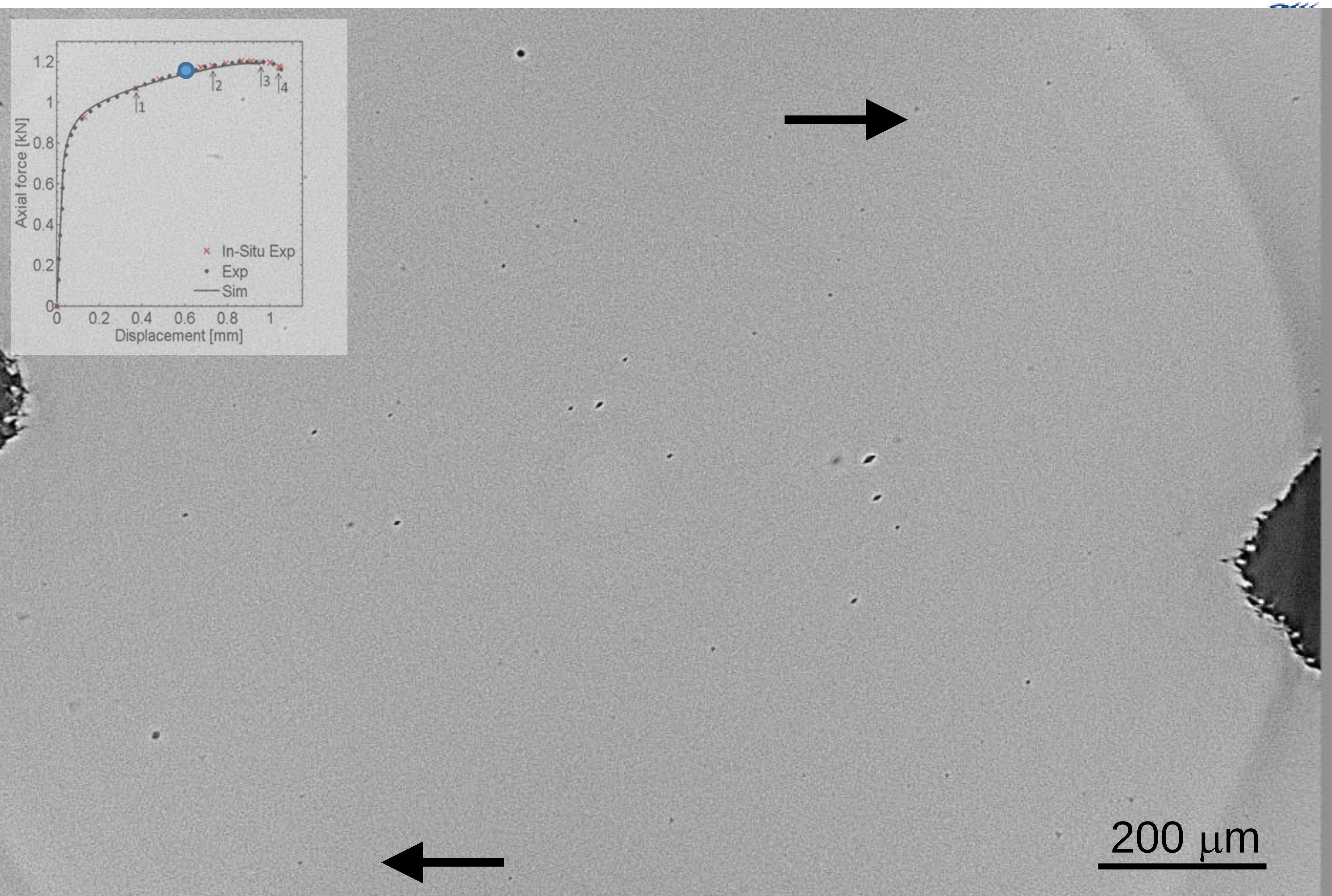

Axial force [kN]
Displacement [mm]
1.2
1
0.8
0.6
0.4
0.2
0
0.2
0.4
0.6
0.8
1
1
2
3
4
In-Situ Exp
Exp
Sim
200 µm

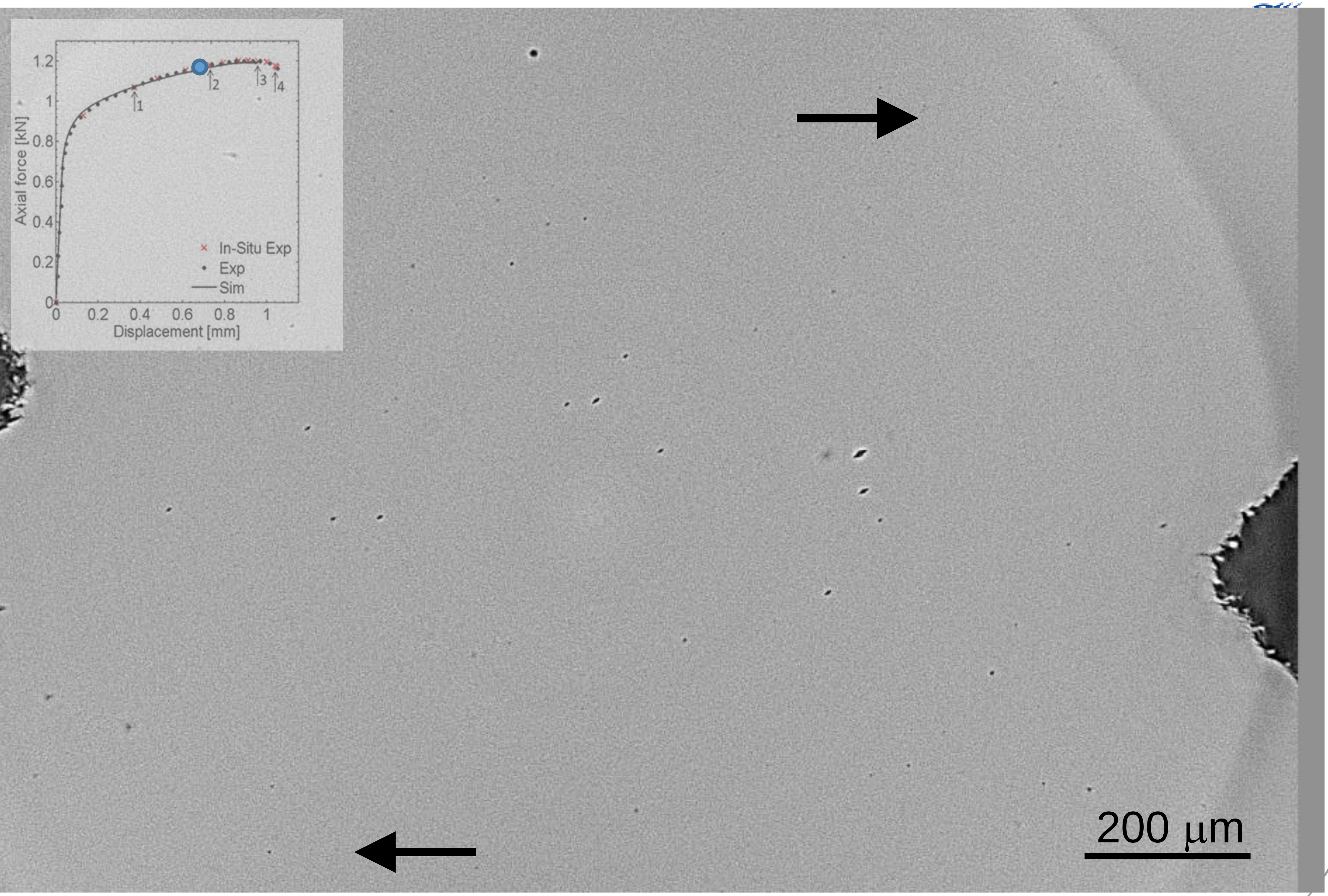

Axial force [kN]
Displacement [mm]
In-Situ Exp
Exp
Sim
1
2
3
4
200 µm

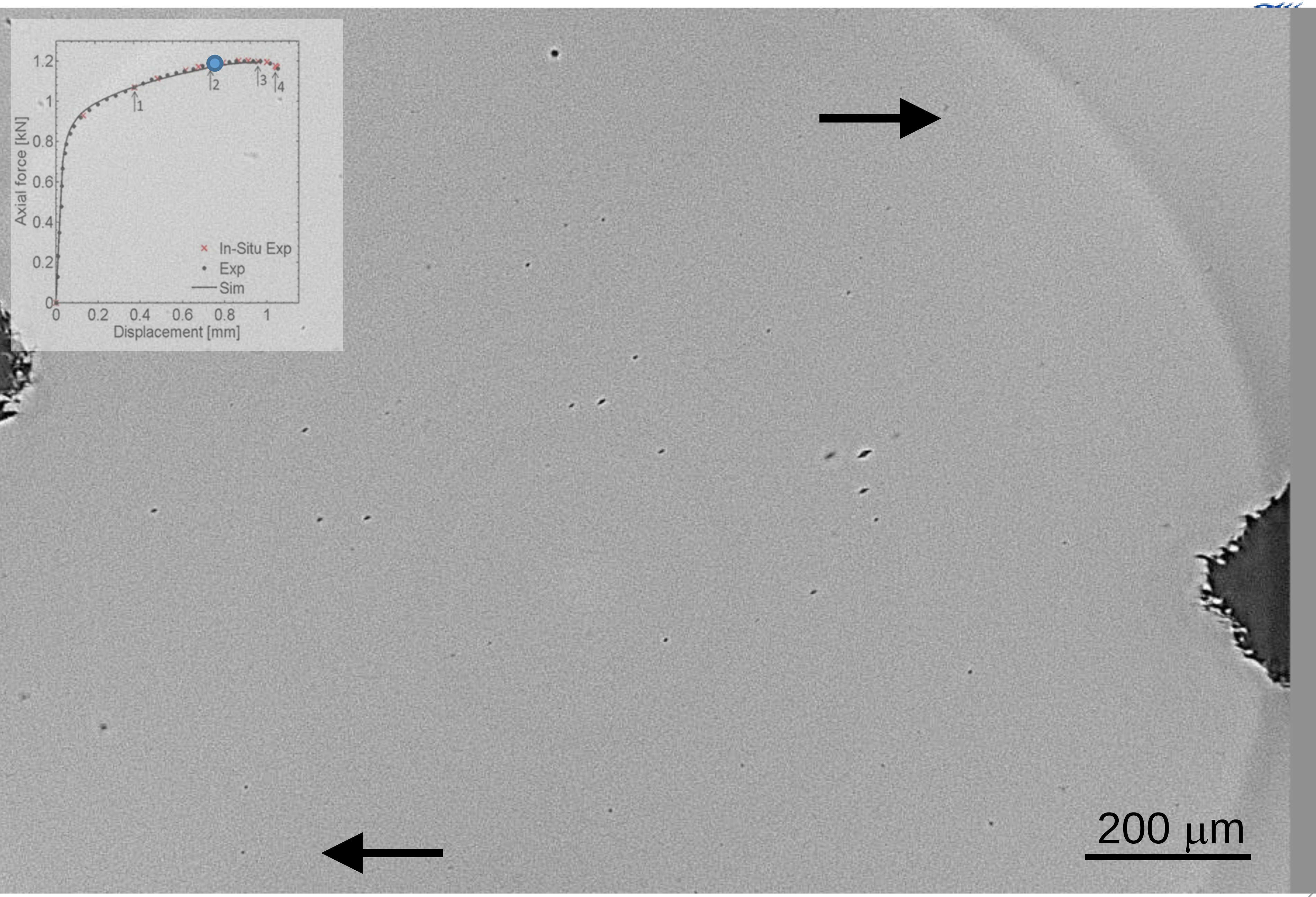

Roth et al IJP 2018

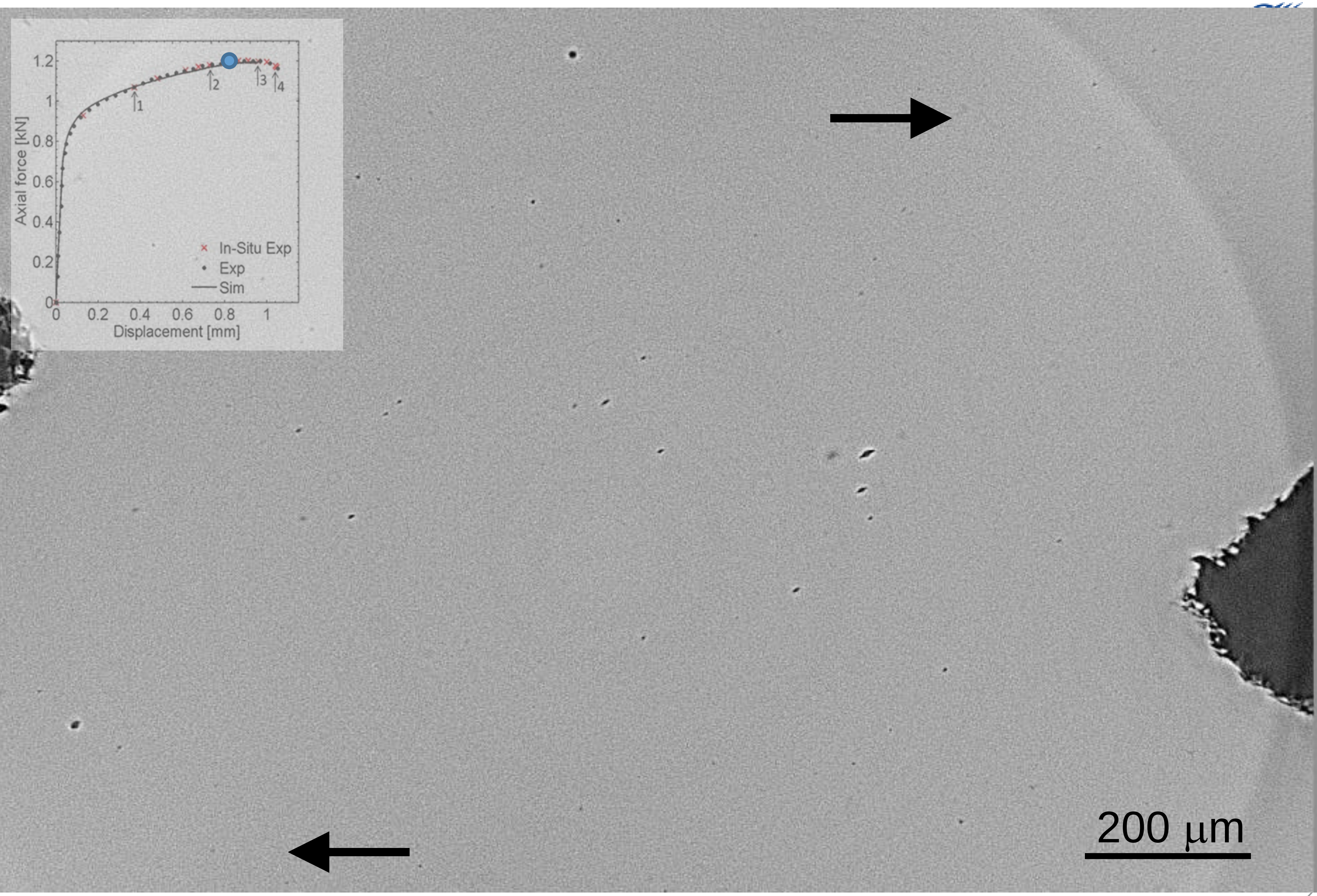

Roth et al IJP 2018

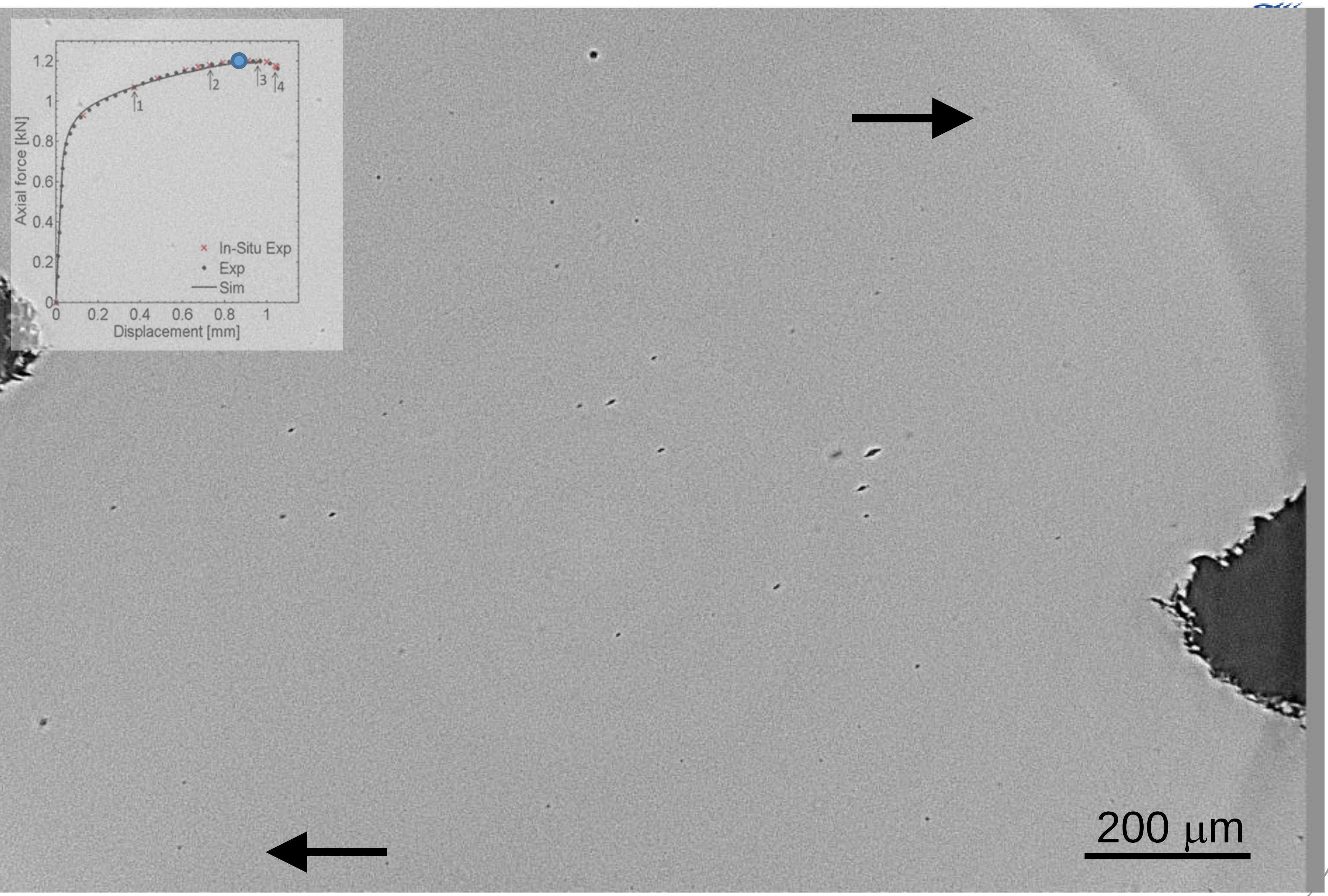

Roth et al IJP 2018

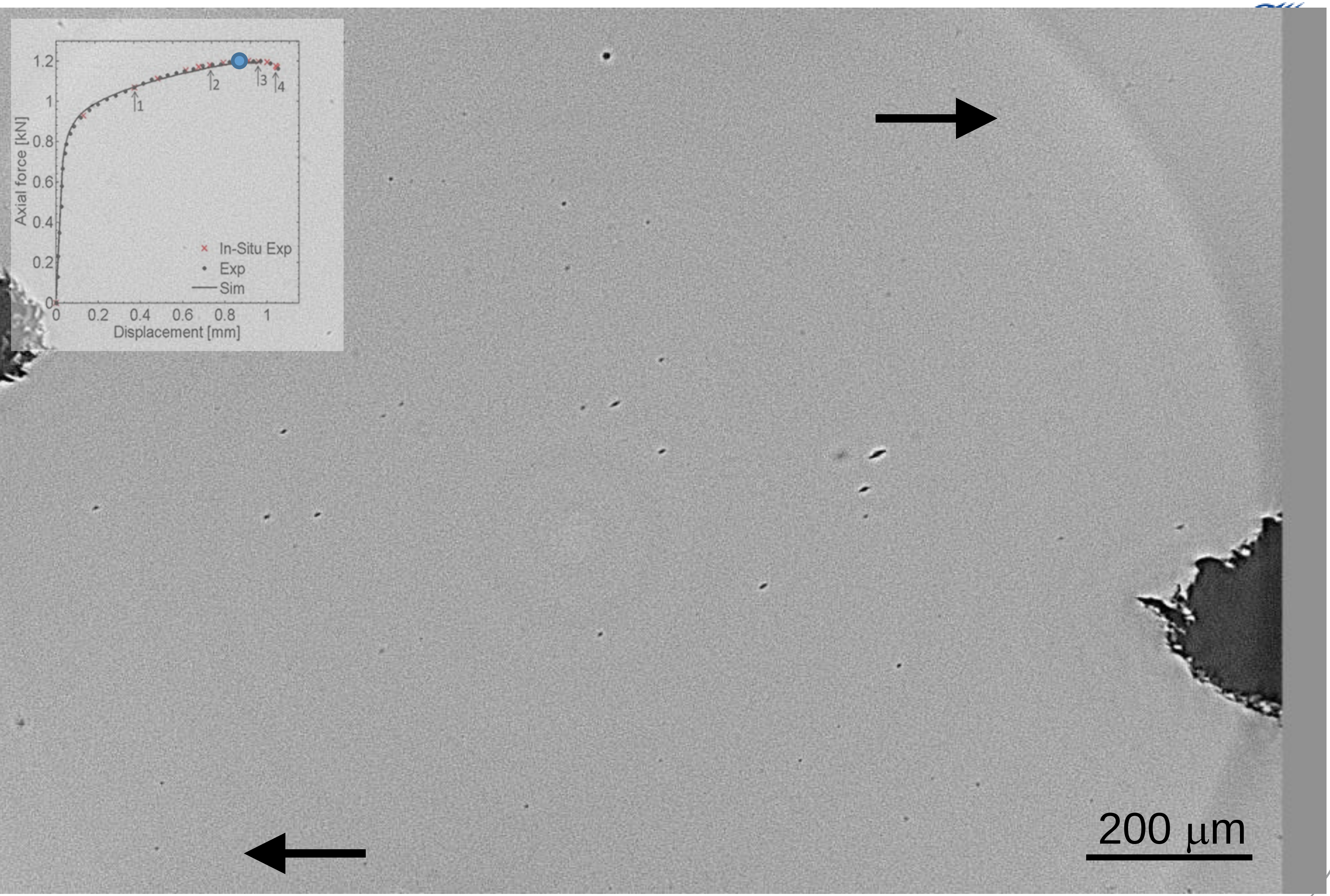

Roth et al IJP 2018

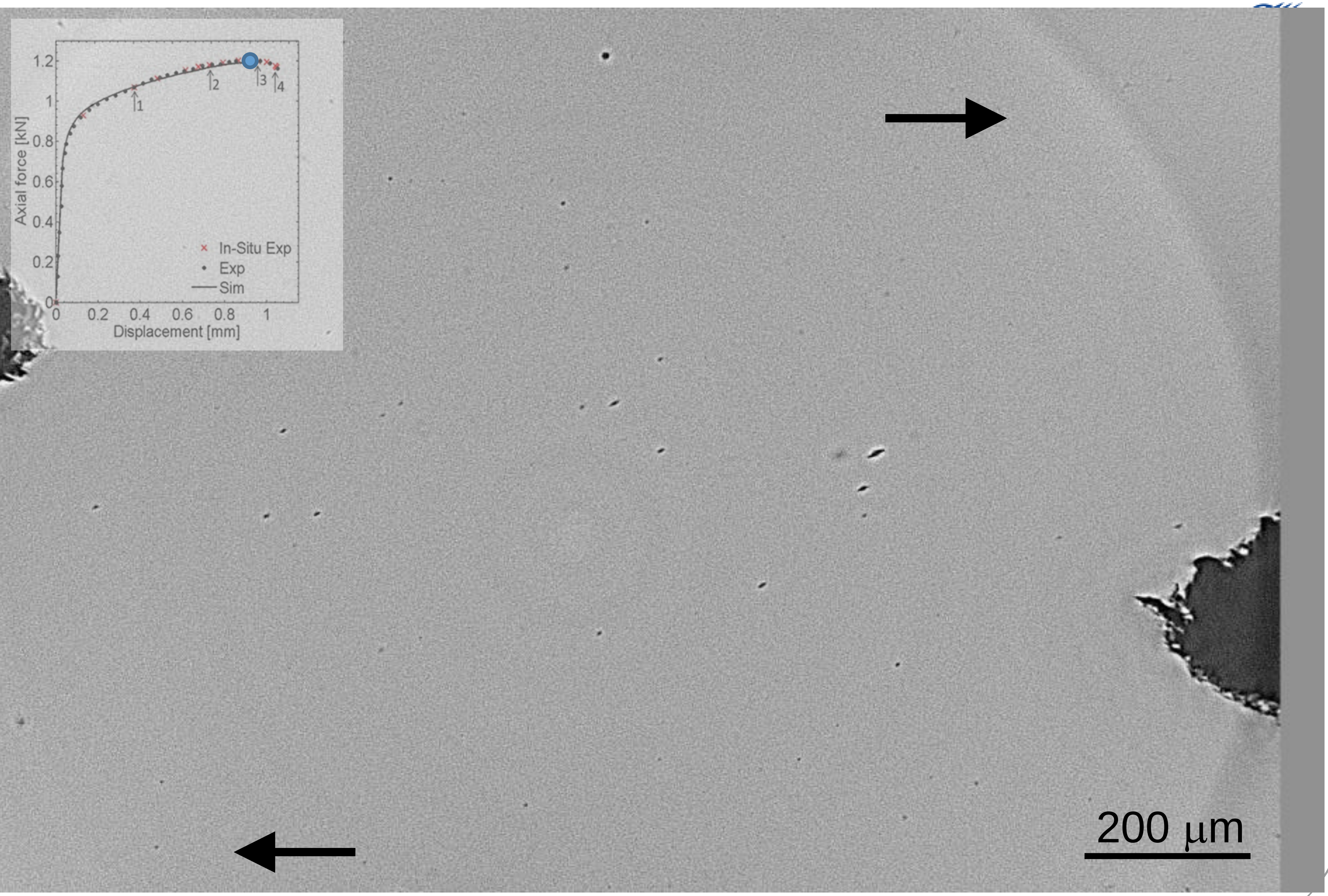

Roth et al IJP 2018

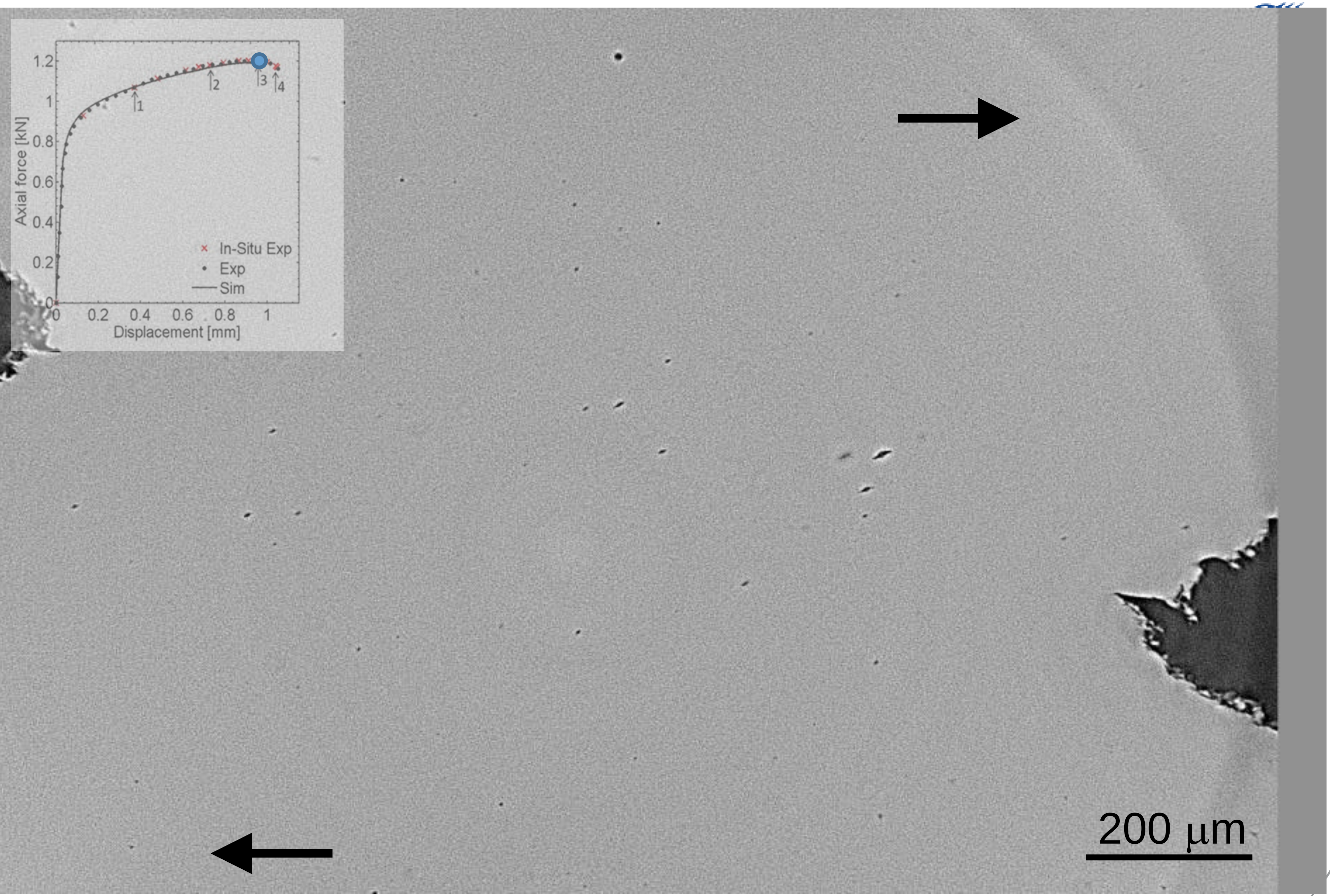

Roth et al IJP 2018

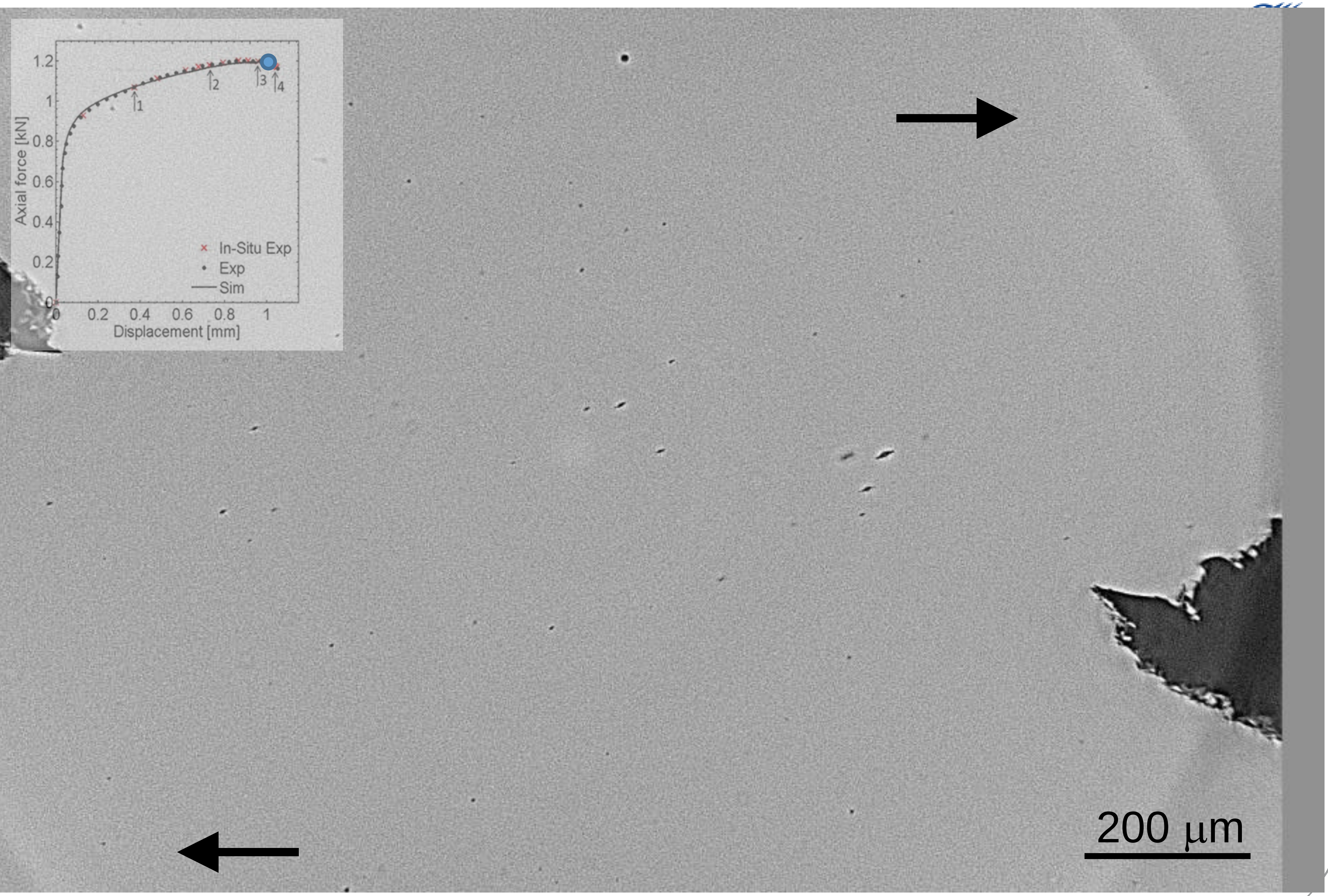

Roth et al IJP 2018

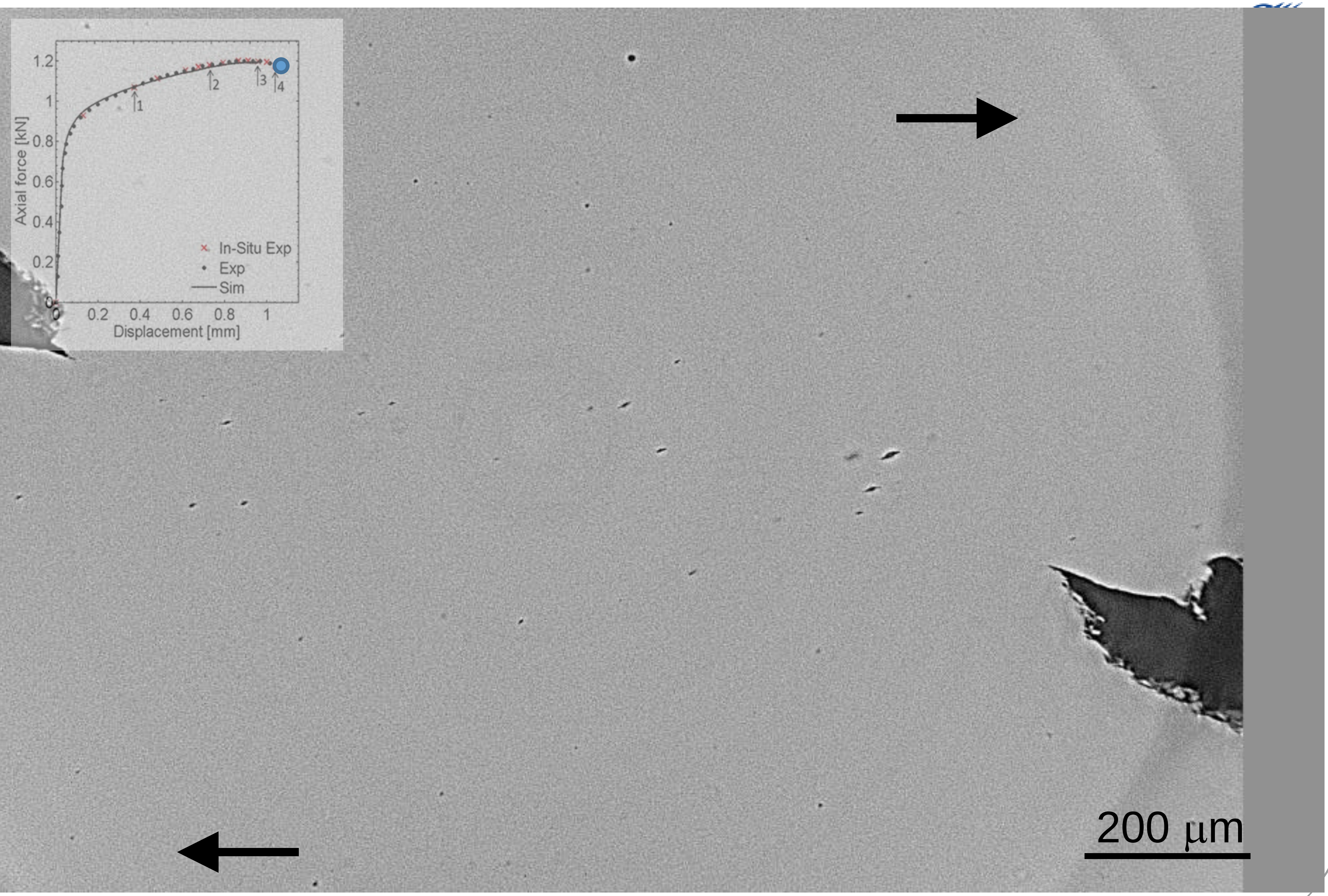

Roth et al IJP 2018

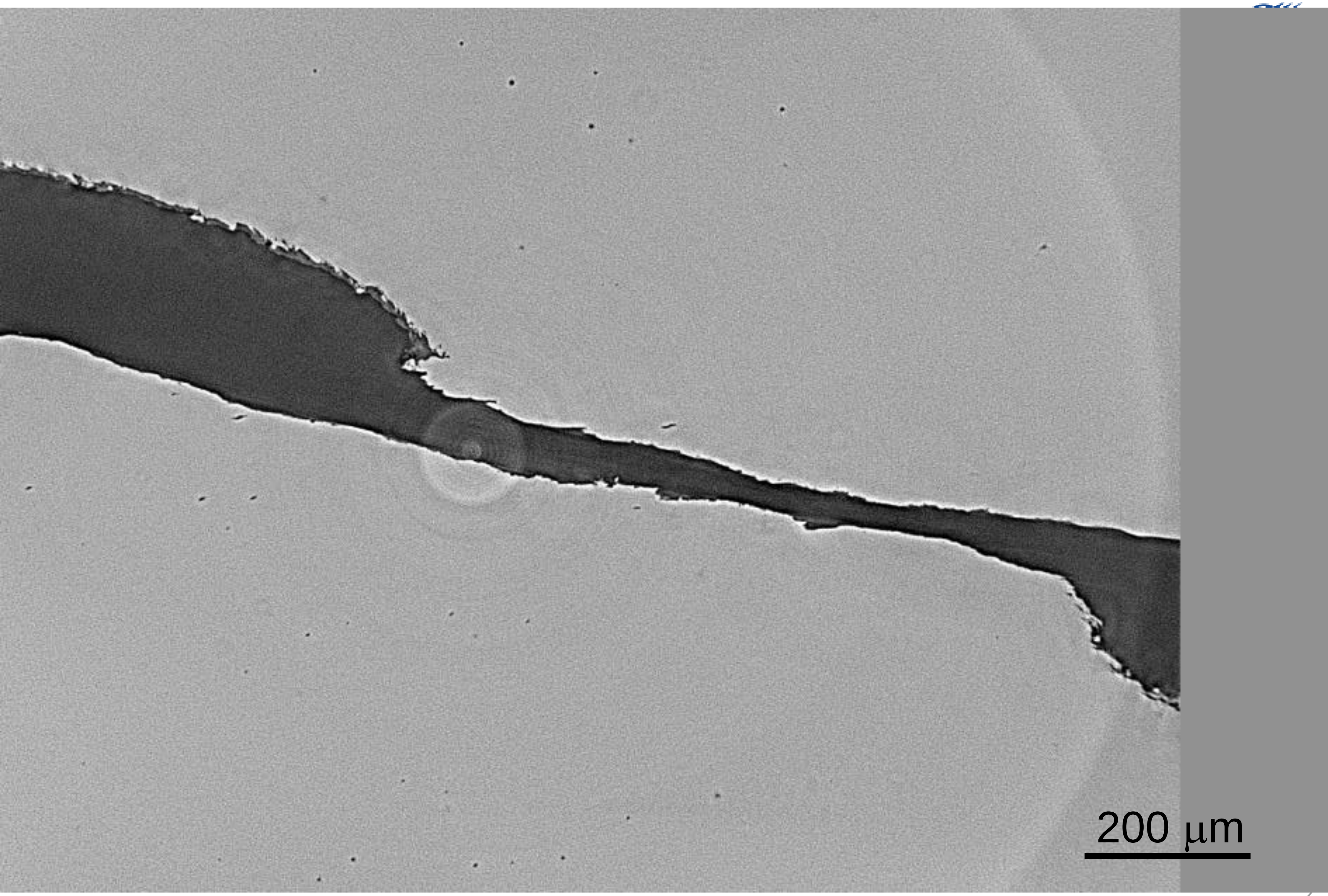

Roth et al IJP 2018

Damage mechanism

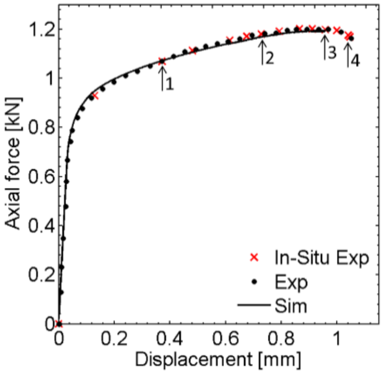

Particle debonding → Void growth along direction of max. principal stress → Nucleation of microcracks

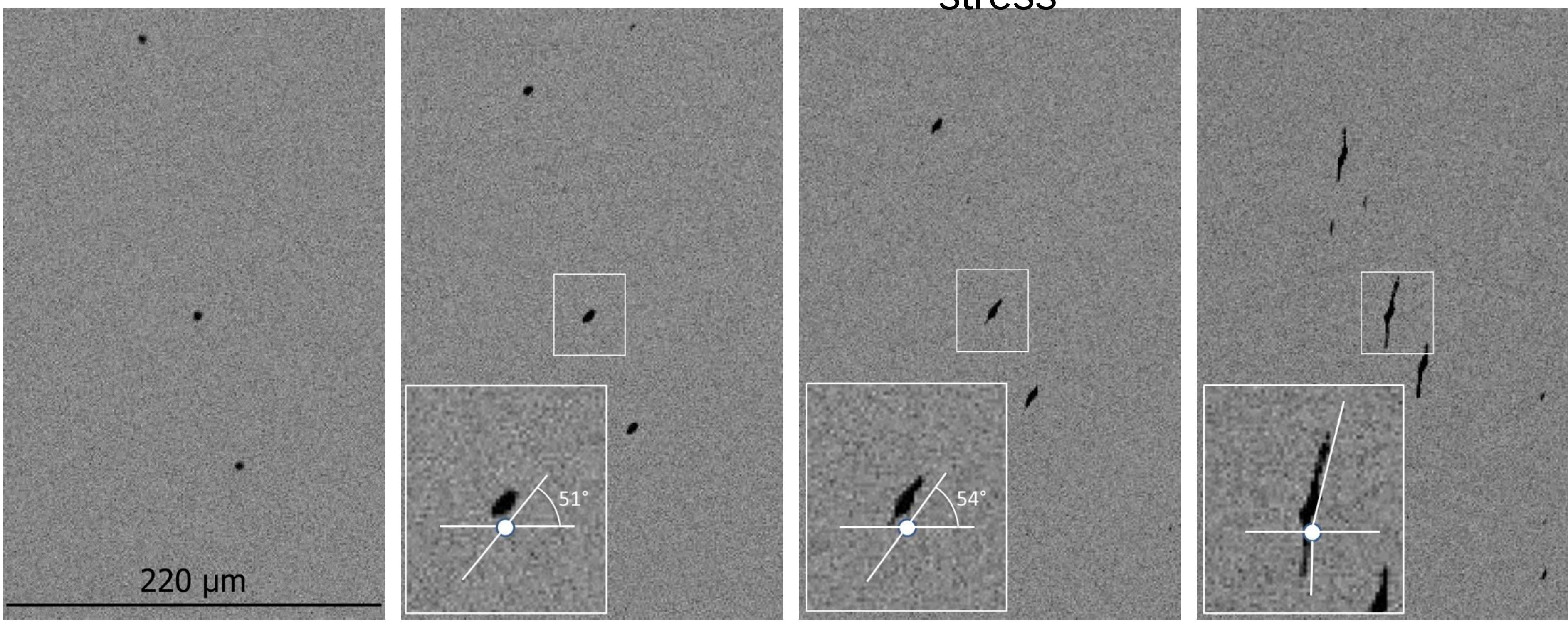

Fractography

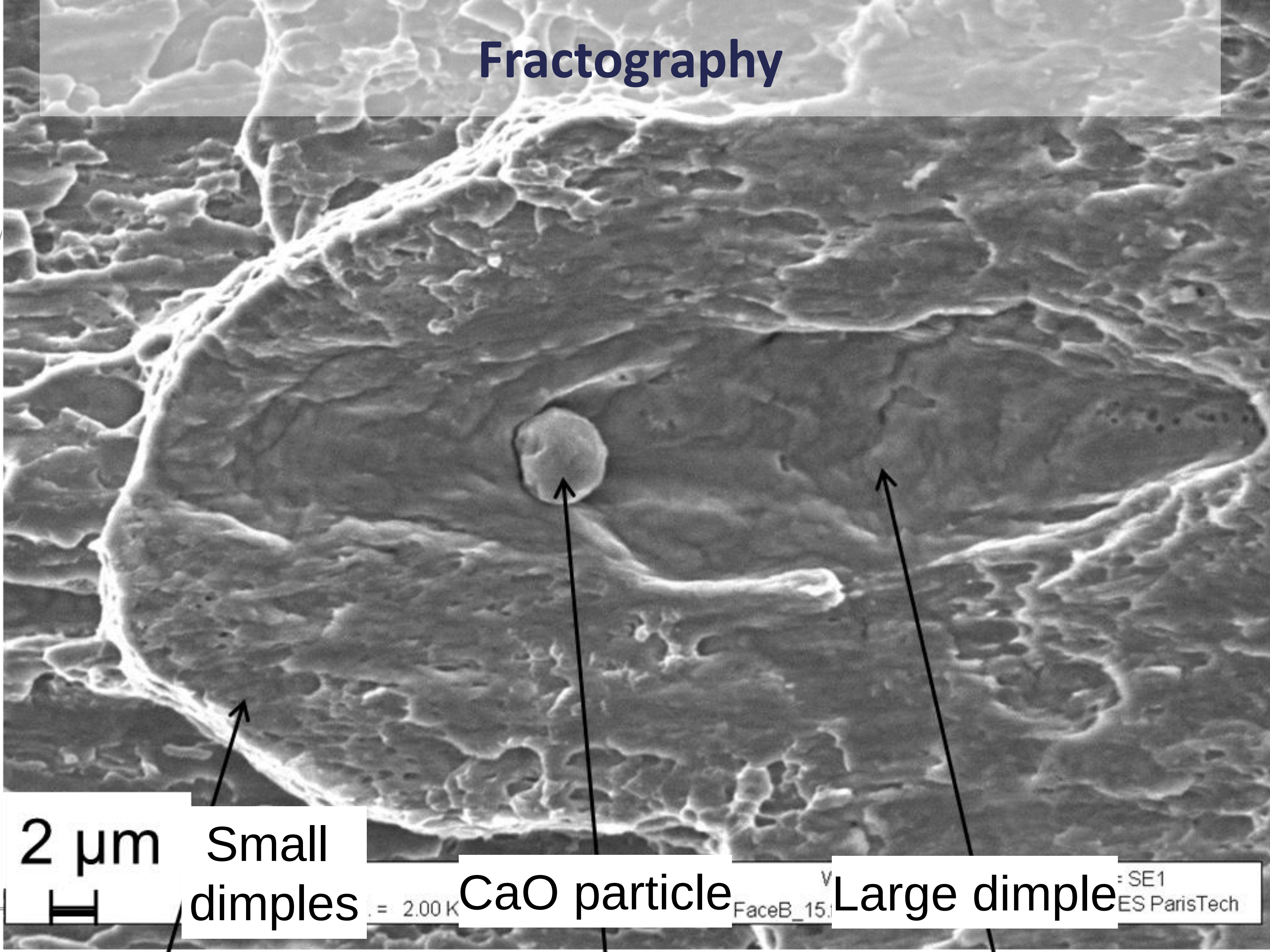

Conclusions on FB600 shear

- Voids nucleate and grow around particles even under shear-dominated loading conditions
- Elongated voids grow along the direction of maximum principal stress (simulation)
- Localization bands form along the direction of maximum shear (simulation)
- Shear localization possible at low void volume fractions (less than 0.02%)

Roth et al IJP 2018

Incrasing resolution

Nucleation/Coalescence observed by enhanced resolution

- ESRF ID22, ID16: Magnified Holotomography (P. Cloetens)

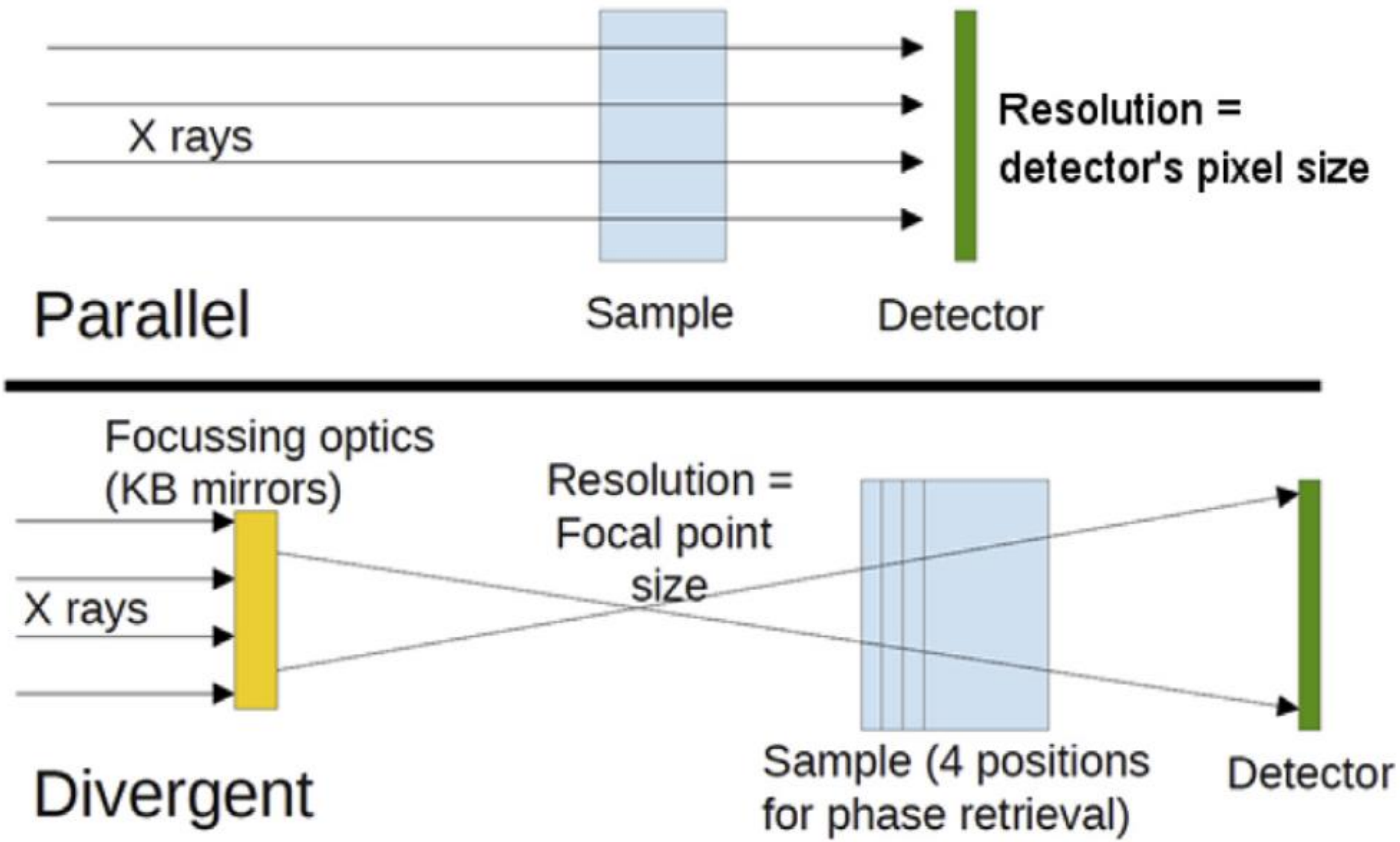

50 nm voxels

[Morgeneyer et al. Polymer 2014]

Outlook: cooperations welcome!

- Mechatronic *in situ* machine
  - 10 kN capacity with load cell
  - Tension-compression
  - Various stress states

  - Leading to fast scanning (1h per sample)

References

- Morgeneyer T.F., Besson J., Proudhon H., Starink M.J., Sinclair I., “Experimental and numerical analysis of toughness anisotropy in AA2139 Al-alloy sheet;” Acta Materialia, 57 (2009): 3902-3915
- Helfen L, Myagotin A, Mikulík P, Pernot P, Voropaev A, Elyyan M, Di Michiel M, Baruchel J, Baumbach T (2011) On the implementation of computed laminography using synchrotron radiation. Rev Sci Instrum 82
- Helfen L, Baumbach T, Mikulík P, Kiel D, Pernot P, Cloetens P, Baruchel J (2005) High-resolution three-dimensional imaging of flat objects by synchrotron-radiation computed laminography. Appl Phys Lett 86
- Morgeneyer T.F., Helfen L., Sinclair I., Proudhon H., Xu F., Baumbach T. , "Ductile crack initiation and propagation assessed via in situ synchrotron radiation computed laminography" Scripta Materialia, 65 (2011) 1010-1013, DOI: 10.1016/j.scriptamat.2011.09.005
- Morgeneyer T.F., Helfen L., Mubarak H., Hild, F., "3D Digital Volume Correlation of Synchrotron Radiation Laminography images of ductile crack initiation: an initial feasibility study", Experimental Mechanics, 53 (2013) 543-556, DOI: 10.1007/s11340-012-9660-y
- Roux S, Hild F, Viot P, Bernard D (2008) Three dimensional image correlation from X-Ray computed tomography of solid foam. Comp Part A 39:1253–1265
- T.F. Morgeneyer, T. Taillandier-Thomas, L. Helfen, et al. "In situ 3D observation of early strain localisation during failure of thin Al alloy (2198) sheet". Acta Materialia, 69 (2014) 78-91 DOI: 10.1016/j.actamat.2014.01.033
- T. Ueda, L. Helfen, T.F. Morgeneyer, "In-situ laminography study of three-dimensional individual void shape evolution at crack initiation and comparison with GTN-type simulations". Acta Materialia, 78 (2014) 254–270 DOI: 10.1016/j.actamat.2014.06.029

References

- T.F. Morgeneyer, H. Proudhon, P. Cloetens, W. Ludwig, Q. Roirand, L. Laiarinandrasana, E. Maire, "Nanovoid morphology and distribution in deformed HDPE studied by Magnifed Synchrotron Radiation Holotomography", Polymer, 55 (2014) 6439-6443,
- A. Buljac, T. Taillandier-Thomas, T.F. Morgeneyer, L. Helfen, S. Roux, F. Hild, "Slant strained band development during flat to slant crack transition in AA 2198 T8 sheet: in situ 3D measurements", International Journal of Fracture, 200 (1) (2016) 49–62, DOI: 10.1007/s10704-015-0052-z
- T.F. Morgeneyer, T. Taillandier-Thomas, A. Buljac, L. Helfen, F. Hild, "On strain and damage interactions during tearing: 3D in situ measurements and simulations for a ductile alloy (AA2139-T3)", Journal of the Mechanics and Physics of Solids, 96 (2016) 550–571, DOI: 10.1016/j.jmps.2016.07.012
- G. Rousselier. T.F. Morgeneyer, S. Ren, M. Mazière, S. Forest "Interaction of the Portevin-Le Chatelier phenomenon with ductile fracture of a thin aluminum CT specimen: experiments and simulations" International journal of fracture, 206 (2017) 95-122
- A. Buljac, F. Hild, L. Helfen, T.F. Morgeneyer, "On deformation and damage micromechanisms in strong work hardening 2198 T3 aluminium alloy",Acta Materialia, 149 (2018) 29-45
- C. C. Roth, T. F. Morgeneyer, Y. Cheng, L. Helfen, D. Mohr "Ductile damage mechanism under shear-dominated loading: In-situ tomography experiments on dual phase steel and localization analysis". International Journal of Plasticity, 109 (2018) 169-192
- S. Ren, T. F. Morgeneyer, M. Maziere, S. Forest and G. Rousselier "Portevin-Le Chatelier effect triggered by complex loading paths in an Al-Cu aluminium alloy" Philosophical Magazine, 2019, accepted for publication

Questions?

Mg$_2$Si particle in AA6061 observed by synchrotron laminography:

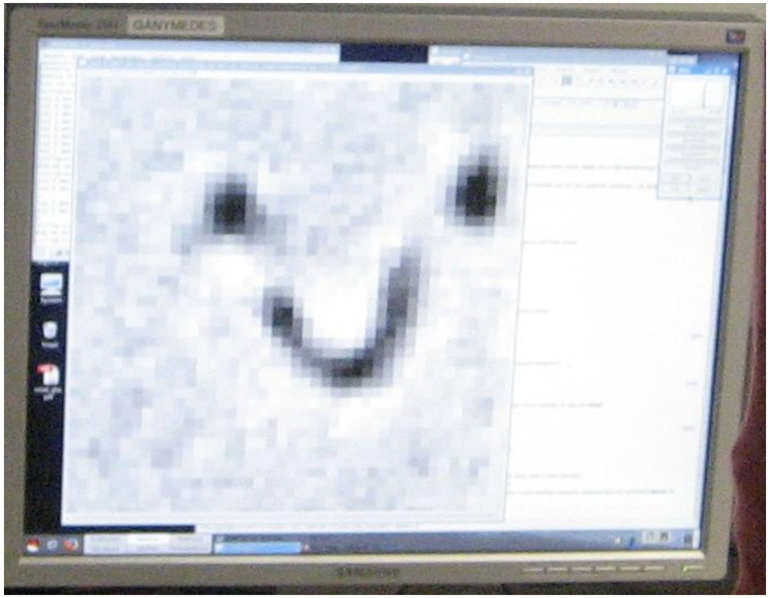

Acknowledgements

'COMINSIDE' project

Beamtime ma1006, mi1149, me1366

Fédération Francilienne de Mécanique : coupe de pouce 2011